COO-3077-136

Courant Institute of
Mathematical Sciences

ERDA Mathematics and Computing Laboratory

Design of Transonic Cascades by Conformal Transformation of the Complex Characteristics

Eldon A. McIntyre Jr.

ERDA Research and Development Report

Mathematics and Computers
November 1976

New York University

UNCLASSIFIED

AEC Computing and Applied Mathematics Center
Courant Institute of Mathematical Sciences
New York University

Mathematics and Computers COO-3077-136

DESIGN OF TRANSONIC CASCADES BY CONFORMAL TRANSFORMATION OF THE COMPLEX CHARACTERISTICS

Eldon A. McIntyre Jr.

November 1976

U. S. Energy Research and Development Administration
Contract No. AT(11-1)-3077

UNCLASSIFIED

TABLE OF CONTENTS

Page

PREFACE.. v

0. INTRODUCTION.................................. 1
   1. The Physical Problem 1
   2. The Mathematical Problem 3

1. THE PARTIAL DIFFERENTIAL EQUATIONS OF TRANSONIC FLOW... 7
   1. The Flow Equations 7
   2. The Hodograph Equations 10
   3. The Characteristic Equations 11
   4. Complex Extension 18

2. TRANSONIC CASCADES.............................. 19
   1. Cascade Geometry 19
   2. Conjugate Characteristic Coordinates 21
   3. The Singular Solution 29
   4. The Complex Characteristic Initial Value Problem for Transonic Flow through a Cascade 32
   5. The Arbitrary Constants in the Singular Solution 38
   6. The Initial Data 41

3. THE COMPUTATION: A CONCEPTUAL OVERVIEW................. 50
   1. The Basic Diagram 50
   2. Subsonic Integration 54
   3. The Finite Difference Scheme 57
   4. Calculating the Flow in the Supersonic Region 62
   5. Using the Existing Method 66

4. A FURTHER REFINEMENT OF THE CHARACTERISTIC TRANSFORMATION 68
   1. The Joukowski Mapping 68
   2. Mapping the Flow onto the Interior of the Unit Circle 71
   3. Modifying the Configuration 73
   4. Conclusion: A Turbine Blade 75

BIBLIOGRAPHY..................................... 77

FIGURES.. 81

Preface

Even a casual reading of newspaper or magazine articles suggests that ours is a world which is vitally concerned with both the production and conservation of energy. People everywhere are searching for new, cheaper, and environmentally safe energy resources, while others are trying to find more efficient ways of using the energy we already have.

This work is consistent with those efforts in that it seeks to further develop a technology which, properly applied, could contribute to the solution of both aspects of the energy problem. To be specific, we are here concerned with developing a procedure for the numerical design of transonic turbine and compressor blade profiles in two dimensions. We say that a flow is transonic if it attains speeds both above and below that of sound. Such a procedure might be used to design more efficient axial flow compressors for use in the production of enriched uranium at gaseous diffusion plants, as well as in the construction of lighter, more efficient airplane engines for better fuel consumption. Improving the design of high speed turbomachinery could be of practical benefit to a great many people.

The techniques used here are a direct result of work on the supercritical wing. First designed by Whitcomb and his associates at the Langley Research Center in Virginia, such airfoils have undergone wind-tunnel and flight testing, the results showing that it is indeed possible to achieve virtually shock-free flow without boundary layer separation. As a consequence of these experimental successes, attempts at providing a purely theoretical basis for the design of supercritical wings have become more frequent and increasingly successful. In fact, wing sections designed by the method used here have been tested also [17], and have shown the theory to be quite functional.

Introduction

1. The Physical Problem

In this section, we use the gas turbine, with particular attention to its use in jet propulsion, to provide a physical context for the mathematical problem under study.

In general, the gas turbine exists in a variety of forms and has many applications, though its operating principle is quite simple. In its basic form, the compressor section raises the pressure and temperature of the gas, the combustion section adds fuel and oxidizes it, thus raising the temperature sharply, and the turbine section fans it out, lowering the pressure considerably and the temperature slightly. The useful work of the system is, of course, delivered to the turbine wheel. Note that because of the work done in compressing the gas, the compressor is usually driven by the turbine.

When used as a power plant, the turbine wheel delivers only a part of its energy to the compressor (when there is a compressor), the remainder being used elsewhere. In a jet propulsion system, however, all of the turbine wheel energy goes to the compressor, the momentum of the craft being a result of Newton's third law and the rearward discharge of gases. A much simplified diagram of such a machine appears in Figure 1. Observe that though there are several types of compressors, we will at all times be restricted to axial flow compressors, so named because the gas flows along the axis (see Figure 2).

If we now look at a blade row of such a structure, or a turbine wheel (see Figure 3), we see that, though quite different, each consists of a pattern of blades mounted on a right circular cylinder. Further, we ignore the radial components of the gas velocity, i.e. we in essence assume that the flow streamlines lie on the cylinder's surface, as in Figure 4. Finally, we develop this cylindrical surface into a plane, obtaining the two dimensional cascade in Figure 5.

These are the structures we want to design. More precisely, we wish to find smooth, transonic, steady-state solutions to the equations for the irrotational flow of an inviscid fluid through a two dimensional cascade.

It should be pointed out that industry has found cascades to be quite useful in blade design work, even though they are only two dimensional idealizations of the physical fact.

2. The Mathematical Problem

In mathematical terms, our problem reduces to finding analytic solutions to a system of partial differential equations for flow about a body. Although we will often be concerned with a single blade, the periodicity of the solution will result in a cascade. There are several difficulties in such a problem:

(1) The equations are nonlinear,

(2) Analytic solutions may not always exist, and

(3) The Equations are of mixed type.

We overcome the first difficulty by use of the hodograph transformation. First used by Chaplygin in his work on gas jets [6], this well-known procedure interchanges the roles played by the independent variables (the planar coordinates x and y) and the dependent variables (the velocity components u and v). The resulting equations are linear, though the boundary data becomes somewhat complicated.

The second difficulty, as well as the third, are results of the transonic nature of the flow and can be presented in the following way. Suppose we wish to design a turbine blade. One procedure is to input a particular blade design with the relevant information, e.g. the geometry of the blade surface, and compute the flow. This is called the direct problem, since we specify the blade and compute the flow. It has been shown by Morawetz [25], however, that the problem of finding a shock-free transonic flow about an arbitrary body is not well-posed, i.e. a smooth solution may not exist. We can get around the issue by instead solving the inverse problem, i.e. we choose data which specify properties of the flow, and then compute the blade profile. Thus the solution will be analytic, and we can then manipulate the data until we get a good blade.

The remaining difficulty is, essentially, that of finding an applicable method for solving the equations. Like Tricomi's equation, the equations of transonic flow are of mixed type (hyperbolic and elliptic) and thus require special algorithms for their solution. The procedure chosen here is the method of characteristics. This technique is usually restricted to hyperbolic systems, but we have used it everywhere, after extending all variables into the complex domain by analytic continuation. The resulting equations are then cast in the form of a complex characteristic initial value problem and solved in complex four-space. Since we are using the hodograph equations, which are linear, we can, by the principle of superposition, break up our expected solution into two parts, a regular part and a singular part, the form of the latter being dictated by the cascade geometry.

The study of transonic problems received a great impetus as a result of experimental successes in achieving virtually shock-free transonic flow in the 1960's [19], [27], [29]. The particular technique of treating these problems as complex characteristic initial value problems, first used by Garabedian and Lieberstein [11], has been carried forward to the design of airfoils [2], [1]. The initial application to compressors is documented by Korn in [21]. It should be mentioned that weak shocks appear under off-design conditions, though the losses remain low.

Nevertheless, certain difficulties have arisen. It has been found difficult to generate blades of large thickness and high camber. The contribution of this work has been to design such blades. This was done by basing the form of the characteristic mapping on the complex velocity of a flow about a Joukowski blade mapped onto the interior of a circle, instead of the complex velocity of a circular cylinder as had been done before.

The plan of this paper is as follows. In Chapter 1 we use basic physical assumptions to derive the characteristic equations and extend them into the complex domain, the result being a system of equations which apply to any transonic flow. In Chapter 2, we present a singular solution which is based on the geometry of a cascade and describe the selection of appropriate initial data, the result being a threefold complex initial value problem which applies to a transonic cascade. Chapter 3 contains a descriptive account of the numerical method of solution (integration paths, finite difference schemes, graphic output, etc.), emphasizing the basic strategy of the computer program, as well as the results of the original program, viz., that we were able to generate a compressor blade but not a turbine blade. Last, in Chapter 4 we introduce the Joukowski transformation and present the resulting turbine blade.

There are, of course, many people who, at one point or another, helped me in this work. In particular, I would like to acknowledge my tremendous debt to Paul R. Garabedian, for his many suggestions, tireless support, and enduring patience. He suggested this problem, and it goes without saying that the work could not have been done without him. I am also grateful to David Korn for his aid and encouragement, and for allowing me to use his programs. Thanks are also due Connie Engle for typing the manuscript.

1. THE PARTIAL DIFFERENTIAL EQUATIONS OF TRANSONIC FLOW

In this chapter we state the basic equations of the flow and introduce the hodograph transformation. The resulting equations, which are of mixed type, are then cast in the form of a characteristic initial value problem in the complex domain.

1. The Flow Equations

The mathematical model for the inviscid flow of a compressible fluid is based on the following assumptions ([7], p. 3-25], as expressed in the accompanying equations. Note that we will use Euler's representation at all times.

(1) The conservation of mass:

$$\rho_t + \nabla\cdot(\rho\vec{q}) = 0 ,$$

where ρ, the density, and $\vec{q}$, the fluid velocity, are functions of space and time, ρ_t is the partial derivative of ρ with respect to t, and

$$\nabla = \hat{i}\,\frac{\partial}{\partial x} + \hat{j}\,\frac{\partial}{\partial y} + \hat{k}\,\frac{\partial}{\partial z} .$$

(2) The conservation of linear momentum:

$$\rho\,\frac{d\vec{q}}{dt} + \nabla P = 0 ,$$

where P represents the pressure, and

$$\frac{d}{dt} = \frac{\partial}{\partial t} + u\frac{\partial}{\partial x} + v\frac{\partial}{\partial y} + w\frac{\partial}{\partial z}$$

is the material derivative. Here and in the following we will let u, v and w respectively denote the x, y and z components of the velocity vector $\vec{q}$.

(3) The equation of state of a polytropic gas:

$$P = A(S)\rho^{\gamma} ,$$

where S is the specific entropy, A is a known function of S, and γ is the adiabatic exponent.

(4) The conservation of energy:

$$\frac{dS}{dt} = 0 .$$

This last equation is somewhat unnecessary for our particular purposes since we assume that the flow is isentropic, i.e. S is constant throughout the medium.

If, in addition, we restrict ourselves to the steady flow of a polytropic gas in two dimensions, the remaining equations reduce to

$$(\rho u)_x + (\rho v)_y = 0 \tag{1.1}$$

$$\rho(uu_x + vu_y) + P_x = 0 \tag{1.2a}$$

$$\rho(uv_x + vv_y) + P_y = 0 \tag{1.2b}$$

and

$$P = A\rho^{\gamma} , \tag{1.3}$$

where A is now a known constant. Observe that we can differentiate (1.3) to get

$$c^2 = \frac{dP}{d\rho} = \gamma A \rho^{\gamma-1} , \tag{1.4}$$

which defines the local speed of sound c. Consequently we can use both (1.3) and (1.4) to eliminate ρ and P from (1.1) and (1.2), and then manipulate the resulting equations to get

$$(c^2-u^2)u_x - uv(u_y+v_x) + (c^2-v^2)v_y = 0 . \tag{1.5}$$

Finally, we assume that the flow is irrotational, i.e.

$$u_y - v_x = 0 , \tag{1.6}$$

which, together with (1.2), implies that

$$q^2 + \frac{2c^2}{\gamma-1} = \frac{2c_0^2}{\gamma-1} , \tag{1.7}$$

where c_0 is the sound speed at $q = 0$. Equation (1.7) is, of course, a form of Bernoulli's law.

In summary, we remark that the system of equations (1.5), (1.6) corresponds to the steady, isentropic, irrotational flow of a polytropic gas in two dimensions. We wish to solve this system for u and v, where we consider c to be a known function of q given by (1.7).

2. The Hodograph Equations

Clearly, equation (1.5) is nonlinear, since the coefficients multiplying the partials of u and v are themselves functions of u and v. One may, however, by use of implicit function theorems or, equivalently, a Legendre transformation ([7], pp. 248-252), rewrite (1.5) and (1.6) as

$$(c^2-u^2)y_v + uv(x_v+y_u) + (c^2-v^2)x_u = 0 \tag{1.8}$$

and

$$x_v - y_u = 0 \ . \tag{1.9}$$

Of course, we have assumed that the Jacobian

$$J = \frac{\partial(u,v)}{\partial(x,y)} \neq 0$$

in the region of interest.

The important point here is that by considering x and y to be functions of the now independent variables u and v we obtain a linear system of first order partial differential equations. Equations (1.8) and (1.9) are called the hodograph equations.

3. The Characteristic Equations

We first rewrite the system (1.8), (1.9) as

(1.10) $$SZ_v + TZ_u = 0 ,$$

where we have set

$$S = \begin{bmatrix} c^2-u^2 & uv \\ 0 & 1 \end{bmatrix} ,$$

$$T = \begin{bmatrix} uv & c^2-v^2 \\ -1 & 0 \end{bmatrix} ,$$

and

$$Z = \begin{bmatrix} y \\ x \end{bmatrix} .$$

We wish to solve this system by the method of characteristics. To do that, we first find equations in the uv-plane for the two-parameter family of loci called characteristics, or characteristic curves, the two parameters being called characteristic coordinates. We then construct equations for the remaining variables, y and x, in terms of the characteristic coordinates, and solve the entire system numerically ([7], pp. 40-45).

Toward that end, we consider the smooth curve C contained in the uv-plane and given by (u(s),v(s)) where s is a real parameter. Then, using the relations

$$\frac{dy}{ds} = y_v \frac{dv}{ds} + y_u \frac{du}{ds} ,$$

and

$$\frac{dx}{ds} = x_v \frac{dv}{ds} + x_u \frac{du}{ds} ,$$

we may rewrite (1.10) in the form

$$AX = B , \tag{1.11}$$

where

$$A = \begin{pmatrix} c^2-u^2 & uv & uv & c^2-v^2 \\ 0 & 1 & -1 & 0 \\ \frac{dv}{ds} & 0 & \frac{du}{ds} & 0 \\ 0 & \frac{dv}{ds} & 0 & \frac{du}{ds} \end{pmatrix} ,$$

$$X = \begin{pmatrix} y_v \\ x_v \\ y_u \\ x_u \end{pmatrix} ,$$

and

$$B = \begin{pmatrix} 0 \\ 0 \\ \frac{dy}{ds} \\ \frac{dx}{ds} \end{pmatrix} .$$

We recall that in two dimensions, however, a characteristic is a curve along which one cannot solve the given equations for the normal derivatives of the dependent variables (in this case y and x), even though the values of these functions are known on that curve. Nevertheless, if we know y and x on C, we can differentiate them to get dy/ds and dx/ds there, which means that we can determine the matrices A and B. Further, if A is nonsingular, we can invert it and get a unique X, which means that we will have determined the derivatives of y and x in all directions, including the normal. Hence, if C is a characteristic, A is singular, i.e.

$$\det A = 0 \ . \tag{1.12}$$

Introducing $\lambda = dv/du$, we assume $du/ds \neq 0$ and set

$$\frac{dv}{ds} = \lambda \frac{du}{ds} \ . \tag{1.13}$$

Then, carrying out the computation of (1.12) we get

$$\det A = \left(\frac{du}{ds}\right)^2 [\lambda^2(c^2-v^2) - 2uv\lambda + c^2-u^2] = 0 \ ,$$

which implies that

$$\lambda^2(c^2-v^2) - 2uv\lambda + c^2-u^2 = 0 \ . \tag{1.14}$$

It is this equation, in practice, which is used to determine the characteristic curves, since we do not know their equations beforehand.

Solving (1.14) for λ, we get two solutions,

$$\lambda_\pm = \frac{uv \pm c\sqrt{q^2 - c^2}}{c^2 - v^2} \ , \tag{1.15}$$

corresponding to two families of characteristic curves which we shall hereafter refer to as C_+ and C_-. We call $\lambda_\pm(u,v)$ the characteristic directions, since they are the slopes of the characteristics through each point of the uv-plane. Clearly they are real and distinct whenever $q^2 > c^2$, i.e. whenever the flow is supersonic. Thus we have determined a two parameter family of curves in the uv-plane along which we wish to solve for y and x.

Suppose now, that we can find two parameters, α and β, such that

$$\beta(u,v) = \text{constant}$$

on each curve in C_+, and

$$\alpha(u,v) = \text{constant}$$

on each curve in C_-, where

$$\frac{\partial(\alpha,\beta)}{\partial(u,v)} \neq 0 \ .$$

We then call α and β characteristic coordinates, since their values at a point in the uv-plane indicate which characteristics intersect there. Thus we may rewrite (1.13) as

$$v_\alpha = \lambda_+ u_\alpha \tag{1.16a}$$

on C_+, and

$$v_\beta = \lambda_- u_\beta \tag{1.16b}$$

on C_-, where we have used partial derivatives since u and v (as well as y and x) are assumed to be functions of both α and β.

Observe then, that in the case of C_+ , (1.11) leads to the augmented matrix

$$[A,B] = \begin{pmatrix} c^2-u^2 & uv & uv & c^2-v^2 & 0 \\ 0 & 1 & -1 & 0 & 0 \\ \lambda_+ u_\alpha & 0 & u_\alpha & 0 & y_\alpha \\ 0 & \lambda_+ u_\alpha & 0 & u_\alpha & u_\alpha \end{pmatrix}$$

which, by use of elementary row operations, can be reduced to

$$\begin{pmatrix} 0 & 0 & 0 & 0 & x_\alpha+\lambda_- y_\alpha \\ 0 & 1 & -1 & 0 & 0 \\ \lambda_+ & 0 & 1 & 0 & y_\alpha/u_\alpha \\ 0 & 0 & \lambda_+ & 1 & x_\alpha/u_\alpha \end{pmatrix} .$$

The last three rows yield no new information, but from the first, we see that we must have

$$x_\alpha + \lambda_- y_\alpha = 0 \tag{1.17a}$$

on every curve of C_+ , or our system will be inconsistent. In a similar way, we arrive at

$$x_\beta + \lambda_+ y_\beta = 0 \tag{1.17b}$$

for every curve in C_-. Thus, equations (1.16), (1.17) form a system of four characteristic equations in four unknowns (u,v,y and x), in terms of the as yet undetermined characteristic coordinates α and β.

Explicit expressions for α and β can be found, however; in fact, Sears has shown [28] that

$$\alpha = f(q) - \theta \tag{1.18a}$$

$$\beta = f(q) + \theta \ , \tag{1.18b}$$

is such a pair of parameters, where of course

$$q = \sqrt{u^2 + v^2}$$

$$\theta = \tan^{-1}\left(\frac{v}{u}\right) \ ,$$

and where

$$f(q) = \frac{1}{2\mu} \sin^{-1}\left[(\gamma-1)\ \frac{q^2}{c_*^2} - \gamma\right] + \frac{1}{2} \sin^{-1}\left[(\gamma+1)\ \frac{c_*^2}{q^2} - \gamma\right] \ . \tag{1.19}$$

Here, c_* is the critical speed, and

$$\mu = \sqrt{\frac{\gamma-1}{\gamma+1}} \ .$$

Note that characteristic coordinates are certainly not unique, since any continuously differentiable monotone function of a characteristic coordinate is itself a characteristic coordinate. Our particular choice of characteristic coordinates (see Section 2.2) will be based on Sears', though they will be, in general, complex, and have additional properties as consequences of that fact.

In passing, we remark that we would have obtained equations (1.16), (1.17) even without the hodograph transformation, with $-1/\lambda_{\pm}$ as the characteristic directions in the xy-plane. Our approach differs in that we will solve (1.16) for u and v in terms of α and β, and then prescribe initial data for y and x in the uv-plane. The advantage gained is that equations (1.17) are linear, since $\lambda_{\pm}$ are functions of u and v alone, and we can use the principle of superposition.

4. Complex Extension

The distinguishing characteristic of a transonic flow is that it contains regions in which the flow speed is above the local speed of sound as well as regions in which it is below. In the former case, i.e. when $q > c$, the system is hyperbolic and, since the characteristic directions $\lambda_{\pm}$ are real and distinct, we can use the method of characteristics. When the flow is subsonic, however, the characteristic directions take on complex values and the method breaks down. The system is elliptic in such a region, and the characteristic curves are not defined.

We resolve this issue by extending all variables into the complex domain and solving the original two dimensional problem in complex four-space. That this can be done is a consequence of the fact that the terms of the coefficient matrices are analytic in all their arguments. It remains to be shown how best this extension can be made, since we will only be interested in that portion of the solution which lies in the real uv-plane.

We now state the general problem:

We wish to solve the complex system (1.16), (1.17) where $\lambda_{\pm}$ are known functions of u and v, and x and y satisfy appropriate initial conditions. We allow all entities to take on complex values.

2. TRANSONIC CASCADES

In this chapter, we use physical criteria derived from the geometry of cascades to further specify the mathematical problem, especially with respect to the form of the singular solution and the assignment of proper initial data. This, in turn, leads to a further development of the characteristic equations.

1. Cascade Geometry

A cascade, as mentioned before, is a two dimensional, periodic array of blades. Steady flow through such a structure is used to represent the regime of an axial flow compressor. It is assumed that a fluid with a prescribed velocity at $x = -\infty$ (called the inlet velocity) passes through the cascade to arrive at another prescribed velocity (called the exit velocity) at $x = +\infty$. For example, in Figure 5 we have a fluid with inlet velocity $\vec{v}_1$ and exit velocity $\vec{v}_2$. The inlet angle α_1 , is the angle between $\vec{v}_1$ and the vertical as is also the case for the exit angle α_2 and $\vec{v}_2$. The net change in angle (not shown in the figure) undergone by the flow from $x = -\infty$ to $x = +\infty$ is called the turning angle.

The gap g is the separation between blades while c is the chord length. In practice we usually use the gap-to-chord ratio g/c, or its inverse, the solidity c/g, which measures the relative distance between blades. We can think of the thickness t as being the maximum blade width along the chord. Here also, we are usually interested in the relative thickness, given by the ratio t/c.

Last (see figure), the stagger angle β specifies the angle at which the blades are stacked. For our purposes, vertical stacking, i.e. $\beta = 90°$, will almost always suffice.

2. Conjugate Characteristic Coordinates

In this section, we use the theory of functions of a complex variable, with special reference to its description of incompressible flow about the unit circle, as a guide in our choice of characteristic coordinates. We remark that throughout, we will be concerned with flow about a single body. In fact, our choice of coordinates will be based on compressible flow about an airfoil ([2], pp. 15-19), the periodicity requirements of cascade geometry being satisfied later as a result of the form of the singular solution.

Clearly, we can consider all quantities, in particular u and v, to be functions of our as yet undetermined (complex) characteristic coordinates α and β. It is in the choice of these coordinates that we have the most freedom, since any analytic function of a characteristic coordinate is itself a characteristic coordinate. We will exploit this freedom by requiring that α and β be not only characteristic coordinates, but conjugate characteristic coordinates, i.e. that

$$\alpha = \bar{\beta}$$

whenever u and v are both real, and conversely. This will simplify our formulation of the problem and reduce the required computation, since we can use the above relationship to identify that part of the solution which lies in the real uv-plane.

To gain an accurate understanding of the role of conjugate characteristic coordinates, we now examine the case of incompressible flow about a body. More specifically, we consider the two dimensional, steady, irrotational flow of an incompressible inviscid fluid about the unit circle in the xy-plane. It can be shown ([24], pp. 174-188), of course, that the complex velocity

$$(2.1) \qquad w = qe^{-i\theta} = u(x,y) - iv(x,y)$$

is an analytic function of the complex variable

$$z = x + iy ,$$

where u and v are, respectively, the x and y components of the flow, as before. This result follows from the fact that, in this illustration, the flow equations reduce to the familiar Cauchy-Riemann equations for u and -v,

$$(2.2a) \qquad u_x = -v_y$$

$$(2.2b) \qquad u_y = v_x .$$

Then, if we assume a velocity u = 1 and v = 0 at infinity, with circulation Γ about the unit circle, we can describe the flow by the complex potential

$$(2.3) \qquad \chi(z) = z + \frac{1}{z} + 2ik \ln z ,$$

where

$$k = \frac{\Gamma}{2\pi} .$$

Moreover, by the standard theory, we know that χ is analytic in z, and further, that

$$w = \frac{d\chi}{dz} = 1 - \frac{1}{z^2} + \frac{2ik}{z} .$$

Inverting this last equation, we see that

$$z = \frac{1}{(1-w-k^2)^{1/2}+ik} . \tag{2.4}$$

We emphasize here that the relationship between z and w as expressed in equation (2.4) has a dual interpretation. The familiar one, based on complex function theory, is that z is an analytic function of w, and hence that the two variables are related by a conformal mapping. For reasons of convenience, we introduce the complex variable,

$$\xi = (1-w-k^2)^{1/2} + ik , \tag{2.5}$$

so that we have

$$z = \frac{1}{\xi} \tag{2.6}$$

and,

$$w = 1 + 2ik\xi - \xi^2 . \tag{2.7}$$

In effect, then, we have a mapping from the z plane to the interior of the unit circle in the ξ plane, and then to the w plane. Figure 6 shows such a mapping for k = 1/2. Observe that, as a result of the branch point at $w = 1-k^2$, the mapping from ξ to w is double-valued. Also, z has a simple pole at $\xi = 0$ (or w = 1). We remark that, up to this point in our illustration, x, y, u and v are all real variables.

On the other hand, we may introduce the hodograph transformation and carry out a computation similar to that of Section 1.3 to get the characteristic equations

(2.8a) $$v_\alpha = \lambda_+ u_\alpha$$

(2.8b) $$x_\alpha = \lambda_+ y_\alpha \ ,$$

which hold on the characteristic planes

$$\beta(u,v) = \text{constant},$$

and

(2.8c) $$v_\beta = \lambda_- u_\beta$$

(2.8d) $$x_\beta = \lambda_- y_\beta \ ,$$

which hold on the characteristic planes

$$\alpha(u,v) = \text{constant},$$

where

$$\lambda_\pm = \pm i \ .$$

Note that since the system (2.2) is of the elliptic type, the characteristic directions $\lambda_\pm$, and characteristic coordinates α and β, must be complex. In addition, x, y, u, and v are now assumed to be complex also, as a result of analytic continuation (see Section 1.4). Moreover, it can be shown that, in this context, w and the complex variable

$$w^* = qe^{i\theta} = u(x,y) + iv(x,y) \tag{2.9}$$

are conjugate characteristic coordinates ([2], pp. 12-13,17), i.e. we may set

$$\alpha = w$$
$$\beta = w^*$$

in (2.8). Of course the w used here is the analytic continuation of that introduced in equation (2.1), since u and v are now complex. Thus we may also view equation (2.4) as a relation between the complex variables x and y, and the conjugate characteristic coordinate w. We note, in passing, that for

$$z^* = x - iy ,$$

we have

$$z^* = \frac{1}{(1-w^*-k^2)^{1/2} - ik} , \tag{2.10}$$

which expresses a relationship between x and y, and the remaining coordinate w^*.

Going further, we may also carry over the variable ξ as defined in equation (2.5), subject to a proper analytic continuation, and in a similar way introduce

$$\eta = (1-w^*-k^2)^{1/2} - ik , \tag{2.11}$$

to get

$$z^* = \frac{1}{\eta} \tag{2.12}$$

and

$$w^* = 1 - 2ik\eta - \eta^2 . \tag{2.13}$$

Clearly, ξ and η are also conjugate characteristic coordinates, since they are analytic functions of w and w^*, and

$$w = \overline{w^*} \Leftrightarrow \xi = \bar{\eta} .$$

These are the coordinates that we use in practice, since unlike w and w^*, their relationships to z and z^* are, respectively, one-to-one for real x and y.

Let us assume therefore, that we have rewritten the characteristic equations (2.8) in terms of ξ and η. We can then use (2.7, 2.13) to solve two of these equations (2.8a,c) explicitly, since

$$u = \frac{w+w^*}{2}$$

and

$$v = \frac{w^*-w}{2i} .$$

Thus the illustration is complete. We point out, however, that although in this case we also know x and y in terms of ξ and η as a result of (2.6), (2.12), this is not generally true in the transonic case. There, we will have to solve the equations corresponding to (2.8b,d) numerically.

We now turn to compressible flow about an airfoil, carrying our formulation over in an analogous way. It has been shown ([2], pp. 21,22) that for such flows, the conjugate characteristic coordinates corresponding to w and w^* are

(2.14a) $$s = h(q)e^{-i\theta}$$

and

(2.14b) $$s^* = h(q)e^{i\theta} ,$$

where

(2.15) $$h(q) = Kq[(c - \sqrt{c^2-c_*^2}\,)^{1/\mu} \; (\sqrt{c^2-q^2} + c)]^{-1} ,$$

and K is a constant such that

$$h(1) = 1 .$$

Continuing our analogy to the incompressible case, we generalize equations (2.7), (2.13) and define ξ and η by

(2.16a) $$s = C_i \xi^i$$

using the summation notation, and

(2.16b) $$s^* = \overline{C_i} \eta^i ,$$

noting that the complex constants C_i are to be determined later. It is clear that, since s and s^* are conjugate characteristic coordinates, ξ and η, as defined in (2.16), will be too.

Thus we may now reformulate the characteristic equations (1.16), (1.17). We wish to solve

(2.17a) $$v_\xi = \lambda_+ u_\xi$$

(2.17b) $$x_\xi + \lambda_- y_\xi = 0$$

on the curves C_+ , given by

$$\xi(u,v) = \text{constant},$$

and

(2.17c) $$v_\eta = \lambda_- u_\eta$$

(2.17d) $$x_\eta + \lambda_+ y_\eta = 0 ,$$

on the curves C_- , given by

$$\eta(u,v) = \text{constant} .$$

We remark that we will have, in effect, solved (2.17a,c) when we have specified the C_i of (2.16), since for each ξ and η we can get s and s^* by (2.16) and in principle invert (2.14) to find q and θ and hence u and v. Nevertheless, we must still solve (2.17b,d) numerically.

Attempts at designing transonic airfoils using these equations have met with much success. It must be remembered, however, that (2.16a,b) were simply taken over, albeit in a more general form, from incompressible flow about a circular cylinder, and there is nothing in this presentation to guarantee their effectiveness. In fact, it was found necessary to modify them to obtain the results of this paper.

3. The Singular Solution

In this section, we use properties of the flow through a cascade to work out the form of the singular solution.

Consider the complex extensions of the planar coordinates x and y. Our immediate goal is to write them in the form

$$x = X_S(\xi,\eta) + X_R(\xi,\eta)$$

$$y = Y_S(\xi,\eta) + Y_R(\xi,\eta) ,$$

where X_R and Y_R are regular, and X_S and Y_S have singularities appropriate to a cascade.

Toward this end, we first let (u_B,v_B) and (u_A,v_A) respectively denote the inlet and exit flow velocities. Assuming the coefficients C_i to be known, we can determine complex numbers ξ_B and ξ_A such that

$$s_B = h(q_B)e^{-i\theta_B} = C_i\xi_B^i \tag{2.18a}$$

and

$$s_A = h(q_A)e^{-i\theta_A} = C_i\xi_A^i , \tag{2.18b}$$

where,

$$q_B^2 = u_B^2 + v_B^2 , \quad \theta_B = \tan^{-1}(\frac{v_B}{u_B}),$$

and

$$q_A^2 = u_A^2 + v_A^2 , \quad \theta_A = \tan^{-1}(\frac{v_A}{u_A}) .$$

Supposing the flow to be from left to right, and remembering that u and v are real when $\eta = \bar{\xi}$, we require a solution such that:

(1) The velocity vector $(u,v) \to (u_B,v_B)$ and $x \to -\infty$ in the real physical plane as $(\xi,\eta) \to (\xi_B,\bar{\xi}_B)$.

(2) We have a source at the point in the real physical plane corresponding to $(\xi_B,\bar{\xi}_B)$.

(3) The velocity vector $(u,v) \to (u_A,v_A)$ and $x \to +\infty$ in the real physical plane as $(\xi,\eta) \to (\xi_A,\bar{\xi}_A)$.

(4) We have a sink at the point in the real physical plane corresponding to $(\xi_A,\bar{\xi}_A)$.

(5) The solution is multiple-valued, i.e. we generate a cascade instead of a single blade.

(6) The stream function ψ is single-valued for any real closed path around any single blade.

All of these conditions can be met by a solution of the form

$$x(\xi,\eta) = X^1(\xi,\eta)\ \ln(\xi-\xi_A) + X^2(\xi,\eta)\ \ln(\xi-\xi_B) + X^3(\xi,\eta) \tag{2.19a}$$

$$y(\xi,\eta) = Y^1(\xi,\eta)\ \ln(\xi-\xi_A) + Y^2(\xi,\eta)\ \ln(\xi-\xi_B) + Y^3(\xi,\eta), \tag{2.19b}$$

where X^i and Y^i, $i = 1,2,3$, are regular functions to be determined numerically. Note that, though we have been able to choose characteristic coordinates such that u and v are real when $\eta = \bar{\xi}$, this is not necessarily true for x and y; their dependence on ξ and η, unlike that of u and v, is still in the form of a pair of unsolved equations. Hence, after solving these equations for the X^i and Y^i, we will choose

(2.20a) $$x_{real} = \text{Re}\,[x(\xi,\bar{\xi})]$$

(2.20b) $$y_{real} = \text{Re}\,[y(\xi,\bar{\xi})]$$

as our real solution.

4. The Complex Characteristic Initial Value Problem for Transonic Flow through a Cascade

In this section, we use the expected form of the solution to derive a final system of characteristic equations, from which we construct three complex characteristic initial value problems, one for each of the three pairs of functions X^i and Y^i, $i = 1,2,3$, of equations (2.19). This, in turn, leads to a further refinement of the singular solution.

Consider the system of characteristic equations (2.17). We recall that we have, in essence, already solved (2.17a,c), since equations (2.14)-(2.16) have the effect of specifying u and v as functions of ξ and η. It follows then, that we need only solve the remaining equations. Since we have already determined the form of the solution, we substitute (2.19) into (2.17b,d) to obtain

$$x_\xi + \lambda_- y_\xi = (X^1_\xi + \lambda_- Y^1_\xi) \ln (\xi-\xi_A) + \frac{X^1+\lambda_- Y^1}{\xi-\xi_A}$$

$$+(X^2_\xi+\lambda_- Y^2_\xi) \ln (\xi-\xi_B) + \frac{X^2+\lambda_- Y^2}{\xi-\xi_B} + X^3_\xi + \lambda_- Y^3_\xi = 0$$

on $\eta =$ constant, and

$$x_\eta + \lambda_+ y_\eta = (X^1_\eta + \lambda_+ Y^1_\eta) \ln (\xi-\xi_A) + (X^2_\eta+\lambda_+ Y^2_\eta) \ln (\xi-\xi_B)$$

$$+ X^3_\eta + \lambda_+ Y^3_\eta = 0$$

on $\xi =$ constant.

We can satisfy the first equation by setting

(2.21a) $$X^1_\xi + \lambda_- Y^1_\xi = 0$$

(2.21b) $$X^2_\xi + \lambda_- Y^2_\xi = 0$$

and

(2.21c) $$X^3_\xi + \lambda_- Y^3_\xi = \frac{X^1+\lambda_- Y^1}{\xi_A-\xi} + \frac{X^2+\lambda_- Y^2}{\xi_B-\xi}$$

on η = constant. Similarly, we can satisfy the second by requiring

(2.21d) $$X^1_\eta + \lambda_+ Y^1_\eta = 0$$

(2.21e) $$X^2_\eta + \lambda_+ Y^2_\eta = 0$$

and

(2.21f) $$X^3_\eta + \lambda_+ Y^3_\eta = 0$$

on ξ = constant. Finally, if X^3 and Y^3 are to be regular solutions of (2.21c), we must have

(2.22a) $$X^1 + \lambda_- Y^1 = 0$$

on $\xi = \xi_A$, and

(2.22b) $$X^2 + \lambda_- Y^2 = 0$$

on $\xi = \xi_B$. Clearly we can use the equations (2.21) to formulate an initial value problem for each of the three pairs of functions X^i, Y^i, $i = 1,2,3$ once we have specified appropriate initial data ([21], pp. 9-12).

To do that, we consider the two functions X^1 and Y^1 and their corresponding equations (2.21a,d). For a properly posed characteristic initial value problem, we must prescribe initial data on one characteristic from each family. We can construct the data to within an additive constant on the characteristic plane $\xi = \xi_A$ by integrating (2.21d) in that plane, subject to the condition (2.22a). Thus we have only to pose initial data on some η characteristic, say $\eta = \eta_A$. We will use the value $\eta_A = \bar{\xi}_A$ in hope of exploiting symmetry. Ideally, since we are only interested in those points for which $\eta = \bar{\xi}$, we would like the initial data on $\eta = \eta_A$ to satisfy

$$X^1(\xi,\eta_A) = X^1(\xi,\bar{\xi}_A) = \overline{X^1(\xi_A,\bar{\xi})}$$

and

$$Y^1(\xi,\eta_A) = Y^1(\xi,\bar{\xi}_A) = \overline{Y^1(\xi_A,\bar{\xi})} .$$

We could then use the Schwarz Reflection Principle to significantly reduce our computation. Unfortunately, this requires that $X^1(\xi_A,\bar{\xi}_A)$ and $Y^1(\xi_A,\bar{\xi}_A)$ be real, which, in general, they are not. To overcome this difficulty, we define two new functions $\hat{X}^1(\xi,\eta)$ and $\hat{Y}^1(\xi,\eta)$ by

$$X^1(\xi,\eta) = \hat{X}^1(\xi,\eta) + iX_A$$
$$Y^1(\xi,\eta) = \hat{Y}^1(\xi,\eta) + iY_A ,$$

where X_A and Y_A are real constants to be determined later, and $\hat{X}^1$ and $\hat{Y}^1$ have the desired symmetry properties in their initial data.

A similar procedure can be followed in posing the initial value problem for X^2 and Y^2 as solutions of (2.21b,e) with initial data prescribed on the characteristic planes $\xi = \xi_B$ and $\eta = \eta_B = \bar{\xi}_B$ in terms of the symmetric functions $\hat{X}^2(\xi,\eta)$ and $\hat{Y}^2(\xi,\eta)$ and the real constants X_B and Y_B.

For X^3 and Y^3, we choose yet another pair of characteristics, say $\xi = \xi_C$ and $\eta = \eta_C = \bar{\xi}_C$ which are far enough away from ξ_A and ξ_B, and η_A and η_B, respectively, to prevent computational error. The choice of initial data for this problem will be discussed later. We can assume $X^3(\xi_C,\bar{\xi}_C)$ and $Y^3(\xi_C,\bar{\xi}_C)$ to be real, since the expected solution uses only their real parts, and therefore assign symmetric initial data directly.

Thus we have a characteristic initial value problem in three parts:

(I) Find $\hat{X}^1(\xi,\eta)$ and $\hat{Y}^1(\xi,\eta)$ satisfying

$$\hat{X}^1_\xi + \lambda_- \hat{Y}^1_\xi = 0 \tag{2.23a}$$

on η = constant, and

$$\hat{X}^1_\eta + \lambda_+ \hat{Y}^1_\eta = 0 \tag{2.23b}$$

on ξ = constant, with initial data $\hat{X}^1(\xi_A,\eta)$ and $\hat{Y}^1(\xi_A,\eta)$ obtained, up to an additive real constant, by solving (2.23b) on $\xi = \xi_A$, subject to the condition

$$(\hat{X}^1 + iX_A) + \lambda_-(\hat{Y}^1 + iY_A) = 0 \ . \tag{2.23c}$$

The initial data on $\eta = \eta_A = \bar{\xi}_A$ are given by

(2.23d) $$\hat{X}^1(\xi,\eta_A) = \overline{\hat{X}^1(\xi_A,\bar{\xi})} \text{ ,}$$

and

(2.23e) $$\hat{Y}^1(\xi,\eta_A) = \overline{\hat{Y}^1(\xi_A,\bar{\xi})} \text{ .}$$

(II) Find $\hat{X}^2(\xi,\eta)$ and $\hat{Y}^2(\xi,\eta)$ satisfying

(2.23f) $$\hat{X}^2_\xi + \lambda_-\hat{Y}^2_\xi = 0$$

on η = constant, and

(2.23g) $$\hat{X}^2_\eta + \lambda_+\hat{Y}^2_\eta = 0$$

on ξ = constant, with initial data $\hat{X}^2(\xi_B,\eta)$ and $\hat{Y}^2(\xi_B,\eta)$ obtained, up to an additive real constant, by solving (2.23g) on $\xi = \xi_B$, subject to the condition

(2.23h) $$(\hat{X}^2+iX_B) + \lambda_-(\hat{Y}^2+iY_B) = 0 \text{ .}$$

The initial data on $\eta = \eta_B = \bar{\xi}_B$ are given by

(2.23i) $$\hat{X}^2(\xi,\eta_B) = \overline{\hat{X}^2(\xi_B,\bar{\xi})} \text{ ,}$$

and

(2.23j) $$\hat{Y}^2(\xi,\eta_B) = \overline{\hat{Y}^2(\xi_B,\bar{\xi})} \text{ .}$$

(III) Find $X^3(\xi,\eta)$ and $Y^3(\xi,\eta)$ satisfying

(2.23k) $$X^3_\xi + \lambda_-Y^3_\xi = \frac{X^1+\lambda_-Y^1}{\xi_A-\xi} + \frac{X^2+\lambda_-Y^2}{\xi_B-\xi}$$

on η = constant, and

(2.23ℓ) $$X^3_\eta + \lambda_+ Y^3_\eta = 0$$

on ξ = constant, with initial data $X^3(\xi_C,\eta)$ and $Y^3(\xi_C,\eta)$ obtained, up to an additive real constant, by solving (2.23ℓ) for Y^3 on $\xi = \xi_C$ where

(2.23m) $$X^3(\xi_C,\eta) = G(\eta) \ ,$$

and G is an as yet undetermined analytic function. For the initial data on $\eta = \eta_C = \bar{\xi}_C$, we set

(2.23n) $$X^3(\xi,\eta_C) = \overline{X^3(\xi_C,\bar{\xi})} \ ,$$

and

(2.23o) $$Y^3(\xi,\eta_C) = \overline{Y^3(\xi_C,\bar{\xi})} \ .$$

5. The Arbitrary Constants in the Singular Solution

In this section, we use previously specified properties of the solution to determine the unknown constants X_A , X_B , Y_A and Y_B , and, in the process, we explain the role they play in the geometry of a given cascade.

Consider a simple closed curve C having a counterclockwise orientation, which lies inside the body, contains the two points $(\xi_A, \bar{\xi}_A)$ and $(\xi_B, \bar{\xi}_B)$ in its interior, and is otherwise arbitrary (see Figure 7). The image of C in complex xy-space under the mapping given by the solution of our problem will be a closed curve in the real physical plane, say Γ, which contains a single blade in its interior. Note that the exterior of C will map onto the interior of Γ, and that Γ will have clockwise orientation.

Substituting $\hat{X}^1+iX_A$, $\hat{X}^2+iX_B$, $\hat{Y}^1+iY_A$, and $\hat{Y}^2+iY_B$ for X^1, X^2, Y^1 and Y^2 in (2.19), respectively, we can show that

$$\oint_\Gamma dx = 2\pi(X_A + X_B) \quad , \tag{2.24a}$$

and

$$\oint_\Gamma dy = 2\pi(Y_A + Y_B) \quad , \tag{2.24b}$$

which implies that

$$X_A + X_B = 0 \tag{2.25a}$$

and

$$Y_A + Y_B = 0 \quad , \tag{2.25b}$$

since we require the solution to be single-valued about such a curve.

Similarly, by requiring the stream function ψ to be single-valued on Γ, we get

$$(2.26)\quad \oint_{\Gamma} d\psi = \oint_{\Gamma} \rho u\, dy - \rho v\, dx = 2\pi\, [\rho_A u_A Y_A + \rho_B u_B Y_B - \rho_A v_A X_A - \rho_B v_B X_B] = 0,$$

which, using (2.25), implies that

$$(2.27)\quad [\rho_A u_A - \rho_B u_B] Y_A = (\rho_A v_A - \rho_B v_B) X_A ,$$

where we assume that ρ_A and ρ_B are already known in terms of the velocity components.

Observe that, had we chosen curves C_1 or C_2 (see figure) containing $(\xi_A, \bar{\xi}_A)$ alone or $(\xi_B, \bar{\xi}_B)$ alone in the interior, respectively, we would have obtained the curves Γ_1 or Γ_2 such that

$$(2.28a)\quad \oint_{\Gamma_1} dx = 2\pi\, X_A ,$$

$$(2.28b)\quad \oint_{\Gamma_1} dy = 2\pi\, Y_A ,$$

$$(2.28c)\quad \oint_{\Gamma_2} dx = 2\pi\, X_B = -2\pi\, X_A ,$$

and

$$(2.28d)\quad \oint_{\Gamma_2} dy = 2\pi\, Y_B = -2\pi\, Y_A .$$

Thus we see that integration along either of these curves increases the x coordinate by $\pm X_A$ and the y coordinate by $\pm Y_A$ which, in the physical plane, corresponds to jumping to another blade of the cascade (see Figure 5).

Based on the above discussion, we define the stagger angle β and gap g by

$$\beta = \tan^{-1} \frac{Y_A}{X_A} , \tag{2.29a}$$

and

$$g^2 = X_A^2 + Y_A^2 . \tag{2.29b}$$

Recall that for g to be a useful description of the blade separation, it must be normalized in such a way that it measures the distance between blades relative to some particular blade parameter, say the chord length. Unfortunately the blade itself and consequently its chord length is not known until after the computation is finished. Hence we use instead the relation

$$g = |\xi_A - \xi_B|^{-1} . \tag{2.30}$$

The reason for this somewhat imperfect choice is that, other parameters remaining constant as $\xi_A \to \xi_B$, our entire model will approach the airfoil case. Equation (2.30) is consistent with that occurrence in that it says the gap becomes infinite, i.e. we have a single blade.

If, in addition, we require $\beta = 90°$, which means that the blades are stacked vertically, we can use (2.29) and (2.30) to find X_A and Y_A , and, after prescribing three of the four inlet and exit velocity parameters, use (2.25) and (2.27) to determine all the remaining constants.

6. The Initial Data

In this section, we present the general form of the initial function and describe the procedure by which we determine its unknown constants.

Recall that the initial data for each of the functions $\hat{X}^1$, $\hat{Y}^1$, $\hat{X}^2$ and $\hat{Y}^2$ have already been determined to within an additive real constant in the previous two sections. It remains for us to prescribe an analytic function $G(\eta)$ to be used as initial data for $X^3(\xi_C,\eta)$ in the condition (2.23m). $Y^3(\xi_C,\eta)$ will then be found by integrating (2.23ℓ) and, since $\eta_C = \bar{\xi}_C$, $X^3(\xi,\eta_C)$ and $Y^3(\xi,\eta_C)$ will be determined by the symmetry conditions (2.23n,o).

Once we have determined G, we compute the solution and plot the streamline $\psi = 0$ in the physical plane. When ψ has been properly initialized, this curve will be the two dimensional cross section of a single turbine blade. Hence, we will refer to the streamline $\psi = 0$ in the physical plane, as well as in the $\xi = \bar{\eta}$ plane, as the body. All other blades in the cascade will, of course, have exactly the same shape. Observe that, as we have said before, the body will not, in general, look like a turbine blade. The basic plan then, is to pick $G(\eta)$ so that it does.

Theoretically, we have a considerable amount of freedom in our choice of initial function, since the only restriction on G is that it be analytic. In practice, however, we proceed in a way similar to that used in the airfoil case ([2], p. 19) and set

$$(2.31)\quad G(\eta) = \sum_{j=1}^{M} (A_{j1} + iA_{j2}) \ln (\eta - B_{j1} - iB_{j2}) + \sum_{j=M+1}^{N} (A_{j1} + iA_{j2}) \eta^j ,$$

where the $A_{j\ell}$ and $B_{j\ell}$, $\ell = 1,2$, are arbitrary constants. G will be completely determined when we have prescribed these 2N+2M real constants.

Note that once we have chosen the $B_{j\ell}$, G will have a logarithmic singularity at each of the points

$$\eta = B_{j1} + iB_{j2} ,$$

which of course lie outside the region of flow. These singularities, which play the role of sources and sinks in the initial plane $\xi = \xi_C$, are used, assuming the $A_{j\ell}$ to be small, to make local adjustments to the streamline representing the body. Our procedure will be to choose the $B_{j\ell}$ and then use physical constraints and automation paths, i.e. polygonal curves in the $\xi = \bar{\eta}$ plane along which we expect the body to pass, to determine the remaining constants in G. Both the $B_{j\ell}$ and the automation paths are chosen by a combination of past experience, and trial and error.

Our physical constraints fall into two categories: those which apply to the nose, and those which apply to the tail ([2], pp. 59-61).

(A) The Nose Constraints

Each blade will have a stagnation point near the leading edge which we call its nose (see Figure 5). The image of that point in the $\xi = \bar{\eta}$ plane will have coordinates $(\xi_N, \bar{\xi}_N)$, where ξ_N satisfies

$$C_i \xi_N^i = 0 . \tag{2.32}$$

This follows from equations (2.14,16) and the fact that h is zero when q is zero. Thus we see that we can determine ξ_N once the C_i are known, though we may still have to choose between several roots.

Since the body passes through the nose, we set

$$\psi^N = 0 ,$$

where the superscript N indicates that ψ is to be evaluated at $(\xi_N, \bar{\xi}_N)$. Initializing ψ in this way has the effect of choosing the streamline $\psi = 0$ as the body. The value of ψ at any other point will be found by integration.

The nose constraints arise from the fact that the values of x_u and x_v at the nose depend on R_C , the radius of curvature of the blade surface at the nose, and α, the angle between the inlet velocity vector and the direction of the central streamline at the nose. Indeed, it can be shown that

$$\left(\frac{\partial x}{\partial u}\right)^N = K^1(R_C, \alpha) \tag{2.33a}$$

$$\left(\frac{\partial x}{\partial v}\right)^N = K^2(R_C, \alpha) , \tag{2.33b}$$

where K^1 and K^2 are known functions. Clearly, then, these equations, which will be our nose constraints, can be introduced as a matter of convenience, making it possible to specify R_C and α as inputs.

(B) The Tail Constraints

Unlike that of the nose, $(\xi_T, \bar{\xi}_T)$, the image of the tail in the $\xi = \bar{\eta}$ plane, is not determined by equations (2.14), since the flow velocity at that point is not zero. Instead, ξ_T is specified as an input parameter of the program, and its final value is determined by trial and error. We remark that, assuming we have chosen a finite value of ξ_T which does in fact locate the tail, equations (2.14) imply that the tail velocity is finite also.

Our first constraint is that the body go through the tail, that is, that

$$\psi^T = 0 \ ,$$

where the superscript T indicates that ψ is to be evaluated at $(\xi_T, \bar{\xi}_T)$.

Second, so that we in fact have a tail, we require

$$\left(\frac{\partial z}{\partial \xi}\right)^T = 0 .$$

Since

$$\frac{\partial z}{\partial \xi} = \frac{\partial z}{\partial w} \frac{\partial w}{\partial \xi} \ ,$$

and

$$\frac{\partial z}{\partial w} = \frac{\partial x}{\partial u} + i \frac{\partial y}{\partial u} \ ,$$

we see that we will have achieved this result if

$$\left(\frac{\partial x}{\partial u}\right)^T = \left(\frac{\partial y}{\partial u}\right)^T = 0 .$$

Thus we have the three tail constraints

$$\psi^T = 0 \tag{2.34a}$$

$$\left(\frac{\partial x}{\partial u}\right)^T = 0 \tag{2.34b}$$

$$\left(\frac{\partial y}{\partial u}\right)^T = 0 . \tag{2.34c}$$

Conditions (2.34b,c) constitute our formulation of the Kutta condition.

(C) The Automation Paths

Finally, we can prescribe certain paths in the subsonic region of the $\xi = \bar{\eta}$ plane which we call automation paths, through which we want the body to pass ([2], pp. 36-39). Choosing a mesh along each path, we obtain the points $(\xi_k, \bar{\xi}_k)$, $k = 1,r$, at which we desire

$$\psi^k = \psi(\xi_k, \bar{\xi}_k) = 0 .$$

Although we will see below that it is usually impossible to satisfy this condition for every index k, we can still use it to justify a least square fit. In substance, choosing automation paths is a more convenient way of prescribing initial data than directly picking the remaining constants in G.

We now use the above three categories of constraints to determine the $A_{j\ell}$ in (2.31). We assume that the $B_{j\ell}$ have already been chosen.

Let $A_{11} = 1$ and set all the other $A_{j\ell} = 0$. Using this initial function, we determine a solution and its corresponding values $(\partial x_1/\partial v)^N$, $(\partial x_1/\partial u)^N$, $\psi_1{}^T$, $(\partial x_1/\partial u)^T$, $(\partial y_1/\partial u)^T$ and $\psi_1{}^k$, $k = 1,r$. Repeating this procedure for each $A_{j\ell}$, we obtain the values $(\partial x_i/\partial v)^N$, $(\partial x_i/\partial u)^N$, $\psi_i{}^T$, $(\partial x_i/\partial u)^T$, $(\partial y_i/\partial u)^T$ and $\psi_i{}^k$, $k = 1,r$, where $i = 1,n$ and $n = 2N$. But, by the principle of superposition, any linear combination of solutions will again be a solution. In fact, we assume that we have constructed such a solution using the as yet unknown constants c_i, i.e. for the solutions x_i, y_i, $i = 1,n$ we have

$$x = \sum_{i=1}^{n} c_i x_i$$

and

$$y = \sum_{i=1}^{n} c_i y_i \, .$$

Our nose and tail constraints then become:

$$\text{(2.35a)} \qquad \sum_{i=1}^{n} c_i \left(\frac{\partial x_i}{\partial u}\right)^N = K^1(R_C,\alpha)$$

$$\text{(2.35b)} \qquad \sum_{i=1}^{n} c_i \left(\frac{\partial x_i}{\partial v}\right)^N = K^2(R_C,\alpha)$$

$$\text{(2.35c)} \qquad \sum_{i=1}^{n} c_i \psi_i{}^T = 0$$

(2.35d) $$\sum_{i=1}^{n} c_i \left(\frac{\partial x_i}{\partial u}\right)^T = 0$$

(2.35e) $$\sum_{i=1}^{n} c_i \left(\frac{\partial y_i}{\partial u}\right)^T = 0 \ ,$$

to which we add the normalization,

(2.35f) $$\sum_{i=1}^{n} c_i = 1 \ .$$

We now introduce a change of interpretation, viz. we view (2.35) as a system of equations to be solved for the c_i. Obtaining them in this manner is equivalent to satisfying the constraints by a proper choice of the $A_{j\ell}$.

At this point, of course, since we have six equations in n unknowns, where six is, in general, less than n, our system is underdetermined. Ideally we would like to remedy the situation by adding the automation conditions

(2.36) $$\sum_{i=1}^{n} c_i \psi_i^k = 0 \ , \qquad k = 1,r \ .$$

Unfortunately, this would leave us with 6+r equations in n unknowns, and, since 6+r is usually greater than n, the system would be overdetermined. For this reason, we do not use (2.36), requiring instead that the body fit the automation paths in a least square sense, subject to the constraints expressed in (2.35).

Our final statement of this problem will be in matrix form. Let the equations (2.35) be written

$$BC = F \ ,$$

where C is the column vector containing the c_i , and B and F have been chosen accordingly. We then define

$$\|C\|_0 = \left\{ \sum_{i=1}^{n} \omega_i^2 c_i^2 \right\}^{1/2}$$

where the ω_i are suitably chosen weights, and we pick the matrix A so that we may write equation (2.36) in the form

$$AC = 0 \ .$$

Thus, we may restate the problem: Minimize the expression

$$\frac{1}{2} \left\{ x_r \|AC\|^2 + \|C\|_0^2 \right\}$$

subject to the constraint

$$BC = F \ .$$

Note that $\|AC\|$ refers to the Euclidean norm of that matrix, and that x_r is an input parameter which is used to weight the importance of the least square fit relative to minimizing the size of the c_i. For example, $x_r = 0$ tells the program to minimize the c_i without attempting any fit at all.

Using Lagrange multipliers, the problem reduces to solving the system

$$BC = F \ ,$$

$$(x_r A^T A + I_0)C + B^T \underset{\sim}{\lambda} = 0 \ ,$$

where

$$I_0 = \begin{pmatrix} \omega_1^2 & 0 & \cdots & 0 \\ 0 & \omega_1^2 & \ddots & \vdots \\ \vdots & & \ddots & 0 \\ 0 & \cdots & 0 & \omega_n^2 \end{pmatrix}$$

and $\underset{\sim}{\lambda}$ is the column vector of multipliers. Here, of course, A^T and B^T denote the respective matrix transposes.

3. THE COMPUTATION: A CONCEPTUAL OVERVIEW

In this chapter we give a descriptive account of the numerical method of solution, emphasizing the basic strategy of the computer program, as opposed to the details of its use.

1. The Basic Diagram

As a starting point for the discussion, we first take a preliminary look at a typical example of the graphic output of the program (see Figure 8).

Figure 8A contains the computed blade profile, indicating the characteristics (or Mach lines) of its supersonic zone, and showing above the Mach number distribution along the blade surface.

Figure 8B , though plotted on a single pair of coordinate axes, variously represents either the initial plane $\eta = \eta_c$, or the $\eta = \bar{\xi}$ plane, which we shall loosely refer to as the hodograph plane. This dual representation is accomplished in the following way: the position of a given point relative to the coordinate axes of the diagram determines its ξ coordinate. Its η coordinate is then given by $\eta = \eta_c$ or $\eta = \bar{\xi}$, depending on which plane is under discussion. The reader is forewarned that while some elements of the graph belong to the initial plane and some to the hodograph plane, there are elements that belong to both planes, depending on the interpretation. In fact, subject to proper interpretation, this figure depicts any plane in which η = constant.

The basic Figure 8B is composed of the following elements:

(i) The sonic line/locus

The curve C is defined to be the set of points at which

$$|C_i \xi^i| = |h(q) e^{-i\theta}| = h(c_*) \quad . \tag{3.1}$$

Note that in the hodograph plane,

$$\xi = \bar{\eta} \Rightarrow s = \overline{s^*} \Rightarrow h(q) \text{ is real.}$$

Thus, equations (2.14)-(2.16) and (3.1) imply that

$$q = c_* \ ,$$

i.e. the flow is exactly sonic; hence we call C the sonic line. Observe that though the sonic line contains the image of the real subsonic regime in its interior, the supersonic regime maps onto another surface entirely (see Section 3.4).

Suppose now we consider C to be a curve in the initial plane $\eta = \eta_c$, whose points, however, still satisfy (3.1). Here, of course, h(q) is complex. Nevertheless, the ξ = constant characteristic through each point of C terminates on the sonic line, i.e. the points of C in the $\eta = \eta_c$ plane are mapped into the sonic line by the characteristic curves. For this reason, we call it the upper sonic locus, the analogous curve on $\xi = \xi_A$ being called the lower sonic locus.

To sum up, the curve C is called the sonic line or the sonic locus, depending on whether we choose $\eta = \bar{\xi}$ or $\eta = \eta_c$.

(ii) The body

This pattern of points, indicated in Figure 8B, represents the $\psi = 0$ streamline in the hodograph plane. We remark in passing, that the subsonic region of flow, which is obviously outside the blade in the physical plane, maps onto the interior of the body image shown here.

(iii) Stagnation points and branch points

The stagnation points are the roots of

$$C_i \xi^i = 0. \tag{3.2}$$

The branch points are the roots of

$$\frac{d}{d\xi} (C_i \xi^i) = 0 . \tag{3.3}$$

Their significance will be discussed later.

(iv) The logarithmic singularities of the initial function

In Section 6, we saw that the initial function $G(\eta)$ has logarithmic singularities at

$$\eta = B_{j1} + iB_{j2} ,$$

(see equation (2.31)), or equivalently, that these points are the locations of the singularities of X^3 and Y^3 in the initial plane $\xi = \xi_c$. Also, by reflection, X^3 and Y^3 have similar singularities at

$$\xi = B_{j1} - iB_{j2} ,$$

in the $\eta = \eta_c = \bar{\xi}_c$ plane. In practice, we input the latter set of singularities, which are shown in the figure, and determine the former by reflection.

There are two basic types of integration paths:

(v) The subsonic paths

These paths are entirely contained inside the sonic line/locus and, aside from those used to search for the body, include

(a) the constraint paths - two paths which go to the nose and tail and are used to compute the respective constraint conditions (see Section 2.6)

(b) the automation paths - paths which indicate the expected location of the body in the hodograph plane (see Section 2.6).

(vi) The supersonic paths

These paths go from the initial ξ-characteristic to the image of the real supersonic regime in (ξ,η) space (see Section 3.4).

2. Subsonic Integration

For the moment, we turn out attention to the simple polygonal path outlined in dark ink in the subsonic region of Figure 8C. We will see how this curve is used to construct a path in the hodograph plane, along which we search for points of the body, or equivalently, zeros of the stream function.

As a first step, we consider this path to be in the initial plane $\eta = \eta_c$. It consists of line segments connecting the points ξ_A , ξ_B , ξ_C , ξ_D , ξ_E and ξ_F in that order. From this information, we can construct its conjugate path, viz. the path connecting η_A , η_B , η_C , η_D , η_E , and η_F , where each η is the complex conjugate of its corresponding ξ, and where we assume the path to be in the $\xi = \xi_c = \bar{\eta}_c$ initial plane. Now, we choose a net of points along each path,

$$\xi_A = \xi_1, \xi_2, \ldots, \xi_M = \xi_F ,$$

and

$$\eta_A = \eta_1, \eta_2, \ldots, \eta_M = \eta_F$$

where

$$\eta_i = \bar{\xi}_i , \qquad i = 1,2,\ldots,M.$$

If we consider all possible pairs of points in this mesh,

$$(\xi_i, \eta_j) , \qquad i,j = 1,2,\ldots,M,$$

we obtain the two-dimensional array of complex numbers outlined schematically in Figure 9.

It is on this grid that we solve (see next section for finite difference procedures) our threefold initial value problem numerically.

Clearly, we can use equations (2.23a-e) to generate initial data for $\hat{X}^1$ and $\hat{Y}^1$ on $\xi = \xi_A$ and $\eta = \eta_A$. Thus we know those functions up to an additive real constant in the first column and last row of the array. We then use equations (2.23a,b) to find their values at all the remaining points. A similar procedure works for $\hat{X}^2$ and $\hat{Y}^2$ in their region of definition, where we generate initial data on $\xi = \xi_B$ and $\eta = \eta_B$.

We now consider X^3 and Y^3 in the quadrant defined by their initial characteristics $\xi = \xi_C$ and $\eta = \eta_C$. Again, we know these functions in their initial planes, having already determined $G(\eta)$ (see equations (2.23k-o) and Section 2.6). Since we already know $\hat{X}^i$ and $\hat{Y}^i$, $i = 1,2,$ everywhere, it follows that we also know X^1, Y^1, X^2 and Y^2 everywhere, and can solve the inhomogeneous equations (2.23k,l) for X^3 and Y^3 over the entire grid. Thus we see that we can determine the unknown functions at every point of the grid for which they are defined. Once this is done, all other functions, e.g. ψ, ρ, etc. can be determined also.

Consider now the diagonal entries of the array. Since the paths are conjugate, we have

$$(\xi_i, \eta_i) = (\xi_i, \bar{\xi}_i) , \qquad i = 1,2,\ldots,M,$$

i.e. each point on the diagonal is in the real hodograph plane.

Hence, for each pair of conjugate initial paths, we obtain a solution along a single path in the real hodograph. Any stream function zeros on the diagonal will map into the body in the real physical plane. Of course, choosing good integration paths (e.g. paths which intersect the body) is the task of the user, and, in the case of automation paths, requires some skill.

In addition, we point out that we can eliminate all our computation below the diagonal, since e.g.

$$\hat{X}^1(\xi_i,\eta_j) = \overline{\hat{X}^1(\bar{\xi}_i,\bar{\eta}_j)} = \overline{\hat{X}^1(\eta_i,\xi_j)} \ .$$

Similar symmetry conditions for the other functions allow us to reduce the amount of calculation by almost a half.

We remark that, except in the case of the constraint and automation paths, we usually prescribe integration paths as a fork with many stems (see Figure 8B). This allows us to pick up more than one body point in a region without having to repeat the entire integration.

3. The Finite Difference Scheme

Consider the grid of an arbitrary path (see Figure 10) in which we have used the shorthand notation

$$P_{ij} = (\xi_i, \eta_j) \ .$$

We assume that values for $\hat{X}^1$ and $\hat{Y}^1$ at P_{11} have been prescribed, and will see how the program determines these functions at other points of the grid.

First, we need to know $\hat{X}^1$ and $\hat{Y}^1$ on their initial ξ-plane, where $\eta = \eta_j$, $j = 1,2,\ldots,M$, i.e. we wish to solve equation (2.23b), subject to the condition (2.23c), where all functions are to be evaluated on $\xi = \xi_A$ (see Section 2.4). To do this, we proceed point by point up the first column of the grid.

As an example, consider the point P_{12}. We already know the solution at P_{11} , and assume the approximations

$$\hat{X}^1_\eta = \frac{\hat{X}^1(P_{12})-\hat{X}^1(P_{11})}{\eta_2 - \eta_1} \ ,$$

and

$$\hat{Y}^1_\eta = \frac{\hat{Y}^1(P_{12})-\hat{Y}^1(P_{11})}{\eta_2 - \eta_1} \ .$$

Substituting in (2.23b), we get

$$\frac{\hat{X}^1(P_{12})-\hat{X}^1(P_{11})}{\eta_2 - \eta_1} + \lambda_+^*\left(\frac{\hat{Y}^1(P_{12})-\hat{Y}^1(P_{11})}{\eta_2 - \eta_1}\right) = 0 \ ,$$

which becomes our first difference equation

(3.4a) $\hat{X}^1(P_{12})-\hat{X}^1(P_{11}) + \lambda_+^*\left(\hat{Y}^1(P_{12})-\hat{Y}^1(P_{11})\right) = 0$.

Here, we have used

$$\lambda_+^* = \frac{\lambda_+(P_{11})+\lambda_+(P_{12})}{2} ,$$

where we determine both $\lambda_\pm(P_{12})$ in the following way. Clearly,

$$h(q(P_{12}))e^{-i\theta(P_{12})} = C_i\xi_1^i ,$$

and

$$h(q(P_{12}))e^{i\theta(P_{12})} = \bar{C}_i\eta_2^i ,$$

implying that

$$h^2(q(P_{12})) = [C_i\xi_1^i][\bar{C}_i\eta_2^i] ,$$

which we invert numerically to find $q(P_{12})$. Similarly, we obtain $\theta(P_{12})$ by solving

$$e^{2i\theta(P_{12})} = \frac{\bar{C}_i\eta_2^i}{C_i\xi_1^i}$$

to get

$$\theta(P_{12}) = \frac{1}{2i}\ln\left[\frac{\bar{C}_i\eta_2^i}{C_i\xi_1^i}\right] .$$

Knowing $q(P_{12})$ and $\theta(P_{12})$, we can find $c(P_{12})$, $u(P_{12})$, and $v(P_{12})$ by way of the standard equations of fluid dynamics, e.g. Bernoulli's law, etc. We then determine $\lambda_\pm(P_{12})$ by substitution into equation (1.15).

We get our second equation by evaluating (2.23c) at P_{12}, which yields

$$(3.4b)\quad \hat{X}^1(P_{12}) + iX_A + \lambda_-(P_{12})[\hat{Y}^1(P_{12}) + iY_A] = 0$$

where X_A, $\lambda_-(P_{12})$ and Y_A are already known.

We can now solve the system (3.4) for $\hat{X}^1(P_{12})$ and $\hat{Y}^1(P_{12})$. In fact, if we continue this procedure, we can determine both functions along the entire path. Thus we have completely determined the initial data for these functions, since we know their values on $\eta = \eta_A$ by reflection.

Let us now consider the interior points of the grid. In general, we determine our solution point by point, going from left to right in each row, starting with the bottom row and working toward the top. For example.

$$P_{11}, P_{12}, P_{22}, P_{13}, P_{23}, P_{33}, P_{14}, P_{24}, P_{34}, P_{44}, P_{15}, \ldots$$

is a typical ordering; note that we stop each row at the diagonal, since the remaining points are known by symmetry (see previous section).

Suppose now, that we know our solution at $P_{i-1,j}$ and wish to find it at P_{ij}. Presumably, we have already computed row j-1 and consequently have values for $P_{i,j-1}$, as indicated in Figure 11.

In principle, we can use equations (2.14)-(2.16) in the same way as we did for the initial data. Unfortunately, this requires the numerical inversion of h(q), which is very time consuming. Instead we find u and v by solving equations (2.17a,c) numerically. We are able to do this, because we have already determined their values on the initial planes by the previous computation.

To be more specific, we wish to solve the following system:

(3.5a) $$v_\xi - \lambda_+ u_\xi = 0$$

(3.5b) $$\hat{X}^1_\xi + \lambda_- \hat{Y}^1_\xi = 0 ,$$

on η = constant, and

(3.5c) $$v_\eta - \lambda_- u_\eta = 0$$

(3.5d) $$\hat{X}^1_\eta + \lambda_+ \hat{Y}^1_\eta = 0 ,$$

on ξ = constant (see Section 2.4), for $u(P_{ij})$, $v(P_{ij})$, $\lambda_\pm(P_{ij})$, $\hat{X}^1(P_{ij})$ and $\hat{Y}^1(P_{ij})$.

We will determine $u(P_{ij})$ and $v(P_{ij})$, and therefore $\lambda_\pm(P_{ij})$, by use of a predictor corrector scheme. Using equations (3.5a,c), we construct the difference equations

(3.6a) $$\hat{v}(P_{ij}) - v(P_{i-1,j}) = \lambda_+(P_{i-1,j})[\hat{u}(P_{ij}) - u(P_{i-1,j})] ,$$

and

(3.6b) $$\hat{v}(P_{ij}) - v(P_{i,j-1}) = \lambda_-(P_{i,j-1})[\hat{u}(P_{ij}) - u(P_{i,j-1})] ,$$

which we solve for the unknowns $\hat{u}(P_{ij})$ and $\hat{v}(P_{ij})$. Observe that since we do not yet know $\lambda_\pm(P_{ij})$, we have had to use $\lambda_+(P_{i-1,j})$ and $\lambda_-(P_{i,j-1})$ which implies that $\hat{u}$ and $\hat{v}$ approximate u and v to first order accuracy. We next compute $\hat{\lambda}_\pm(P_{ij})$, based on $\hat{u}(P_{ij})$ and $\hat{v}(P_{ij})$, and use them in (3.6) to get the corrected system

$$(3.7a)\quad v(P_{ij}) - v(P_{i-1,j}) = \tilde{\lambda}_+[u(P_{ij}) - u(P_{i-1,j})] \ ,$$

$$(3.7b)\quad v(P_{ij}) - v(P_{i,j-1}) = \tilde{\lambda}_-[u(P_{ij}) - u(P_{i,j-1})] \ ,$$

where

$$\tilde{\lambda}_+ = \frac{\hat{\lambda}_+(P_{ij}) + \lambda_+(P_{i-1,j})}{2}$$

and

$$\tilde{\lambda}_- = \frac{\hat{\lambda}_-(P_{ij}) + \lambda_-(P_{i,j-1})}{2} \ .$$

After solving the system (3.7) for $u(P_{ij})$ and $v(P_{ij})$ and then making a final determination of $\lambda_\pm(P_{ij})$, we can solve the difference equations which result from equations (3.5b,d),

$$(3.8a)\quad \hat{X}^1(P_{ij}) - \hat{X}^1(P_{i-1,j}) + \left[\frac{\lambda_-(P_{ij}) + \lambda_-(P_{i-1,j})}{2}\right][\hat{Y}^1(P_{ij}) - \hat{Y}^1(P_{i-1,j})] = 0$$

and

$$(3.8b)\quad \hat{X}^1(P_{ij}) - \hat{X}^1(P_{i,j-1}) + \left[\frac{\lambda_+(P_{ij}) + \lambda_+(P_{i,j-1})}{2}\right][\hat{Y}^1(P_{ij}) - \hat{Y}^1(P_{i,j-1})] = 0,$$

to get $\hat{X}^1(P_{ij})$ and $\hat{Y}^1(P_{ij})$.

We state for once and for all that this is the method used to find $\hat{X}^1$, $\hat{Y}^1$, $\hat{X}^2$, $\hat{Y}^2$ and, with slight modification, X^3 and Y^3 at all points of the grid for which they are defined. It will always be successful, except in regions where the system is ill-conditioned, i.e. when

$$\begin{vmatrix} 1 & \lambda_- \\ 1 & \lambda_+ \end{vmatrix} = \lambda_+ - \lambda_- = 0 \ , \qquad \Rightarrow q = c \ .$$

Thus our scheme will break down near the sonic line.

4. Calculating the Flow in the Supersonic Region

In this section we explain the basic reasoning behind our choice of supersonic paths.

The essential difficulty with the calculation in the supersonic region is that although we want our integration paths to start at $\xi_A, \xi_B, \xi_C, \eta_A, \eta_B$, and η_C, in keeping with our choice of initial characteristics, we must avoid all points of (ξ,η) space at which

$$\lambda_+ = \lambda_- ,$$

since our difference equations will be ill-conditioned there, and the procedure will break down.

To begin with, we consider the geometry of the complex four-space (ξ,η) (see [30] for a more detailed account). We first observe that there is a two dimensional set of points which we shall call the complex sonic surface, whereon

$$q^2 - c^2 = 0$$

(q and c complex). This surface intersects the $\xi = \bar{\eta}$ plane along the sonic line, whose interior, we recall, maps into the region of subsonic flow in the physical plane. Observe that the real supersonic regime in (ξ,η) space, though attached to the $\xi = \bar{\eta}$ plane along a portion of the sonic line, which we shall call the real sonic segment, is not contained in that plane, since for $q > c$, $h(q)$ is complex, and hence

$$s = h(q)e^{-i\theta} \neq \overline{h(q)}e^{-i\theta} = \overline{h(q)e^{i\theta}} = \overline{s^*} ,$$

which implies that

$$\xi \neq \bar{\eta} .$$

In fact, standard theory shows ([9], pp. 526-535) that the characteristics in the supersonic regime are real, and all terminate on the sonic line.

The specific task at hand, then, is to construct integration paths which will enable us to compute the solution at points in the supersonic region. Put another way, we want to choose integration paths which start in the subsonic region of the $\xi = \bar{\eta}$ plane, and twist around the complex sonic surface to get to points corresponding to the real supersonic region.

To do this, we use the sonic loci. In the $\eta = \eta_A$ plane, there is a segment of the (upper) sonic locus whose points are connected to the real sonic segment of the $\xi = \bar{\eta}$ plane by ξ characteristics. Let us connect this segment to the initial characteristics by a path P_u (see Figure 12A), choosing a net of points

$$\xi_1, \xi_2, \xi_3, \ldots, \xi_k, \xi_{k+1}, \xi_{k+2}, \ldots, \xi_N ,$$

where ξ_i , $i \geq k$, are points along the sonic locus. The same situation occurs in the $\xi = \xi_A$ plane, where we choose a path P_L (see Figure 12B) and net

$$\eta_1, \eta_2, \ldots, \eta_j, \eta_{j+1}, \eta_{j+2}, \ldots, \eta_M ,$$

subject to the following restrictions:

(i) we require that for every ξ-characteristic passing through P_u and η-characteristic passing through P_L, we have

$$(3.9) \qquad \lambda_+(\xi,\eta) \neq \lambda_-(\xi,\eta) .$$

Thus, we will have avoided the complex sonic surface, and our numerical procedure will work up to the sonic segment.

(ii) we require that $\eta_j, \eta_{j+1}, \ldots, \eta_M$ be conjugate points of $\xi_k, \xi_{k+1}, \ldots, \xi_N$ in reverse order, i.e.

$$(3.10) \qquad \eta_j = \bar{\xi}_N \ , \ \eta_{j+1} = \bar{\xi}_{N-1}, \ \ldots, \ \eta_M = \bar{\xi}_1 \ ,$$

where we have assumed that each net has the same number of points on the sonic locus, or rather, that

$$N-k+1 = M-j+1 .$$

We can best understand these restrictions by looking at the resultant grid (see Figure 13).

We first remark that the circled diagonal points in the diagram are in the $\eta = \bar{\xi}$ plane, by relation (3.10) and further, because of the position of their preimages on the sonic loci, that they are points on the real sonic segment. Second, we state that our numerical method of solution (see previous section) works here, since (3.9) holds everywhere, up to the diagonal. Of course, we cannot go beyond the diagonal, since

$$\lambda_+ = \lambda_-$$

there. Observe, also, that since our paths are asymmetric, we no longer obtain real subsonic points on the main diagonal.

We now come to the entire point of this procedure, which is that the triangular submatrix of points beneath the diagonal (see the figure) belongs to the real supersonic regime. We recall that the surface in four-dimensional space which corresponds to the real supersonic domain, is attached to the $\eta = \bar{\xi}$ plane along the sonic line, and further, that it is swept out by characteristics which terminate at the real sonic segment. Thus, we might expect that $\xi_k, \ldots, \xi_N$ and $\eta_j, \eta_{j+1}, \ldots, \eta_M$ together sweep out the desired region, or, put another way, that the points under discussion yield solution values in the supersonic regime.

We note that the preimage of the real sonic segment is best located by observing the pattern of body points in the subsonic region after the blade has begun to take shape.

5. Using the Existing Method

In this section, we discuss attempts at using the direct analogue of the airfoil program in the design of compressor and turbine blades.

(A) A Compressor Blade

Dr. D. Korn's first attempt was relatively successful. The blade in Figure 8A,B is closed and of a reasonable shape, though it has a high gap-to-chord ratio and may suffer from boundary layer separation. Subsequent blades have been designed, and are undergoing wind tunnel testing now.

It should also be noted that this result was obtained by using

$$s = 1 - 2B\xi - \xi^2$$

and

$$s^* = 1 - 2\bar{B}\eta - \eta^2$$

for equations (2.16), where the imaginary part of B controls the lift ([2], p. 69). This results, of course, in a ξ-plane configuration quite similar to that of an airfoil.

(B) An Unsuccessful Turbine Blade

The method failed in the turbine case (Fig. 14). This was not totally unexpected, since the blade was of such high camber and large thickness as to be unlike anything done before.

The choice of constants in equations (2.16) was, here and in the successful configuration, essentially determined by prescribing the graph elements (see Section 4.4), e.g. the locations of the nose, the branch points, etc.

Although the placement of a branch point at (1,0) seemed successful in magnifying the region near ξ_A to allow more room for the placement of automation paths between it and the sonic locus, we were still unable to produce a closed blade. It appeared that the lower surface had an unnecessarily high curvature, which caused it to cross the upper surface. Obviously, this case was physically unreasonable.

Based on the airfoil experience and hundreds of runs, it had become clear that the method failed in the case of extremely thick and highly cambered blades.

4. A FURTHER REFINEMENT OF THE CHARACTERISTIC TRANSFORMATION

In this chapter, we return to equations (2.16) of Section 2.2, which, we recall, were arrived at by mapping flow about the unit circle onto its interior. Here, we derive a new expression for the complex velocity by instead mapping the flow about a Joukowski blade onto the interior of the unit circle. Using this result as a basis, we modify the configuration, or equivalently, choose new constants in (2.16) and obtain a turbine blade.

1. The Joukowski Mapping

This section shows how the desired physical properties of the flow (blade thickness, camber, and velocity at infinity) are used to determine a specific Joukowski mapping.

By means of the transformation ([24], pp. 194,195)

$$z = \frac{1}{2}\left(\zeta + \frac{1}{\zeta}\right) , \tag{4.1}$$

a pair of circles tangent at $\zeta = 1$ (see Figure 15) are mapped into the z plane (see Figure 17) in such a way that the circle $\gamma_A = \{\zeta: \zeta = t_0 + ae^{i\theta}, 0 \leq \theta < 2\pi\}$ is mapped onto the circular arc C_A, and circle $\gamma_B = \{\zeta: \zeta = \zeta_0 + be^{i\theta}, 0 \leq \theta < 2\pi\}$ is mapped onto the Joukowski profile C_B.

For a flow about C_B with circulation Γ and complex velocity U at infinity, the complex potential is given by

$$X(\zeta) = U(\zeta - \zeta_0) + \bar{U}\left(\frac{b^2}{\zeta-\zeta_0}\right) + \frac{i\Gamma}{2\pi} \ln \left(\frac{\zeta-\zeta_0}{b}\right) . \tag{4.2}$$

Using (4.1) and (4.2), we get the complex velocity,

$$w(\zeta) = \frac{d\chi}{dz} = \frac{d\chi}{d\zeta}\,\frac{d\zeta}{dz} = \left[U - \frac{\bar{U}b^2}{(\zeta-\zeta_0)^2} + \frac{i\Gamma}{2\pi(\zeta-\zeta_0)}\right]\frac{2\zeta^2}{(\zeta^2-1)}$$

$$= \frac{[2\pi U(\zeta-\zeta_0)^2 + i\Gamma(\zeta-\zeta_0) - 2\pi\bar{U}b^2]\zeta^2}{\pi(\zeta^2-1)(\zeta-\zeta_0)^2} \; .$$

In addition, the Kutta condition for a cusped tail requires that $\zeta = 1$ be a root of the numerator, so that

$$w(\zeta) = \frac{2\zeta^2[U(\zeta-\zeta_0) + \bar{U}(1-\bar{\zeta}_0)]}{(\zeta+1)(\zeta-\zeta_0)^2} \; , \tag{4.3}$$

and

$$\Gamma = 4\pi[u_0\beta_0 + (1-\alpha_0)v_0] \; , \tag{4.4}$$

where we have set $\zeta_0 = \alpha_0 + i\beta_0$ and $U = u_0 - iv_0$.

The flow will be completely determined by equations (4.1)-(4.4) once we have properly chosen the as yet undetermined constants. In practice we specify the velocity at infinity U, the velocity angle at the tail θ_T, and a thickness parameter t, which are then used to determine t_0, a, ζ_0, and b. Because of the symmetry of the circular arc, θ_T is essentially the blade camber. In the following, we assume that U and θ_T are given.

The complex velocity at the tail, $w_T = u_T - iv_T$ is given by

$$w_T = w(1) = \frac{2\,\mathrm{Re}\,(\bar{U}(1-\zeta_0))}{(1-\zeta_0)^2} \; ,$$

so that

$$\tan\theta_T = \frac{v_T}{u_T} = \frac{-\,\mathrm{Im}\,[(1-\bar{\zeta}_0)^2]}{\mathrm{Re}\,[(1-\bar{\zeta}_0)^2]} = \frac{2\beta_0(\alpha_0-1)}{(1-\alpha_0)^2-\beta_0^2} \; .$$

Solving for β_0, we get

$$\beta_0 = (1-\alpha_0)\left(\frac{\cos\theta_T \pm 1}{\sin\theta_T}\right) .$$

These two equations define a pair of straight lines in the ζ-plane along which ζ_0 must be chosen to get the desired θ_T. In our configuration we have assumed $\theta_T < 0$, $\alpha_0 < 0$, and $\beta_0 > 0$ which requires the choice of the minus sign in the above (see line ℓ in Figure 16). The location of ζ_0 on this line will be determined by the thickness parameter t.

Next, we determine t_0 and a, the center and radius, respectively, of γ_A. Since γ_A is tangent to γ_β at $\zeta = 1$, and since γ_A also passes through $\zeta = -1$, it is clear that t_0 must be at the intersection of line ℓ and the imaginary axis. Hence,

$$t_0 = \left(\frac{\cos\theta_T - 1}{\sin\theta_T}\right)i$$

and

$$a = |1-t_0| = \frac{\sqrt{2(1-\cos\theta_T)}}{|\sin\theta_T|} .$$

We now define the thickness parameter t as

$$t = b - a > 0 ,$$

which is the distance of ζ_0 from t_0 along ℓ. If t=0, i.e. we have the case of zero thickness, $\gamma_A = \gamma_B$ and the profile coincides with the circular arc. As t increases, the body will thicken about the arc.

Using the above equations, we can now generate Joukowski profiles by specifying U, θ_T and t.

2. Mapping the Flow onto the Interior of the Unit Circle

In this section we map the flow in the ζ-plane onto the interior of the unit circle in the ξ-plane, thus determining the functions $z(\xi)$ and $w(\xi)$.

This is accomplished by means of the transformation

$$\xi = \frac{b}{\zeta - \zeta_0}\,, \tag{4.5}$$

or, solving for ζ,

$$\zeta = \zeta_0 + \frac{b}{\xi}\,. \tag{4.6}$$

Substituting (4.6) in equations (4.1) and (4.3), we get

$$z(\xi) = \frac{1}{2}\left\{\zeta_0 + \frac{b}{\xi} + \frac{\xi}{b+\xi\zeta_0}\right\} \tag{4.7}$$

and

$$w(\xi) = \frac{2(b+\xi\zeta_0)^2[\xi\bar{U}(1-\bar{\zeta}_0)+Ub]}{[\xi(1+\zeta_0) + b]b^2}\,. \tag{4.8}$$

Clearly then, w is a rational function of ξ which, in addition to its branch points, has

(1) a pole at

$$\xi = \frac{-b}{1+\zeta_0}\,,$$

(2) a zero at

$$\xi = \frac{Ub}{\bar{U}(\bar{\zeta}_0-1)}\,,$$

which corresponds to the nose of the blade, and

(3) a double zero at

$$\xi = \frac{-b}{\zeta_0}\,.$$

The new elements introduced here are the pole and the double zero. The Joukowski transformation suggests that the location of the pole is primarily determined by the thickness of the blade, whereas the position of the double zero is primarily determined by the camber (see Section 3).

3. Modifying the Configuration

In this section we see how the physical characteristics of the Joukowski blade affect the configuration in the ξ-plane, viz. the location of the pole, double zero, and branch points of w.

The three parameters of interest are: (a) the thickness of the blade, (b) its camber, and (c) the angle of the flow at infinity, which respectively correspond to t, θ_T and U of Section 1. Note that, in the following figures, an additional rotation has been introduced so that the nose is always located at -1.

(a) Blade thickness (Figure 18)

Here we vary t while keeping θ_T and U constant.

As can be seen in the figure, the blade becomes thicker as t increases, and the pole moves away from the nose. The double zero is off the page and relatively unimportant.

(b) Blade camber (Figure 19)

Here we vary θ_T while keeping t and U constant.

As θ_T increases negatively, the blade camber increases, the pole approaches the nose, and the double zero comes into view.

(c) Angle of the flow at infinity (Figure 20)

We fix t, θ_T , and $|U| = 1$, while varying the argument of U.

This in no way changes the shape or size of the body in the z-plane, but dramatically affects the imaginary coordinate of the pole, as well as the relative positions of the branch points.

Our procedure then is to use the Joukowski blade to get a preliminary estimate for the configuration, and then to vary the locations in accordance with our design goals.

4. Conclusion: A Turbine Blade

In Figure 21, we exhibit a turbine blade. Observe that, as a result of our particular choices for the constants in equations (2.16), the configuration, especially the sonic line (or locus), is quite different. Furthermore, it happened that, rather than choose the C_i directly, it was easier to determine them by prescribing certain basic elements of the transformation.

In this case, we assumed the equations to be of the fourth degree, which meant that we could satisfy five conditions in the ξ-plane (Figure 21B).

(1) We put the leading edge stagnation point, the nose, at -1+0i, i.e. we required

$$C_i \xi_N^i = 0 \tag{4.9a}$$

where

$$\xi_N = -1+0i.$$

(2) We placed a branch point at $\xi_{BP} = 1+0i$ to make room between the body and the sonic line, i.e. we required

$$\frac{d}{d\xi}\left(C_i \xi^i\right)\Big|_{\xi=\xi_{BP}} = 0 . \tag{4.9b}$$

(3) Further, we specified the velocity at that point (a Mach number of .9 and a flow angle of 148.93 degrees), which led to a second equation,

(4.9c) $$C_i \xi_{BP}^i = h(q_{BP})\, e^{-i\theta_{BP}} .$$

(4) Finally, we required a double zero, as dictated by the Joukowski transformation, which we placed at

$$\xi_D = -.35 + 1.4i .$$

This led to the two equations,

(4.9d) $$C_i \xi_D^i = 0 ,$$

and

(4.9e) $$\frac{d}{d\xi} (C_i \xi^i) \Big|_{\xi=\xi_D} = 0 .$$

The last requirement is, of course, the essence of this work. Note that ξ_D is in the same general area as in the incompressible case (Figure 19D).

We remark that, having determined the C_i by the five equations (4.9), the locations of ξ_A and ξ_B were found as a consequence of the prescribed inlet and exit velocities.

Thus, though the pressure distribution along the blade indicates probable boundary layer separation, it is clear that the method works, i.e. we can design highly cambered blades of large thickness. It is hoped that a physically practical blade will be designed and tested in the near future.

Bibliography

[1] Bauer, F., Garabedian, P., Jameson, A., and Korn, D., Supercritical Wing Sections II, A Handbook, Lecture Notes in Economics and Mathematical Systems, Vol. 108, Springer-Verlag, New York, 1975.

[2] Bauer, F., Garabedian, P., and Korn, D., Supercritical Wing Sections, Lecture Notes in Economics and Mathematical Systems, Vol. 66, Springer-Verlag, New York, 1972.

[3] Bergman, S., Integral Operators in the Theory of Linear Partial Differential Equations, Springer-Verlag, New York, 1969.

[4] Bers, L., Mathematical Aspects of Subsonic and Transonic Gas Dynamics, John Wiley and Sons, Inc., New York, 1958.

[5] Casamassa, J., and Bent, R., Jet Aircraft Power Systems, McGraw-Hill, New York, 2 ed., 1957.

[6] Chaplygin, S., On Gas Jets, Scientific Annals of the Imperial University of Moscow, Physico-Mathematical Division, Pub. No. 21, Moscow, 1904.

[7] Courant, R., and Friedrichs, K. O., Supersonic Flow and Shock Waves, Interscience-Wiley, New York, 1948.

[8] Forsythe, G., and Wasow, W., Finite Difference Methods for Partial Differential Equations, Wiley, New York, 1960.

[9] Garabedian, P., Partial Differential Equations, Wiley, New York, 1964.

[10] Garabedian, P., and Korn, D., "Numerical Design of Transonic Airfoils," Numerical Solution of Partial Differential Equations, II, ed. by B. Hubbard, Academic Press, New York, 1971, pp. 253-271.

[11] Garabedian, P., and Lieberstein, H., "On the Numerical Calculation of Detached Bow Shocks in Hypersonic Flow," J. Aero. Sci., Vol. 25, pp. 109-118 (1958).

[12] Graham, L., Jones, R., and Boltz, F., "An Experimental Investigation of Three Oblique-Wing and Body Combinations at Mach Numbers between 0.60 and 1.40," NASA TM X-62, 256, Ames Research Center, 1973.

[13] Johnson, I., and Bullock, R., eds. Aerodynamic Design of Axial Flow Compressors, Revised National Aeronautics and Space Administration, Washington, D. C., 1965 (NASA SP-36).

[14] Judge, A., Gas Turbines for Aircraft, Macmillan, New York, 1959.

[15] Kacprzynski, J., "A Second Series of Wind Tunnel Tests of the Shockless Lifting Airfoil, No. 1," Project Report 5x5/0063, National Research Council of Canada, Ottawa, 1972.

[16] Kacprzynski, J., "Wind Tunnel Test of a Shockless Lifting Airfoil, No. 2," Lab. Tech. Rep. LTR-HA-5x5/0067, Natl. Res. Council of Canada, Ottawa, 1973.

[17] Kacprzynski, J., Ohman, L., Garabedian, P., and Korn, D., "Analysis of the Flow Past a Shockless Lifting Airfoil in Design and Off-Design Conditions," Aeronautics Report LR-554, National Research Council of Canada, Ottawa, 1971.

[18] Keenan, J., Elementary Theory of Gas Turbines and Jet Propulsion, 1946.

[19] Koppe, E., and Meier, G., "Erfahrungen mit optischen Methoden bei der Untersuchung transsonischer Strömungen," Zeit. Flugwissenschaften, Vol. 13, pp. 143-157 (1965).

[20] Korn, D., Computation of Shock-Free Transonic Flows for Airfoil Design, Report NYU-NYO-1480-125 (1969).

[21] Korn, D., Numerical Design of Transonic Cascades, ERDA Research and Development Report, Mathematics and Computers, January 1975, No. COO-3077-72.

[22] Korn, D., "Transonic Design in Two Dimensions," Lecture Notes in Economics and Mathematical Systems, Vol. 430, Springer-Verlag, New York, 1975.

[23] Lighthill, M., "The Hodograph Transformation in Transonic Flow, II and III," Proc. Roy. Soc. London, Vol. A191, pp. 341-369 (1949).

[24] Markushevich, A., Theory of Functions of a Complex Variable, Volume II, Trans. R. Silverman, Prentice-Hall, Englewood Cliffs, N. J., 1965.

[25] Morawetz, C., "Non-Existence of Transonic Flow Past a Profile," Comm. Pure Appl. Math., Vol. 17, pp. 357-367 (1964).

[26] Nieuwland, G., "Transonic potential flow around a family of quasi-elliptical airfoil sections," N.L.R. Report TR.T172 (1967).

[27] Pearcey, H., "The Aerodynamic Design of Section Shapes for Swept Wings," Advan. Aero. Sci., Vol. 3, 1962.

[28] Sears, W., General Theory of High-Speed Aerodynamics, Princeton University Press, Princeton, 1954.

[29] Spee, B., and Uijlenhoet, R., "Experimental Verification of Shock-Free Transonic Flow around Quasi-Elliptical Airfoil Sections," N.L.R. Report, MP 68003 U (1969).

[30] Swenson, E., "Geometry of the Complex Characteristics in Transonic Flow," Comm. Pure Appl. Math., Vol. 21, pp. 175-185 (1968).

[31] Swenson, E., "Numerical Computation of Hypersonic Flow Past a Two-Dimensional Blunt Body," Courant Inst. Math. Sci., New York Univ., Report NYO-1480-1 (1964).

[32] Whitcomb, R., "Review of NASA Supercritical Airfoil," Ninth International Congress on Aeronautical Sciences, Haifa, Israel, 1974.

[33] Whitcomb, R., "The Upside Down Wing," Science News Item in Time Magazine, February 21, 1969, p. 66.

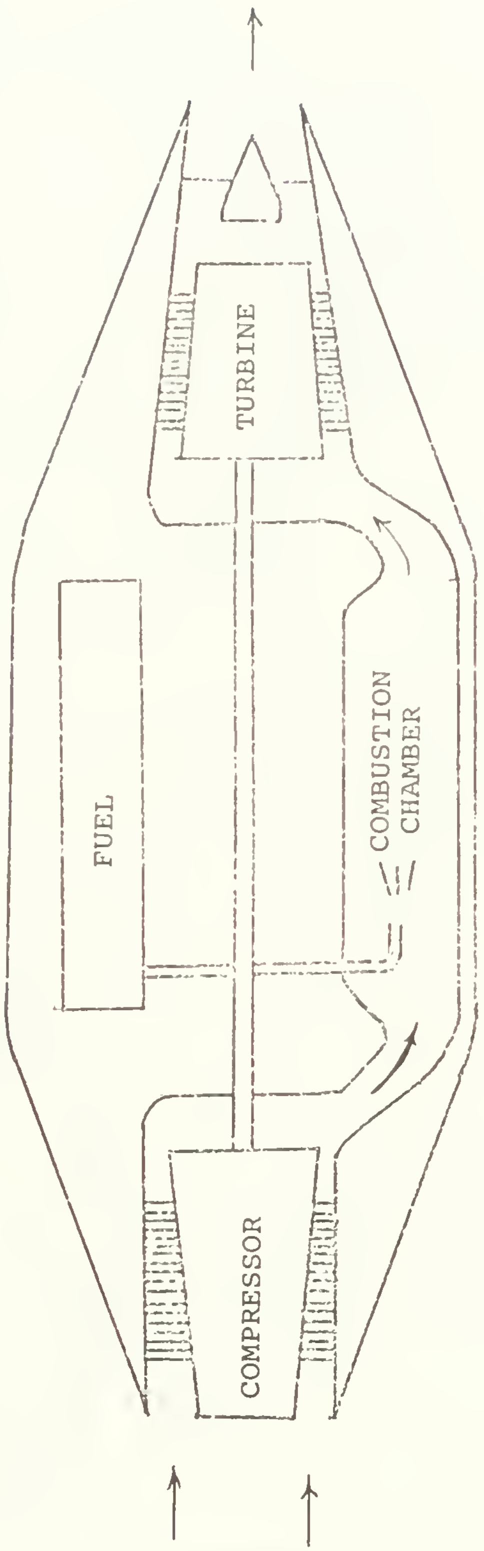

Figure 1

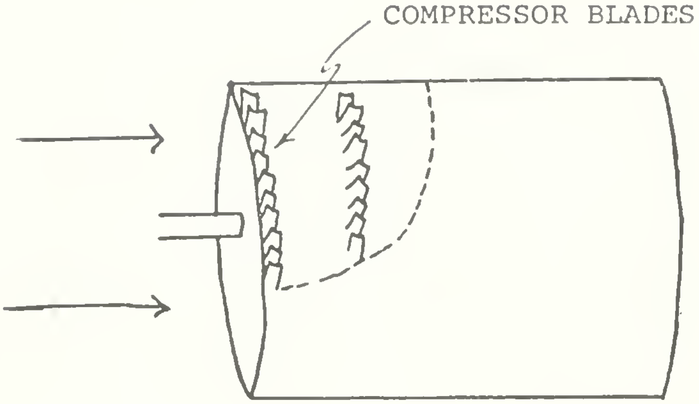

Figure 2

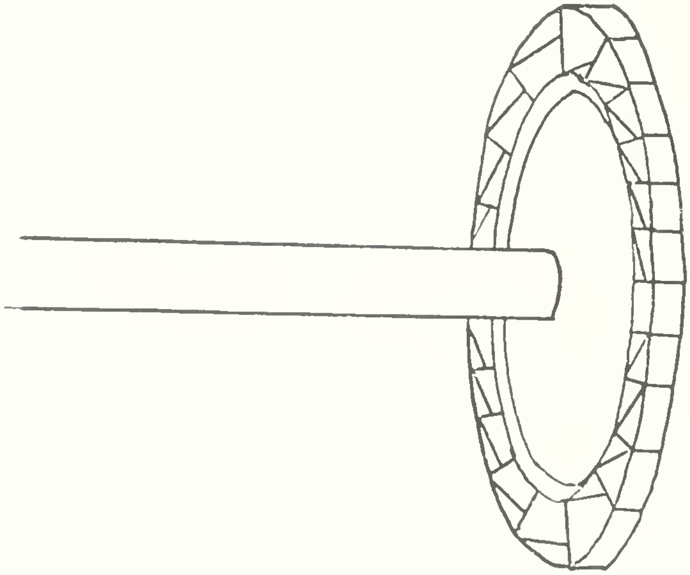

Figure 3

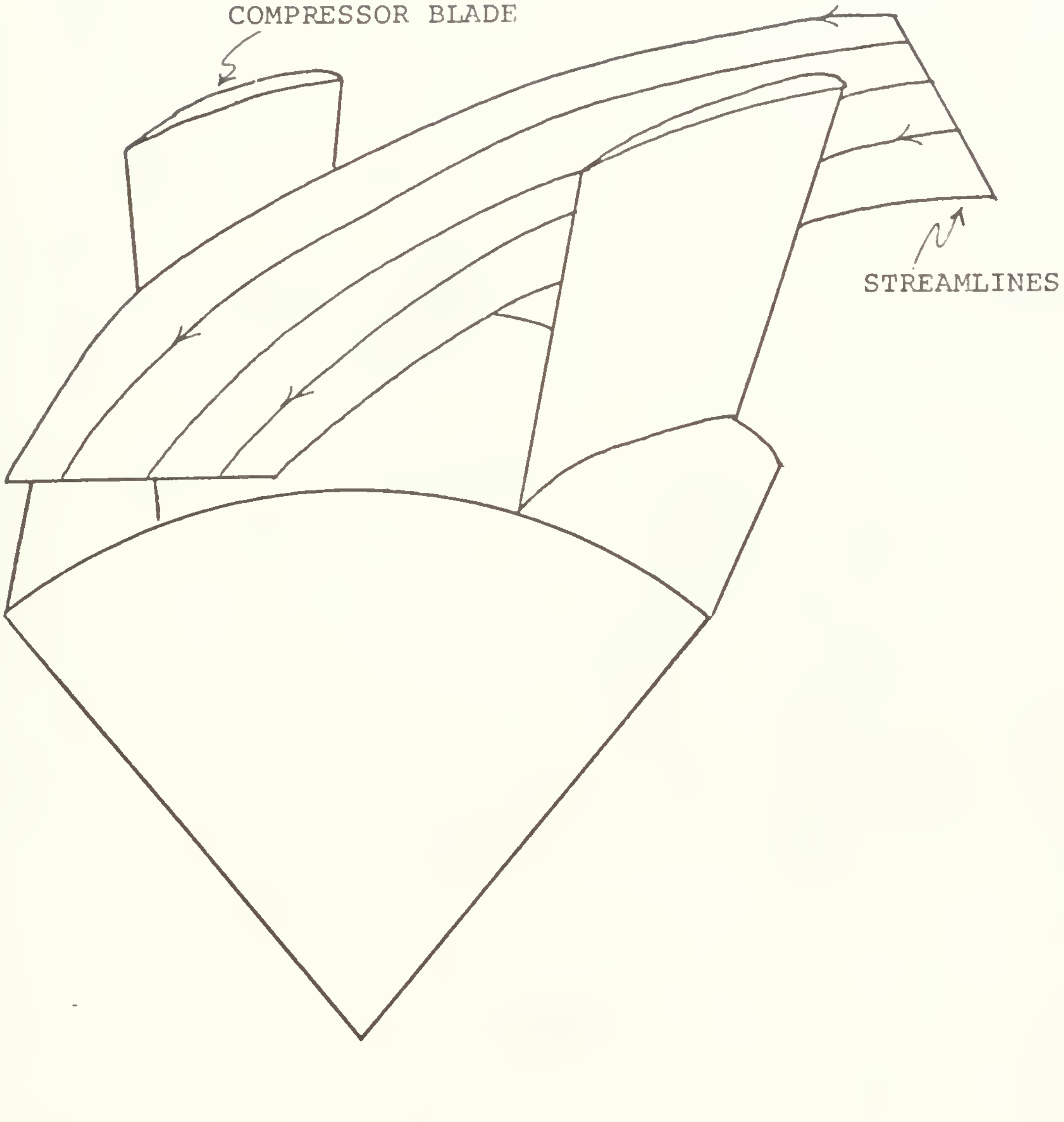

Figure 4

A CASCADE

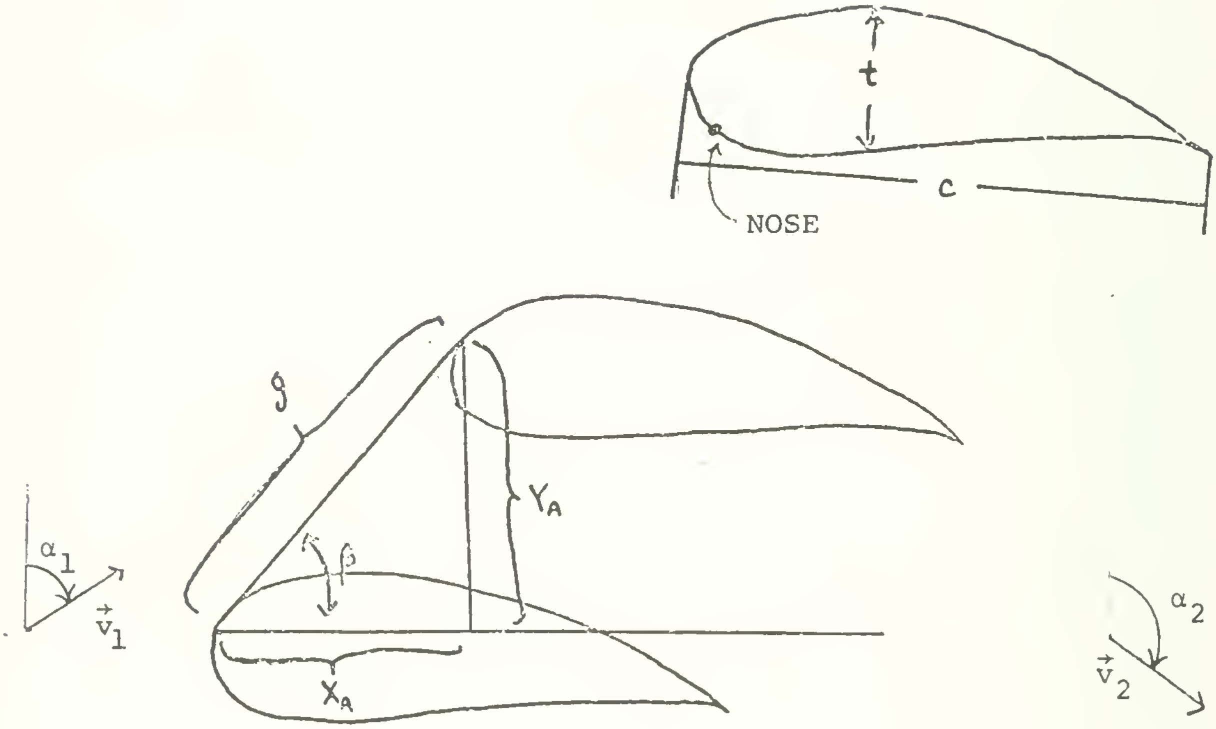

Figure 5

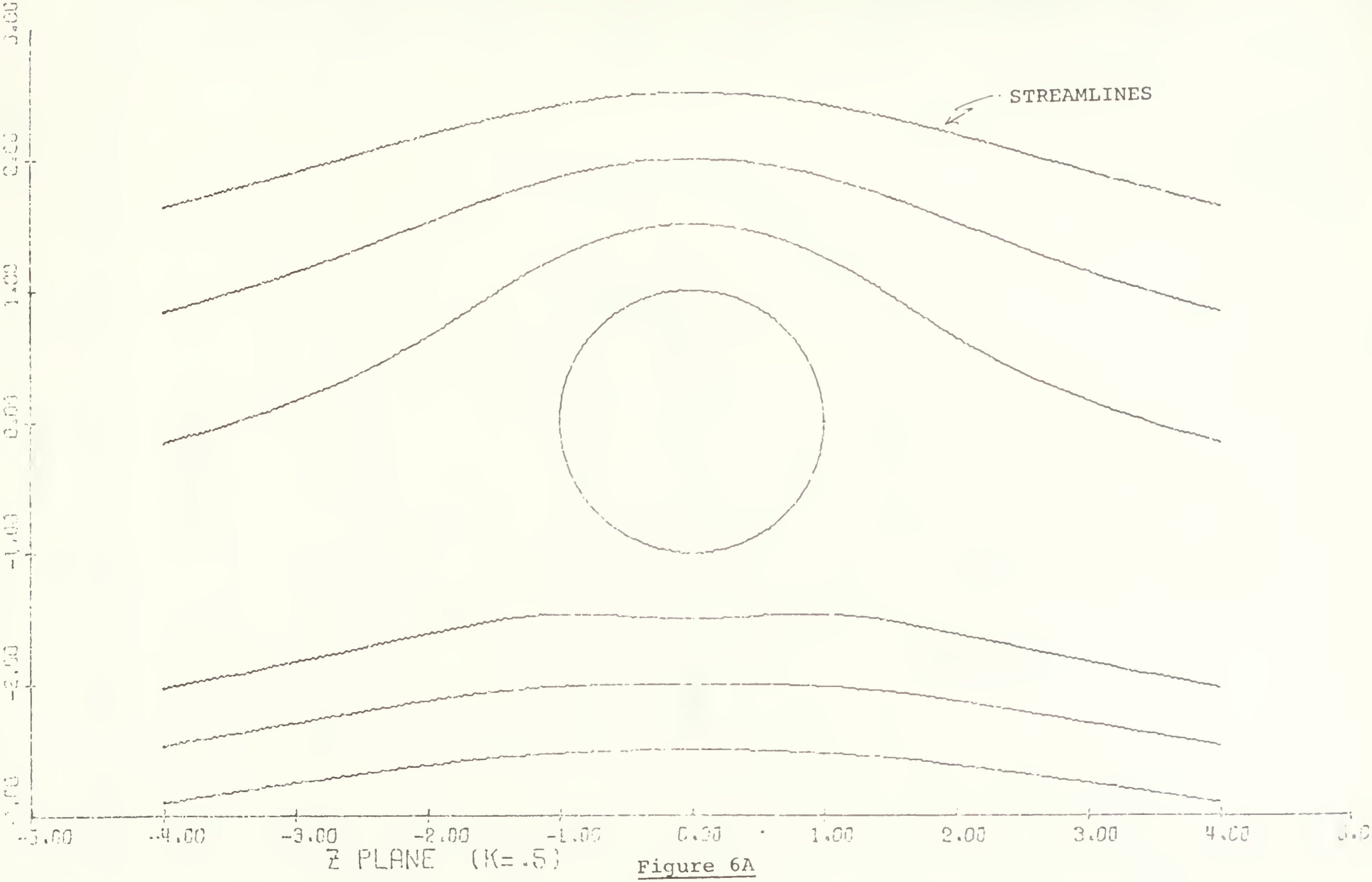
STREAMLINES
3.00
2.00
1.00
0.00
-1.00
-2.00
-3.00
-5.00
-4.00
-3.00
-2.00
-1.00
0.00
1.00
2.00
3.00
4.00
5.00
Z PLANE (K=.5)

Figure 6A

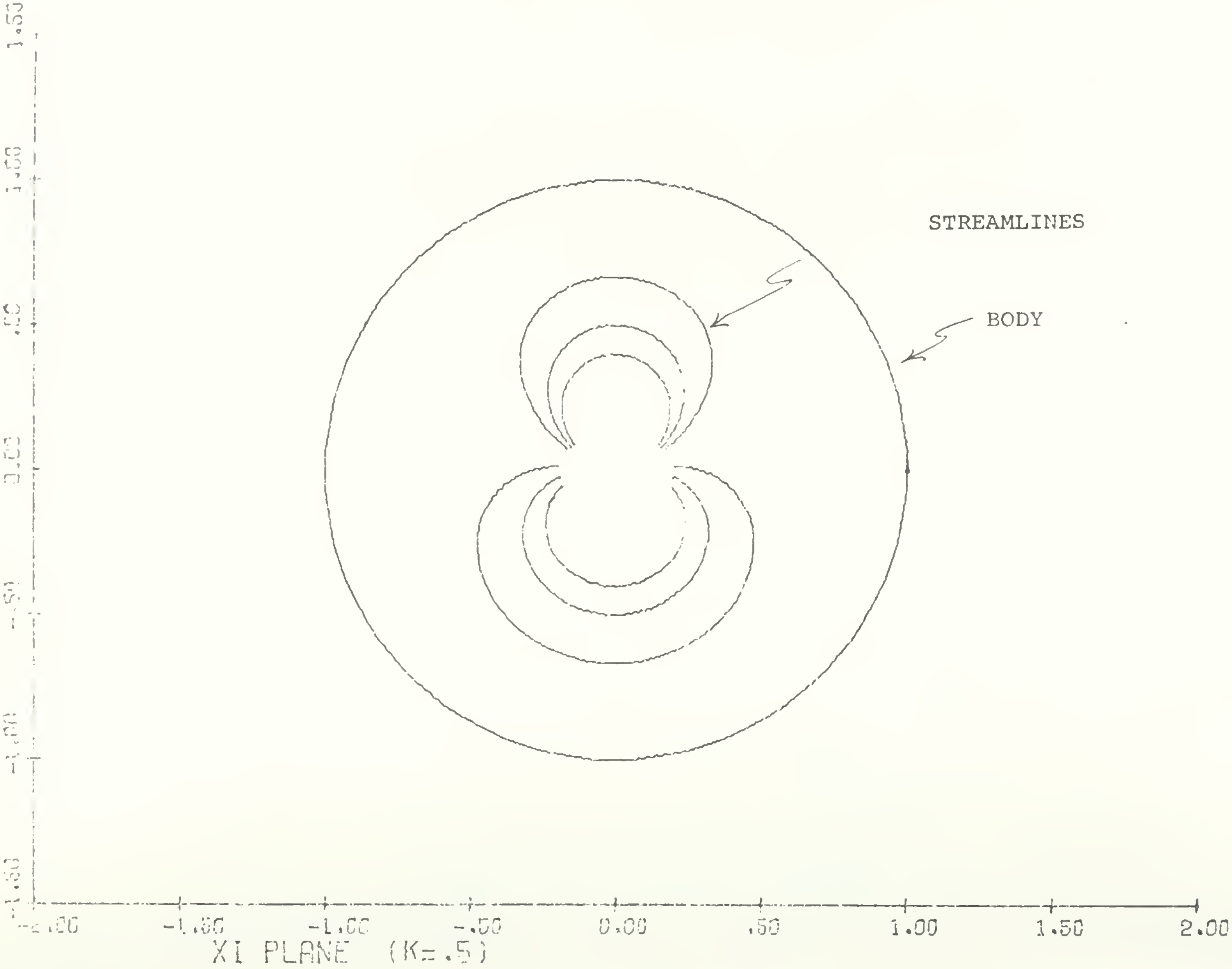
STREAMLINES
BODY
1.50
1.00
.50
0.00
-.50
-1.00
-1.50
-2.00
-1.50
-1.00
-.50
0.00
.50
1.00
1.50
2.00
XI PLANE (K=.5)

Figure 6B

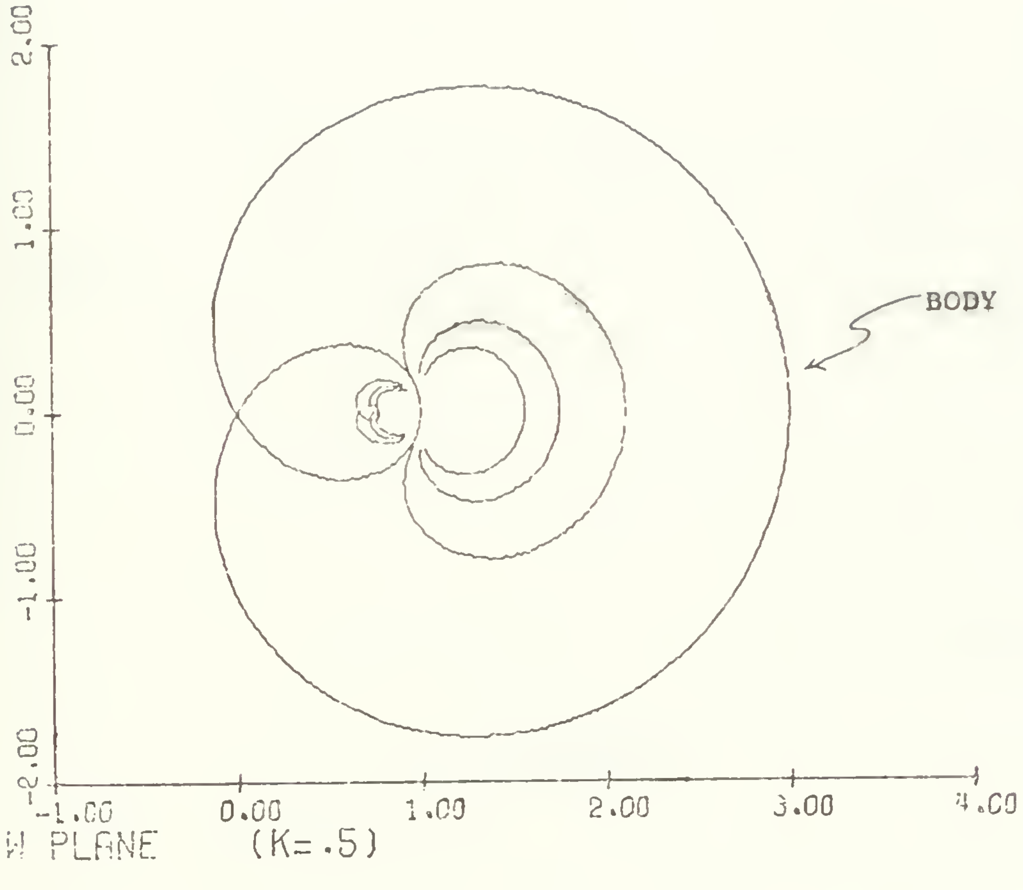

Figure 6C

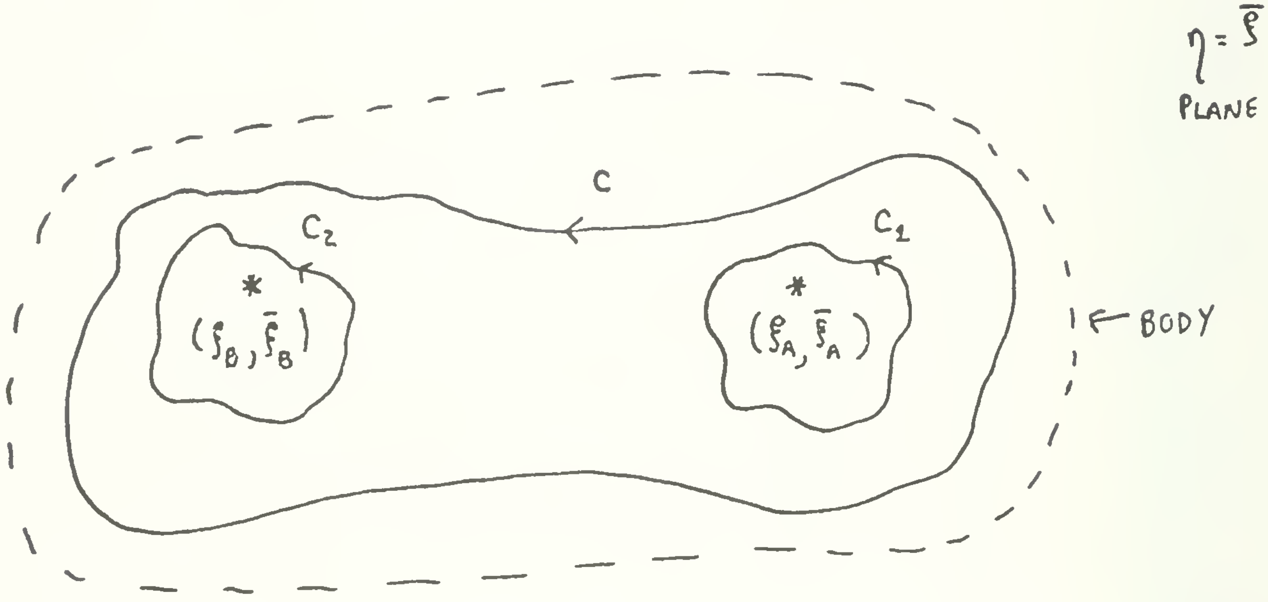$\eta = \bar{\zeta}$
PLANE
C
C_2
C_1
*
$(\zeta_B, \bar{\zeta}_B)$
*
$(\zeta_A, \bar{\zeta}_A)$
BODY

Figure 7

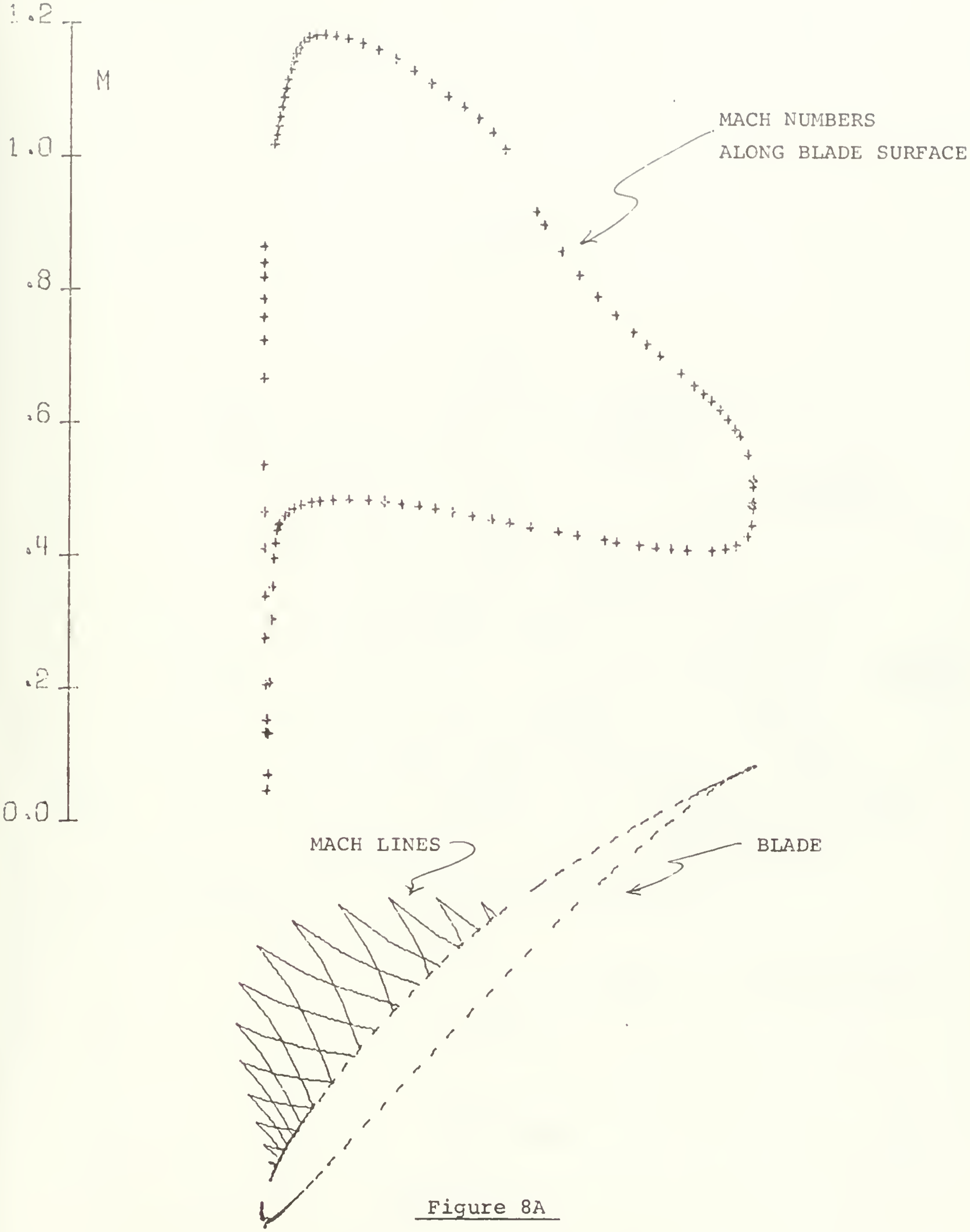

Figure 8A

G/C=2.49 M1=.700 M2=.519 DFL TH= 10.00

[illegible] 78 EM1= .700 EM2= .519 M= .600

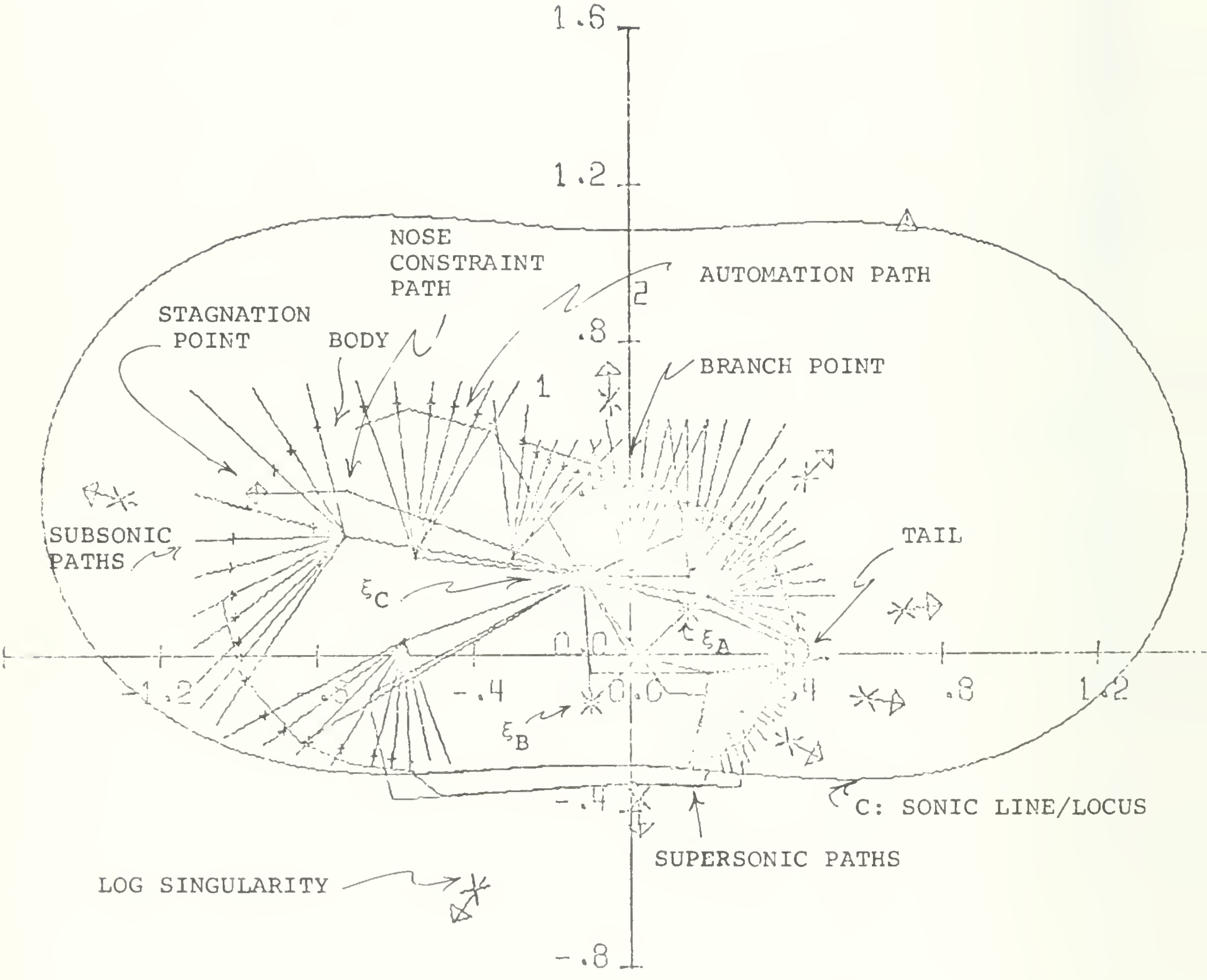

Figure 8B

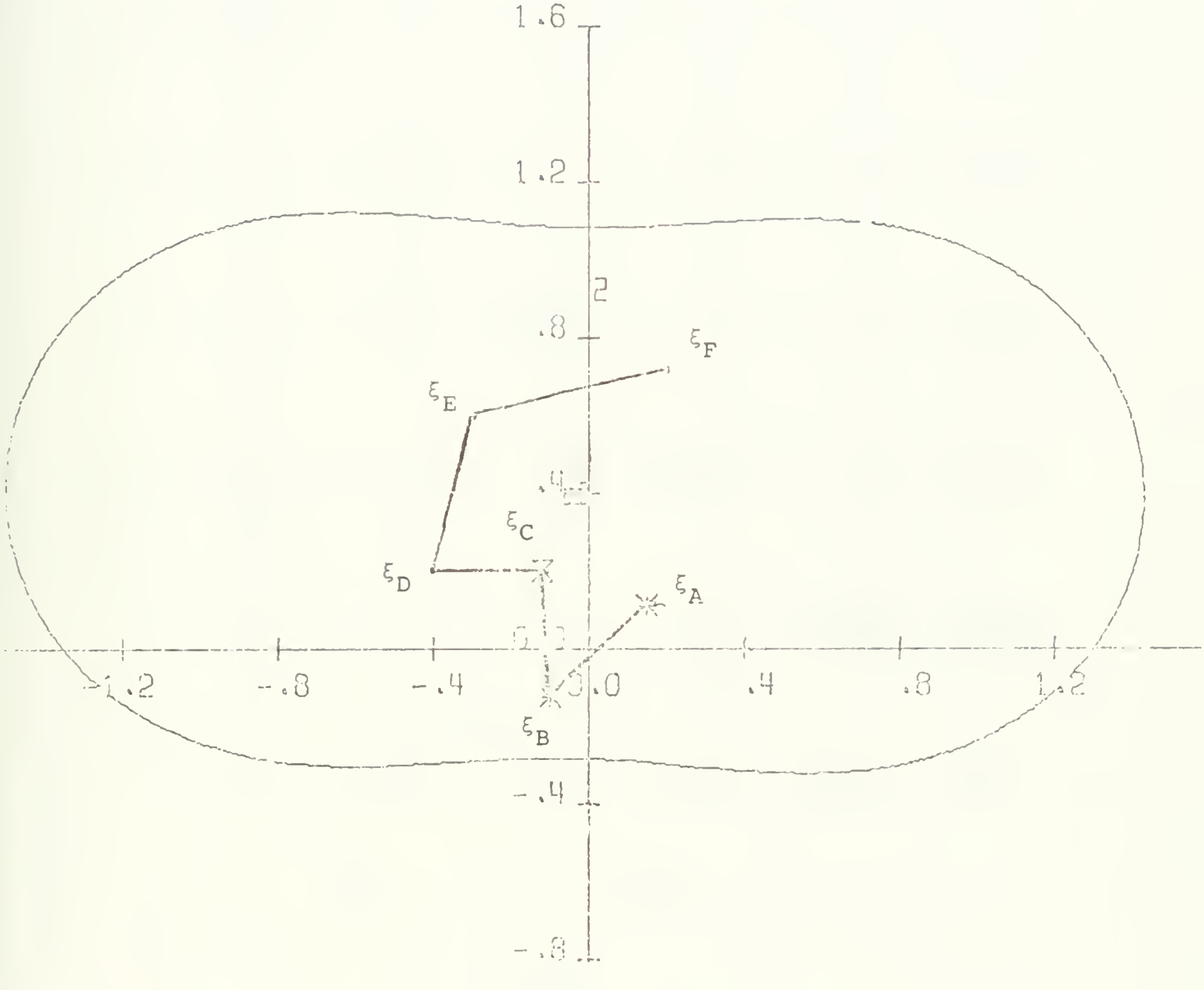

Figure 8C

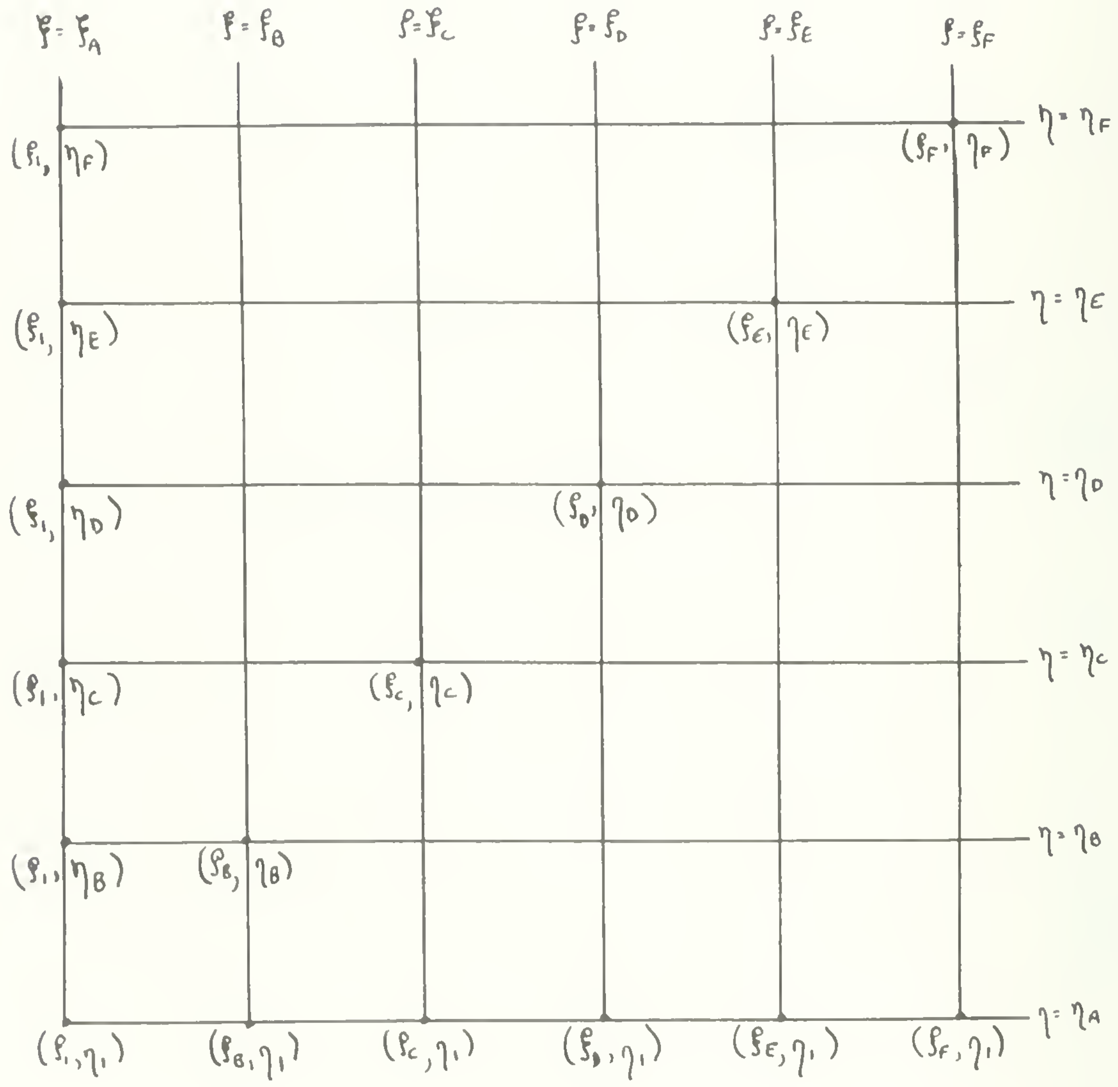
$\xi = \xi_A$
$\xi = \xi_B$
$\xi = \xi_C$
$\xi = \xi_D$
$\xi = \xi_E$
$\xi = \xi_F$
$\eta = \eta_F$
(ξ_1, η_F)
(ξ_F, η_F)
$\eta = \eta_E$
(ξ_1, η_E)
(ξ_E, η_E)
$\eta = \eta_D$
(ξ_1, η_D)
(ξ_D, η_D)
$\eta = \eta_C$
(ξ_1, η_C)
(ξ_C, η_C)
$\eta = \eta_B$
(ξ_1, η_B)
(ξ_B, η_B)
$\eta = \eta_A$
(ξ_1, η_1)
(ξ_B, η_1)
(ξ_C, η_1)
(ξ_D, η_1)
(ξ_E, η_1)
(ξ_F, η_1)

Figure 9

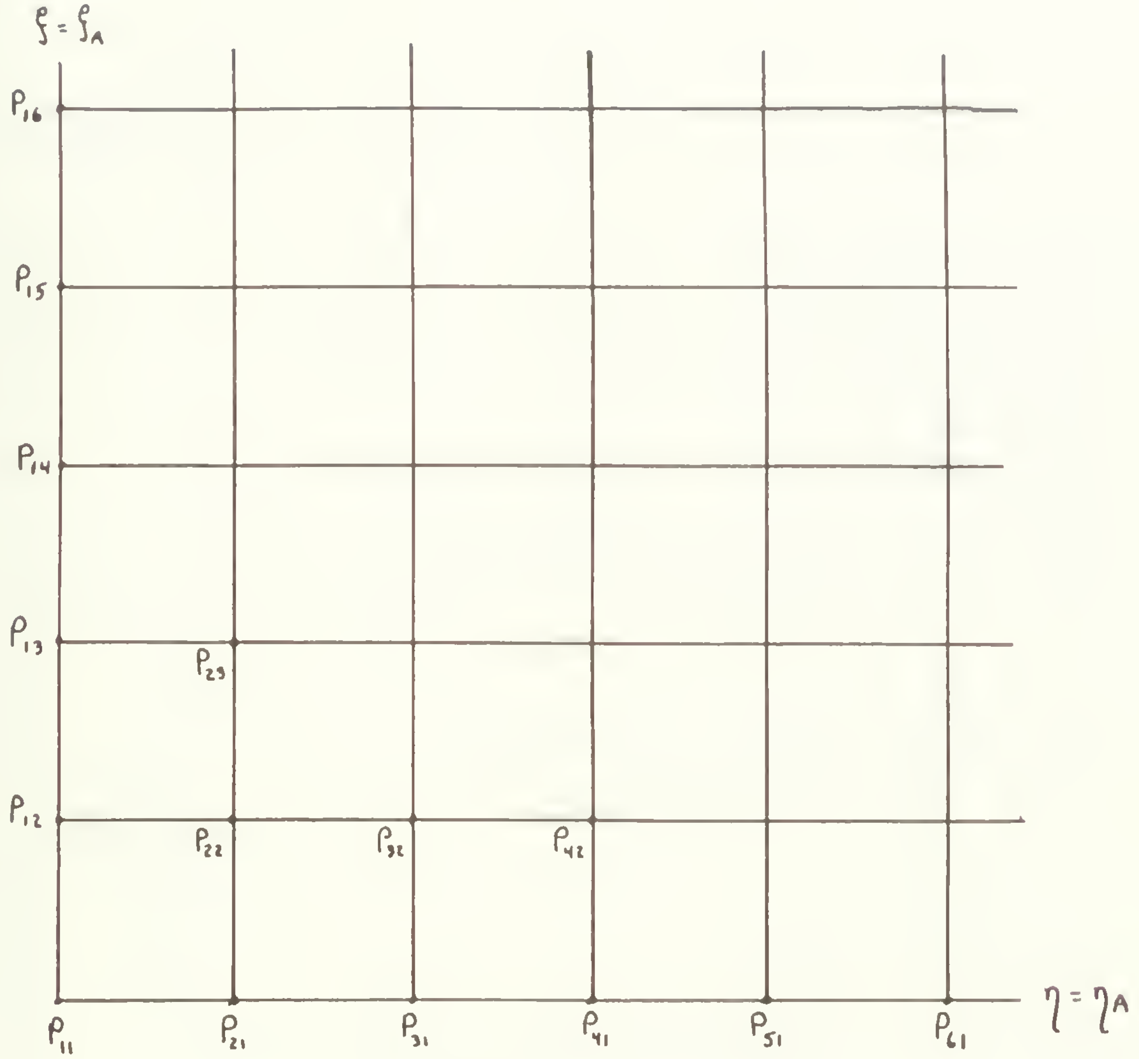

Figure 10

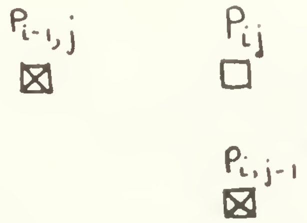

☒ - KNOWN POINTS OF $\hat{X}^1$ AND $\hat{Y}^1$

☐ - UNKNOWN POINTS OF $\hat{X}^1$ AND $\hat{Y}^1$

Figure 11

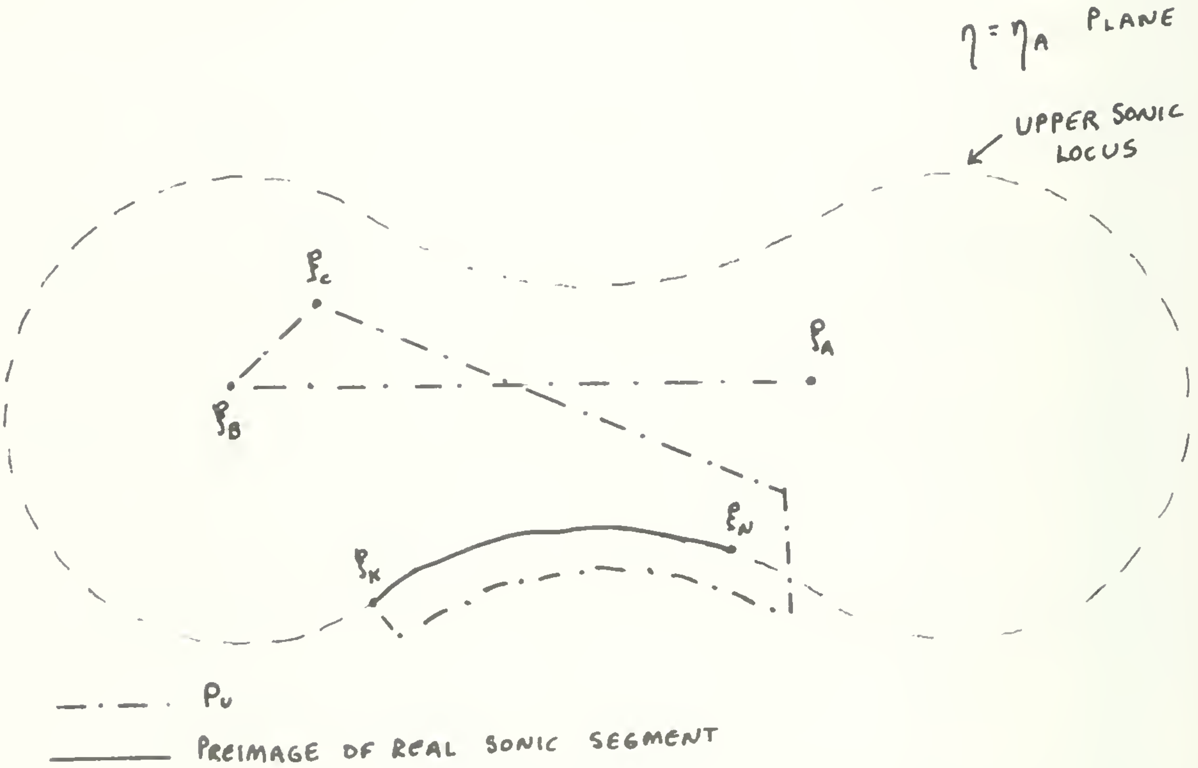

Figure 12A

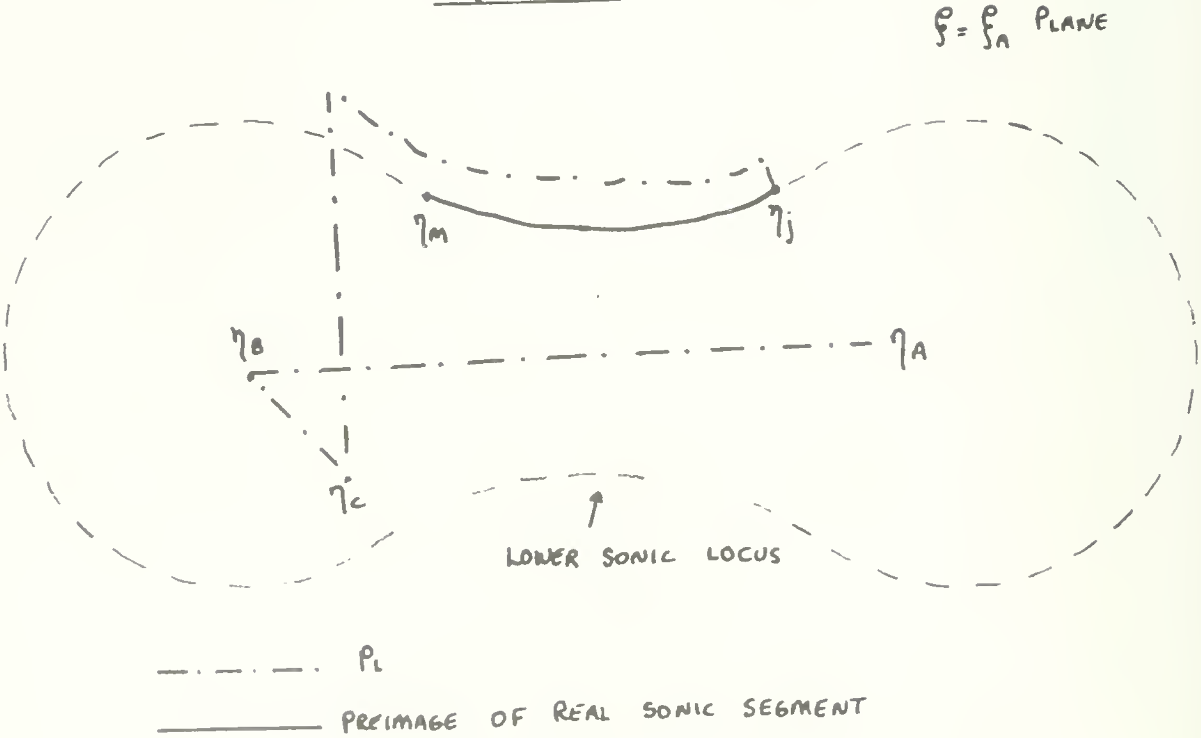

Figure 12B

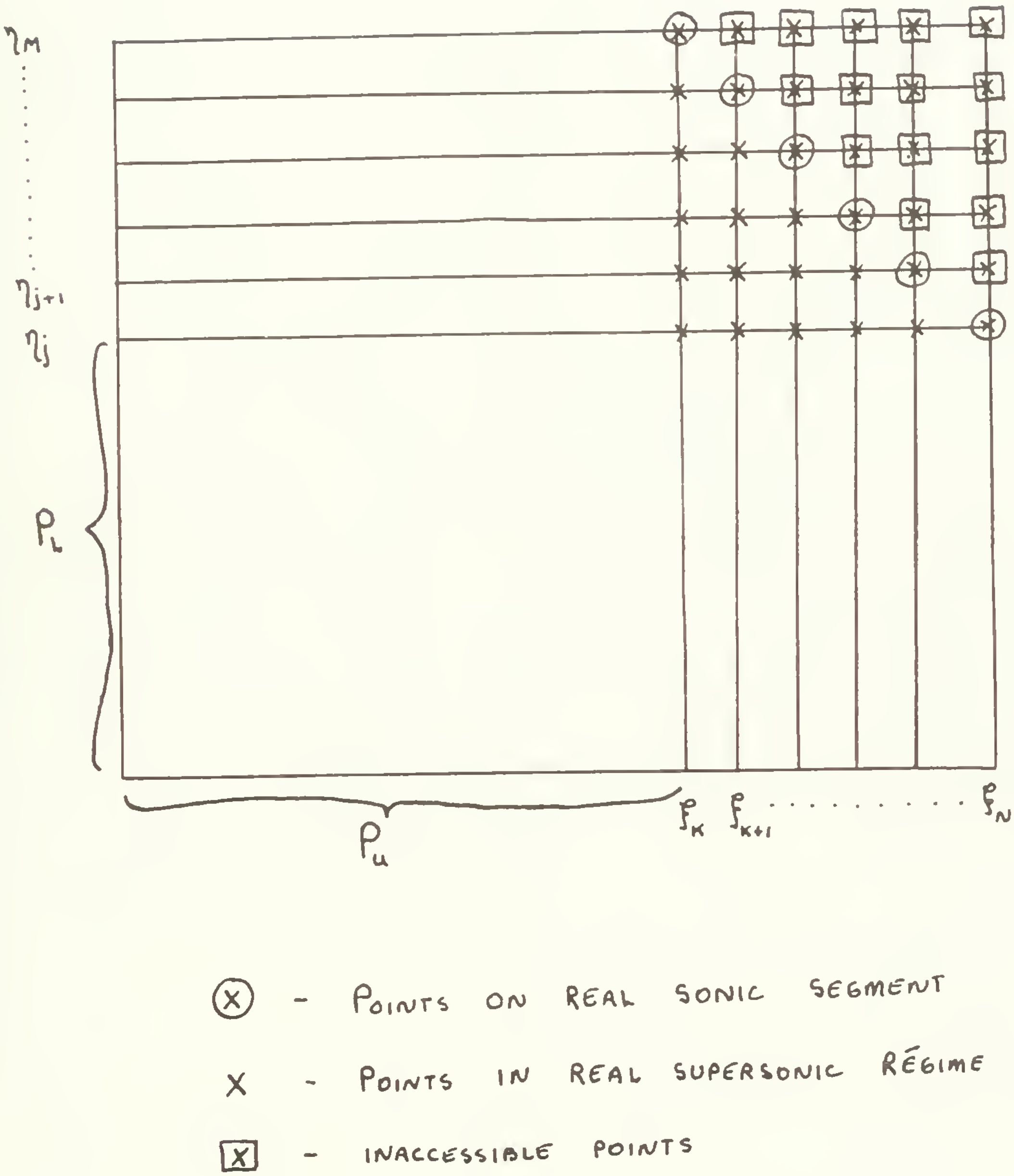
η_M
η_{j+1}
η_j
P_L
P_u
ξ_K
ξ_{K+1}
ξ_N
ⓧ - POINTS ON REAL SONIC SEGMENT
× - POINTS IN REAL SUPERSONIC RÉGIME
☒ - INACCESSIBLE POINTS

Figure 13

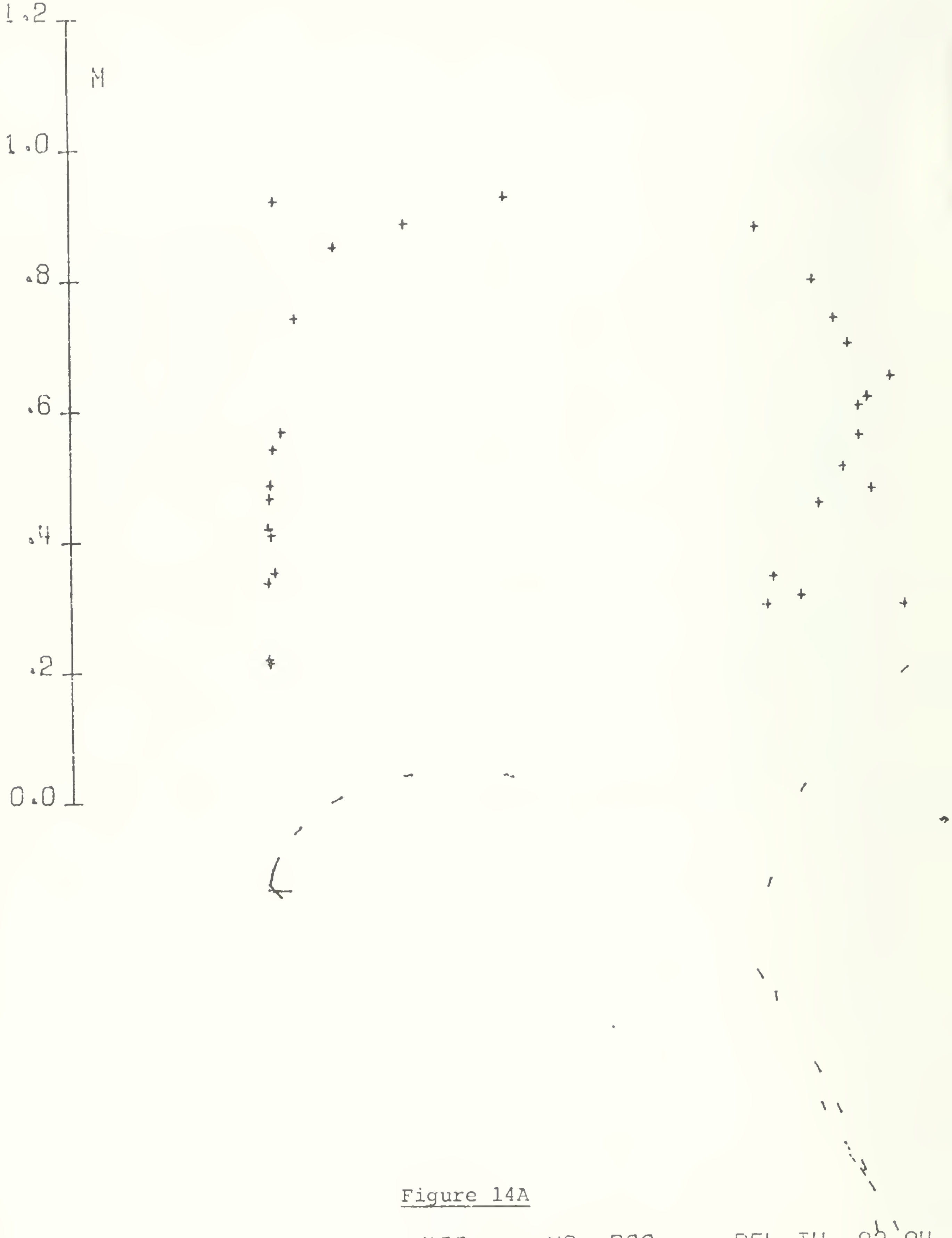

Figure 14A

G/C=1.18 M1=.400 M2=.700 DEL TH= 83.94

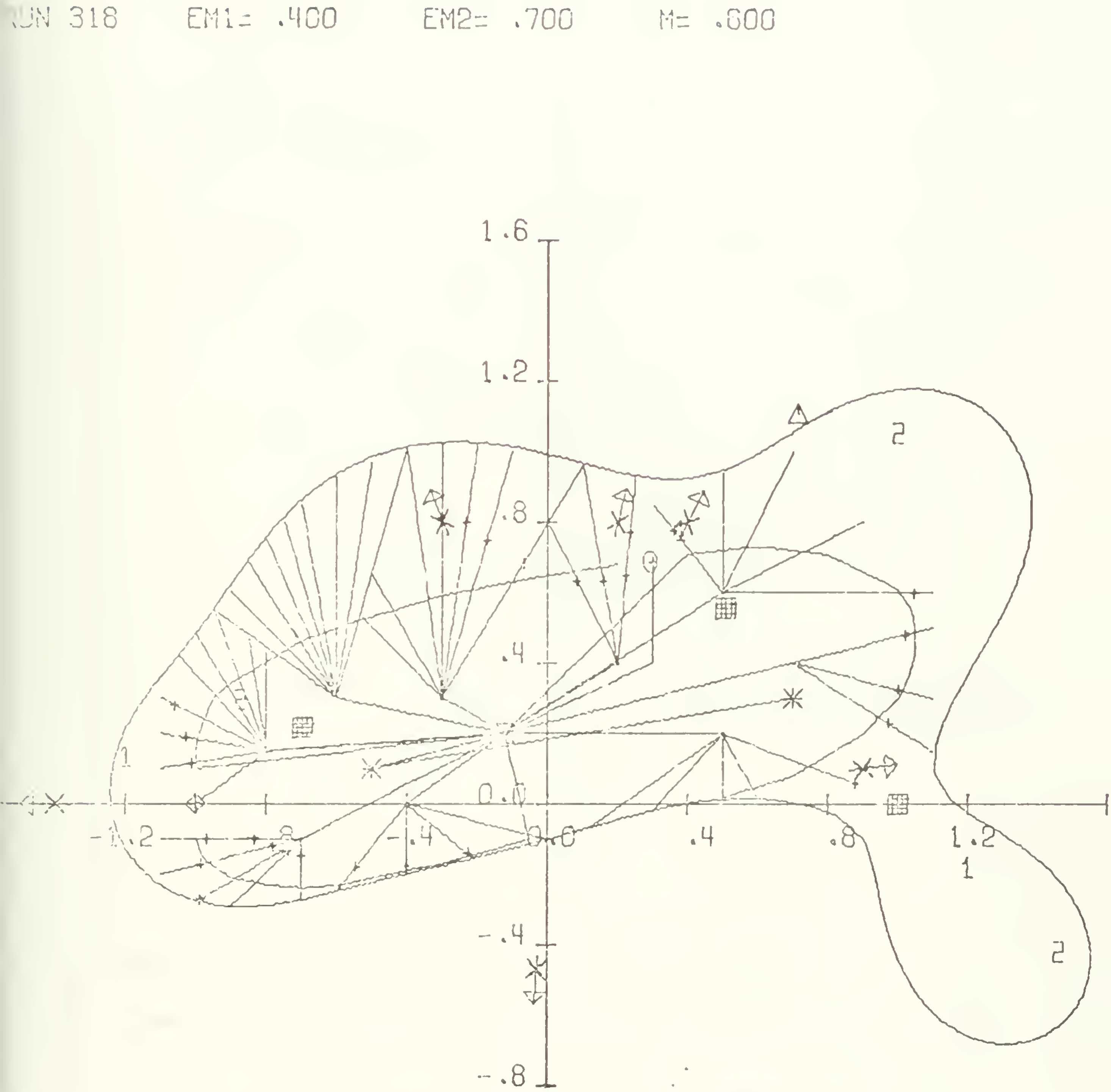

Figure 14B

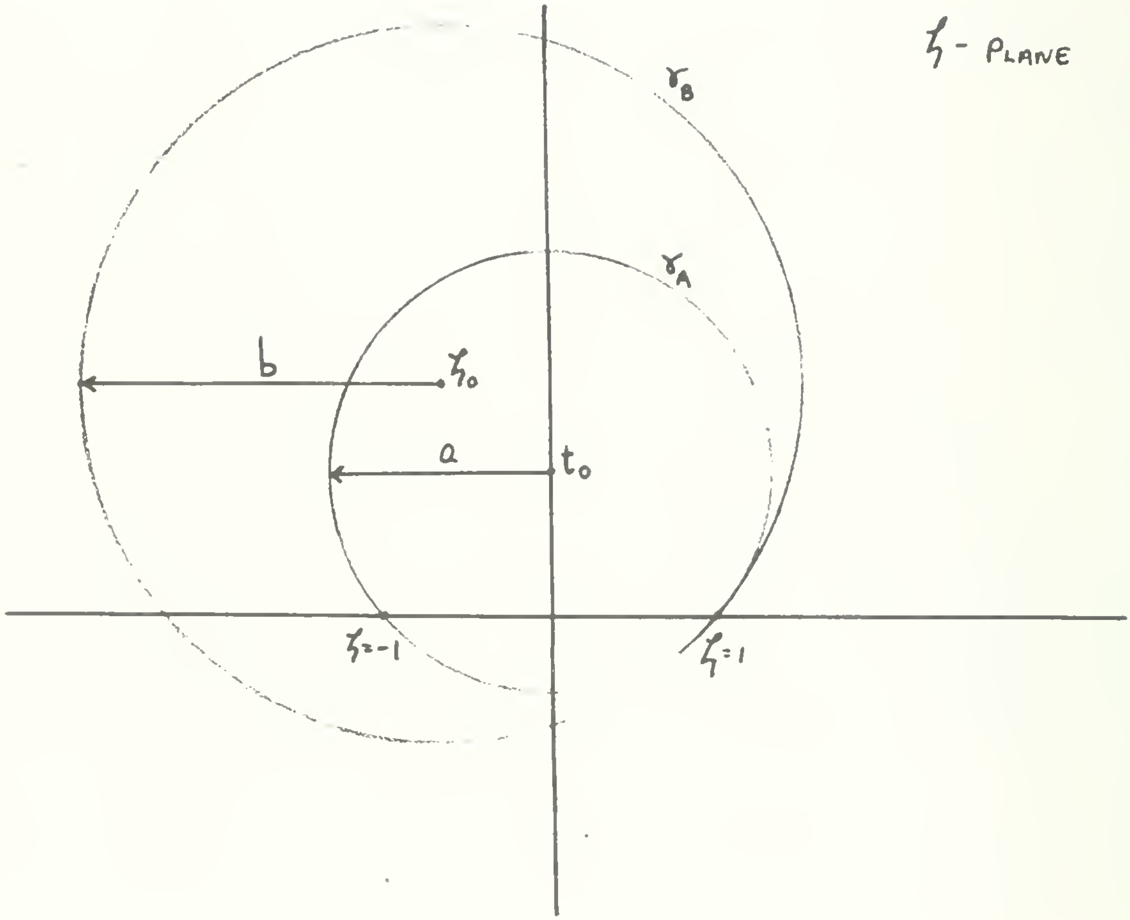

$\gamma_A = \{\zeta : \zeta = t_0 + ae^{i\theta},\ 0 \le \theta < 2\pi\}$ – MAPPED INTO THE CIRCULAR ARC

$\gamma_B = \{\zeta : \zeta = \zeta_0 + be^{i\theta},\ 0 \le \theta < 2\pi\}$ – MAPPED INTO THE BODY

$\zeta = 1$ - MAPPED INTO THE TAIL

Figure 15

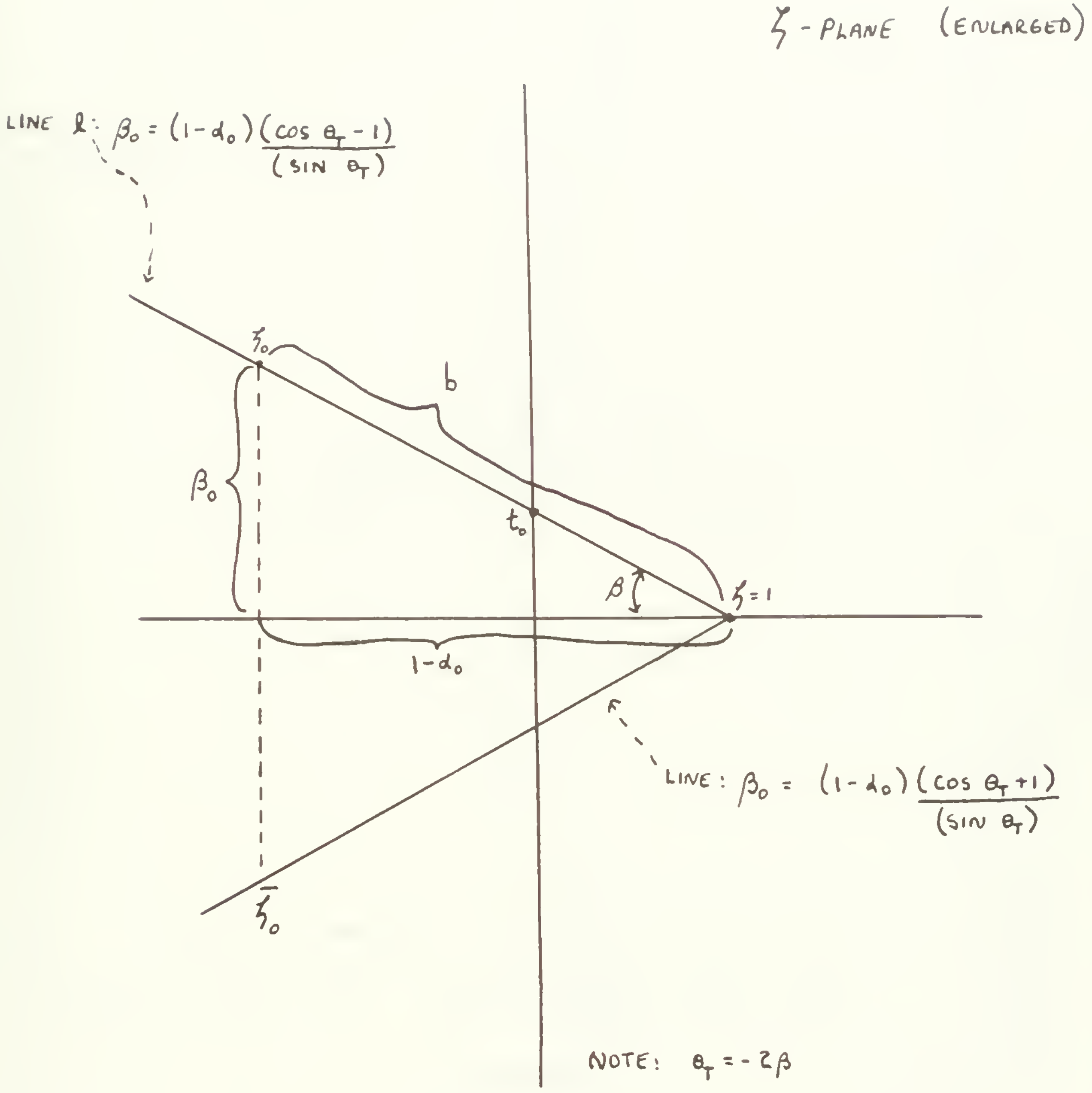
ζ - PLANE (ENLARGED)
LINE ℓ: $\beta_0 = (1-\alpha_0)\dfrac{(\cos\theta_T - 1)}{(\sin\theta_T)}$
ζ_0
b
β_0
t_0
β
$\zeta = 1$
$1-\alpha_0$
LINE: $\beta_0 = (1-\alpha_0)\dfrac{(\cos\theta_T + 1)}{(\sin\theta_T)}$
$\bar{\zeta}_0$
NOTE: $\theta_T = -2\beta$

Figure 16

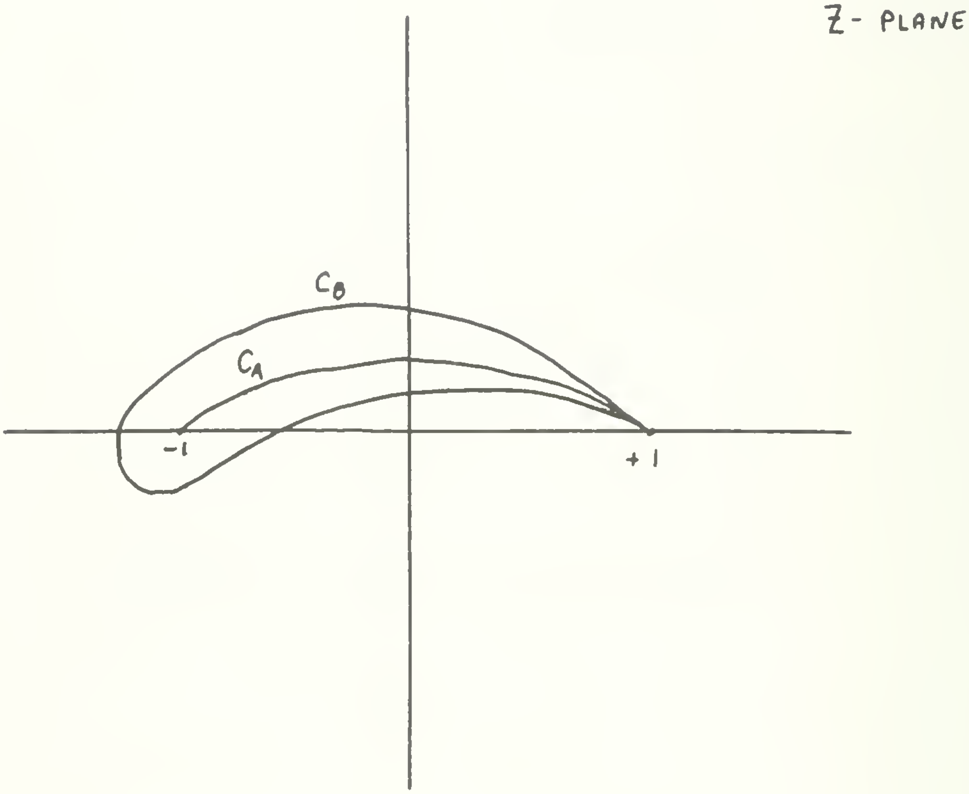

C_A IS THE CIRCULAR ARC (THE IMAGE OF γ_A)

C_B IS THE JOUKOWSKI PROFILE (THE IMAGE OF γ_B)

Figure 17

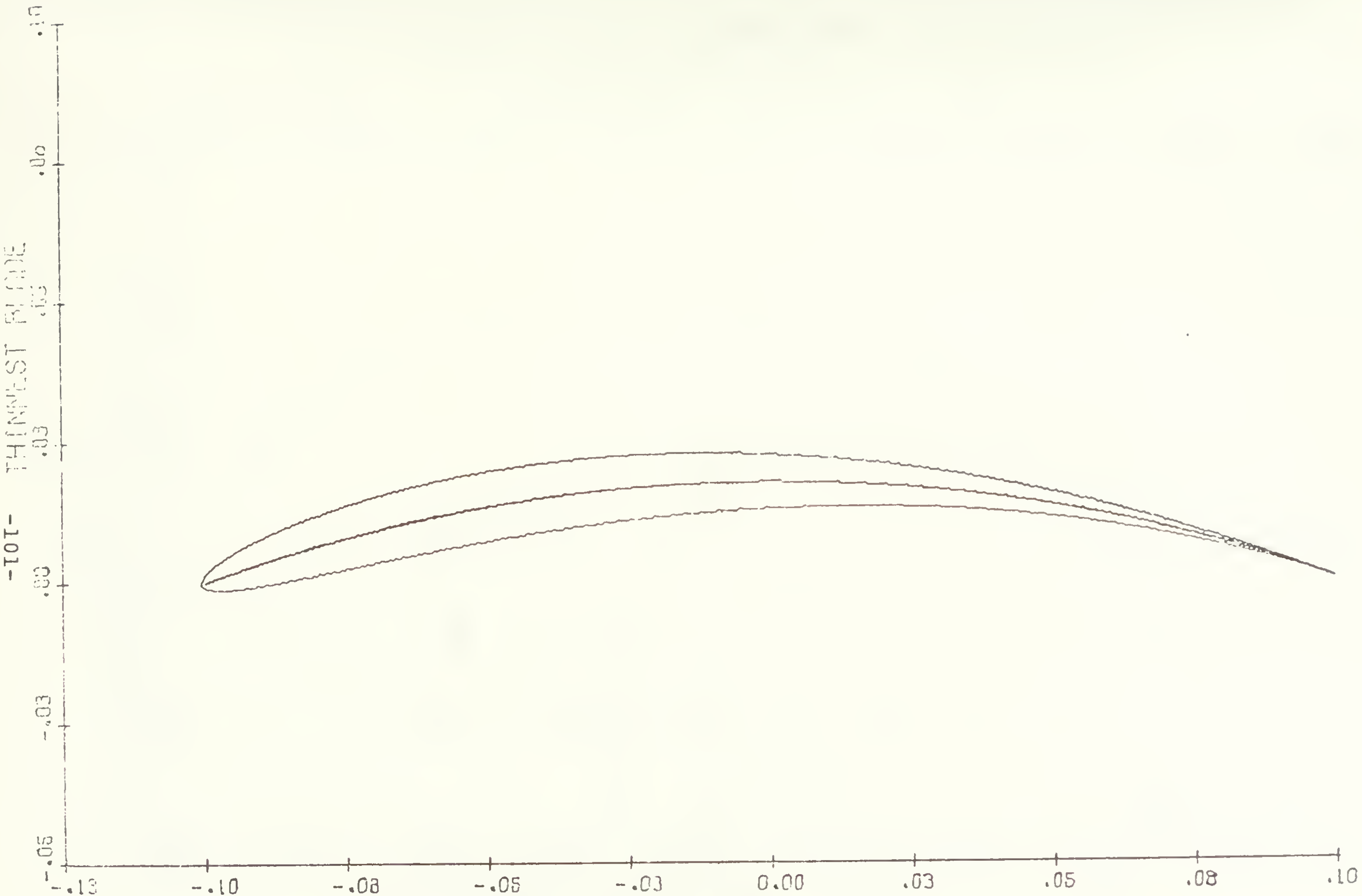

THKNSS=.05 CAMBER=-20. U=1.

Figure 18A

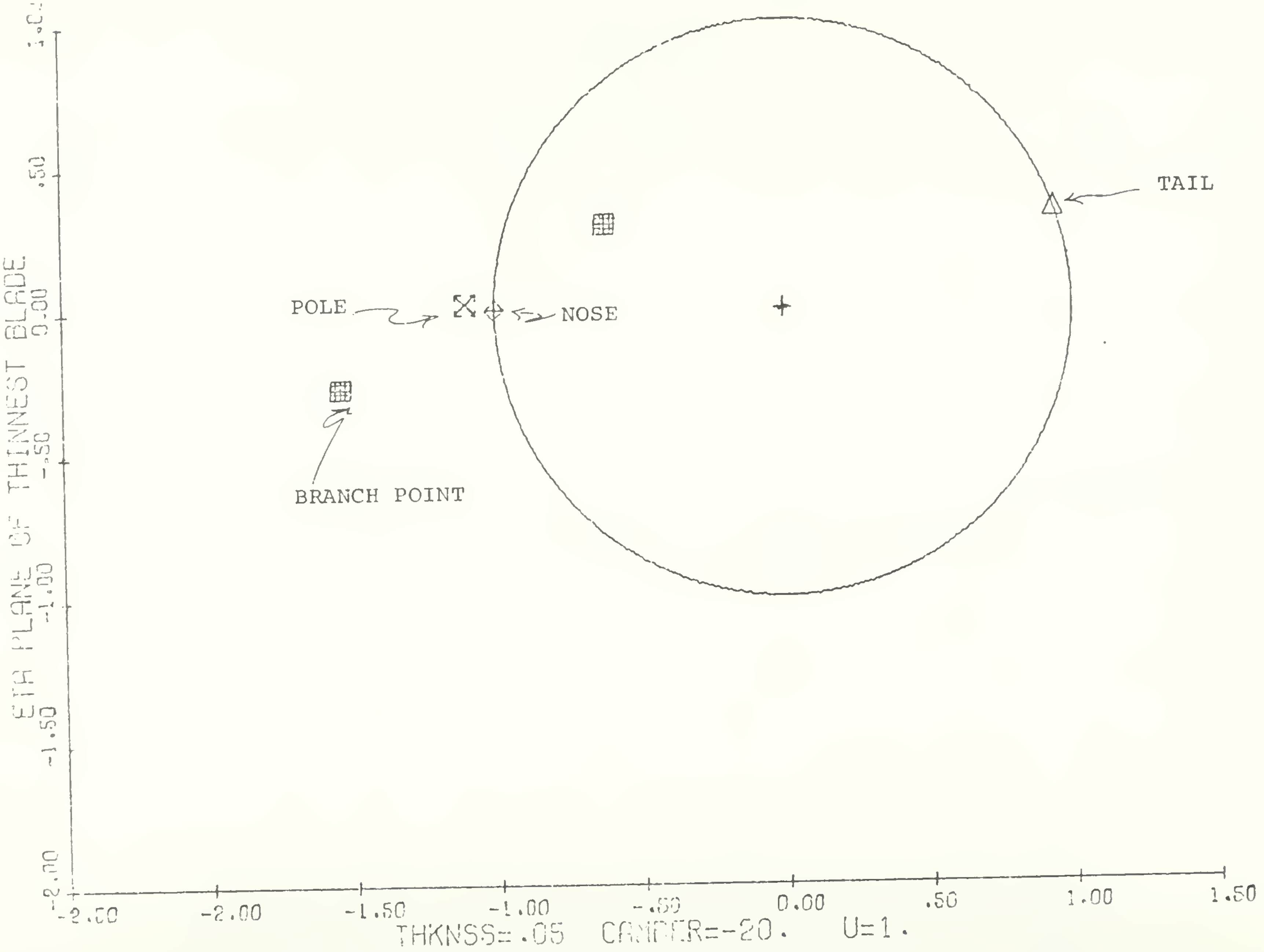
TAIL
POLE
NOSE
BRANCH POINT
ETA PLANE OF THINNEST BLADE
1.00
.50
0.00
-.50
-1.00
-1.50
-2.00
-2.50
-2.00
-1.50
-1.00
-.50
0.00
.50
1.00
1.50
THKNSS=.05 CAMBER=-20. U=1.

Figure 18B

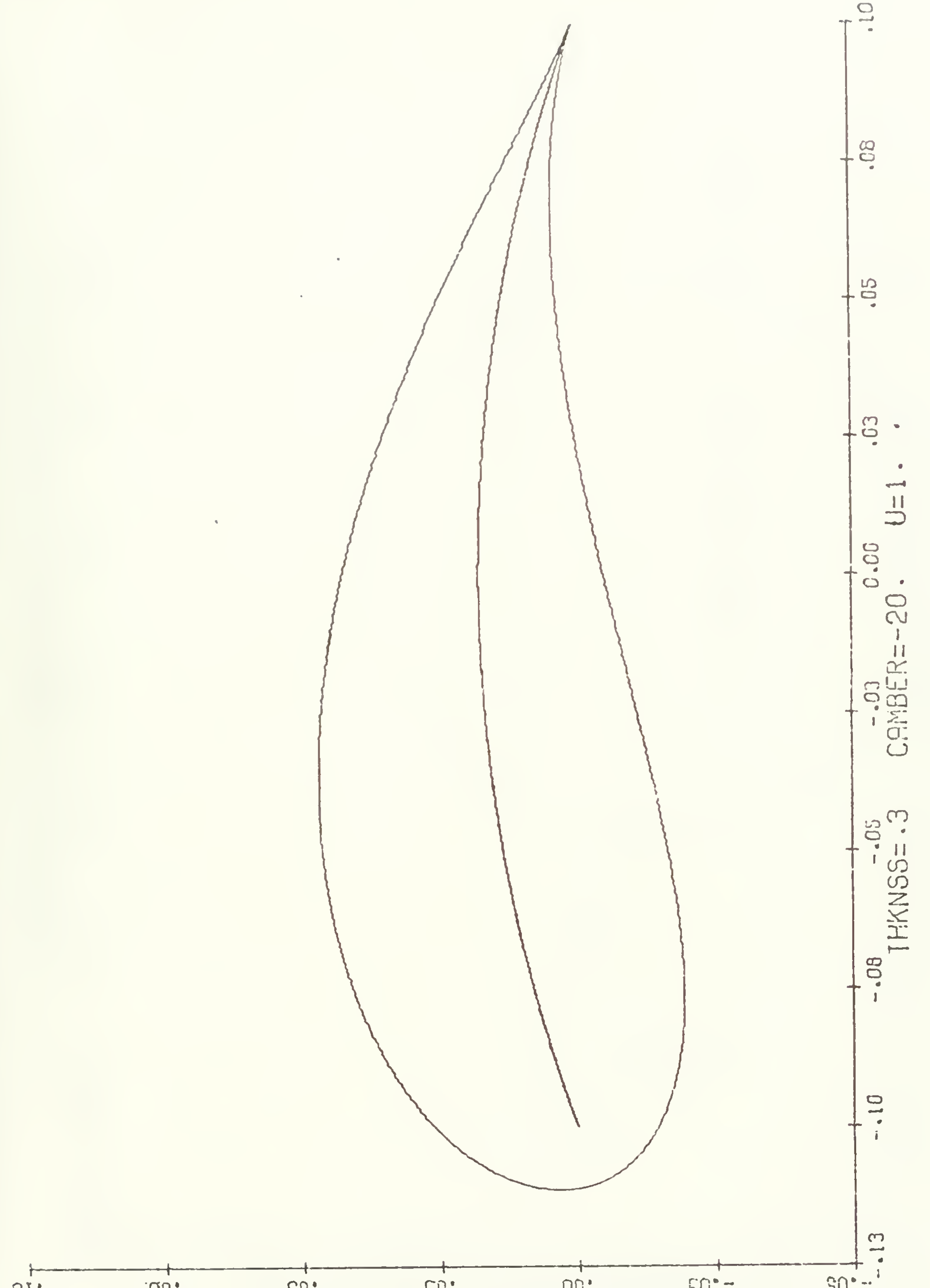
THKNSS=.3 CAMBER=-20. U=1.
-.13
-.10
-.08
-.05
-.03
0.00
.03
.05
.08
.10
-.05
-.03
.00
.03
.05
.08
.10
THICKEST BLADE

Figure 18C

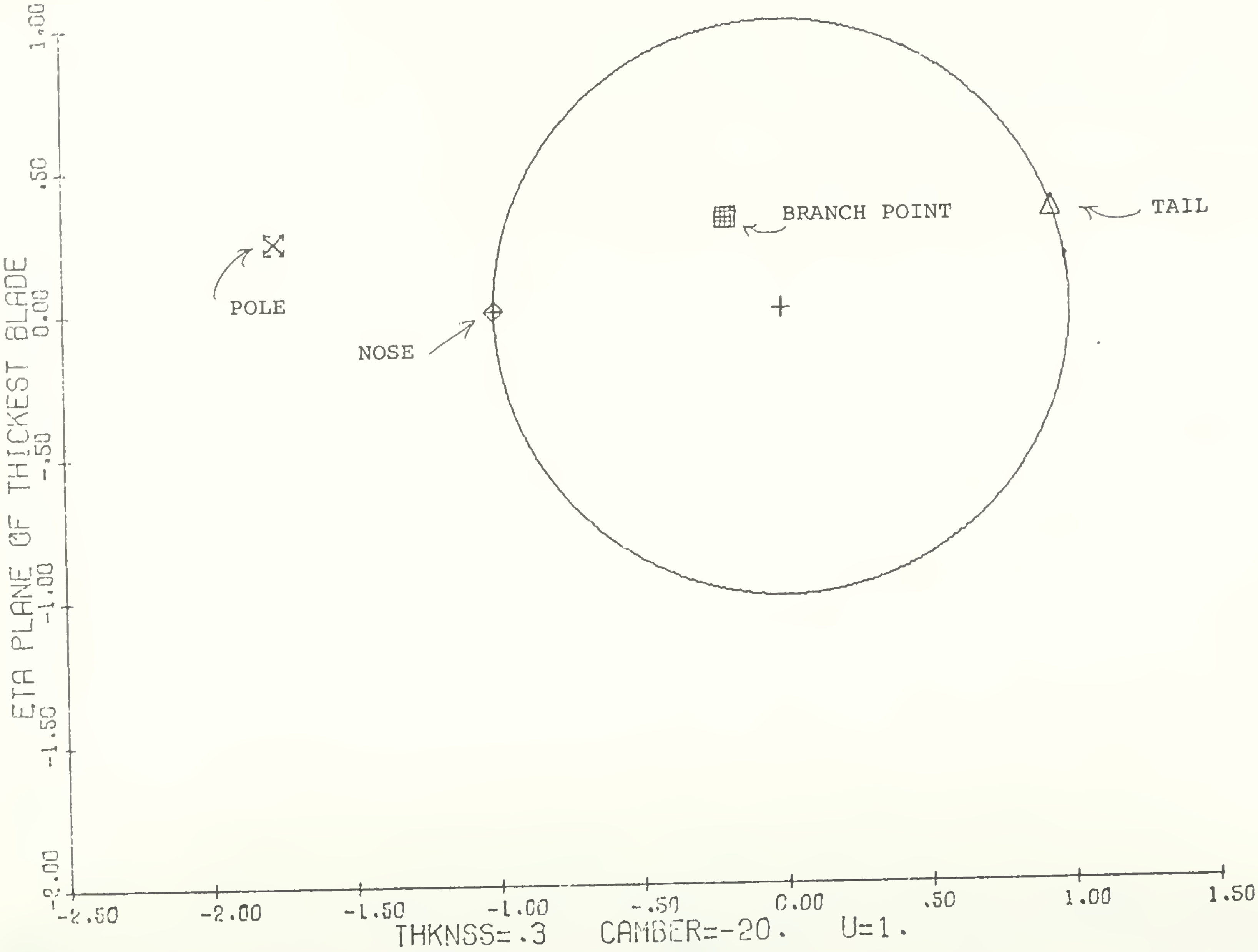
ETA PLANE OF THICKEST BLADE
1.00
.50
0.00
-.50
-1.00
-1.50
-2.00
-2.50
-2.00
-1.50
-1.00
-.50
0.00
.50
1.00
1.50
THKNSS=.3 CAMBER=-20. U=1.
POLE
NOSE
BRANCH POINT
TAIL

Figure 18D

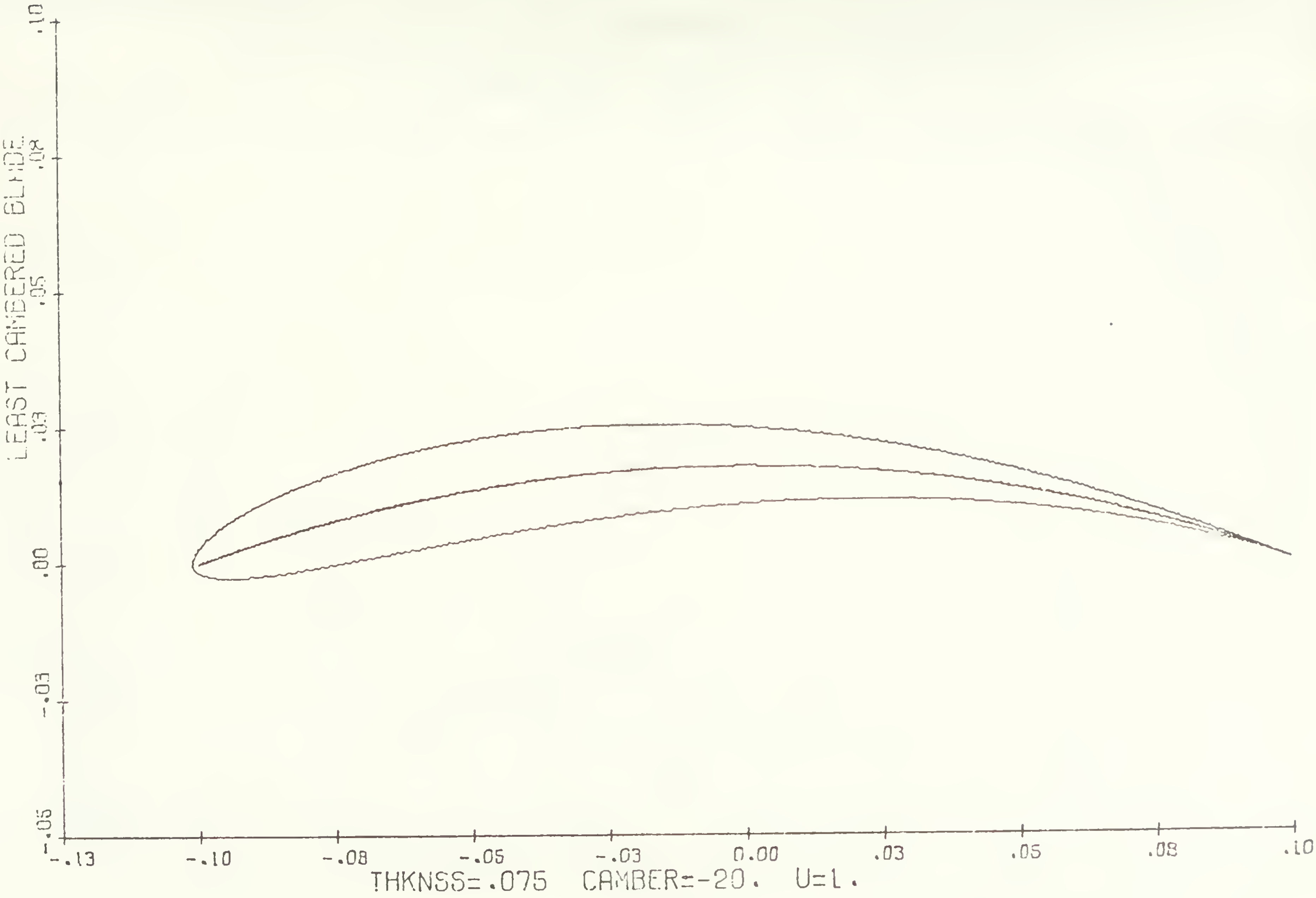
LEAST CAMBERED BLADE
.10
.08
.05
.03
.00
-.03
-.05
-.13
-.10
-.08
-.05
-.03
0.00
.03
.05
.08
.10
THKNSS=.075 CAMBER=-20. U=1.

Figure 19A

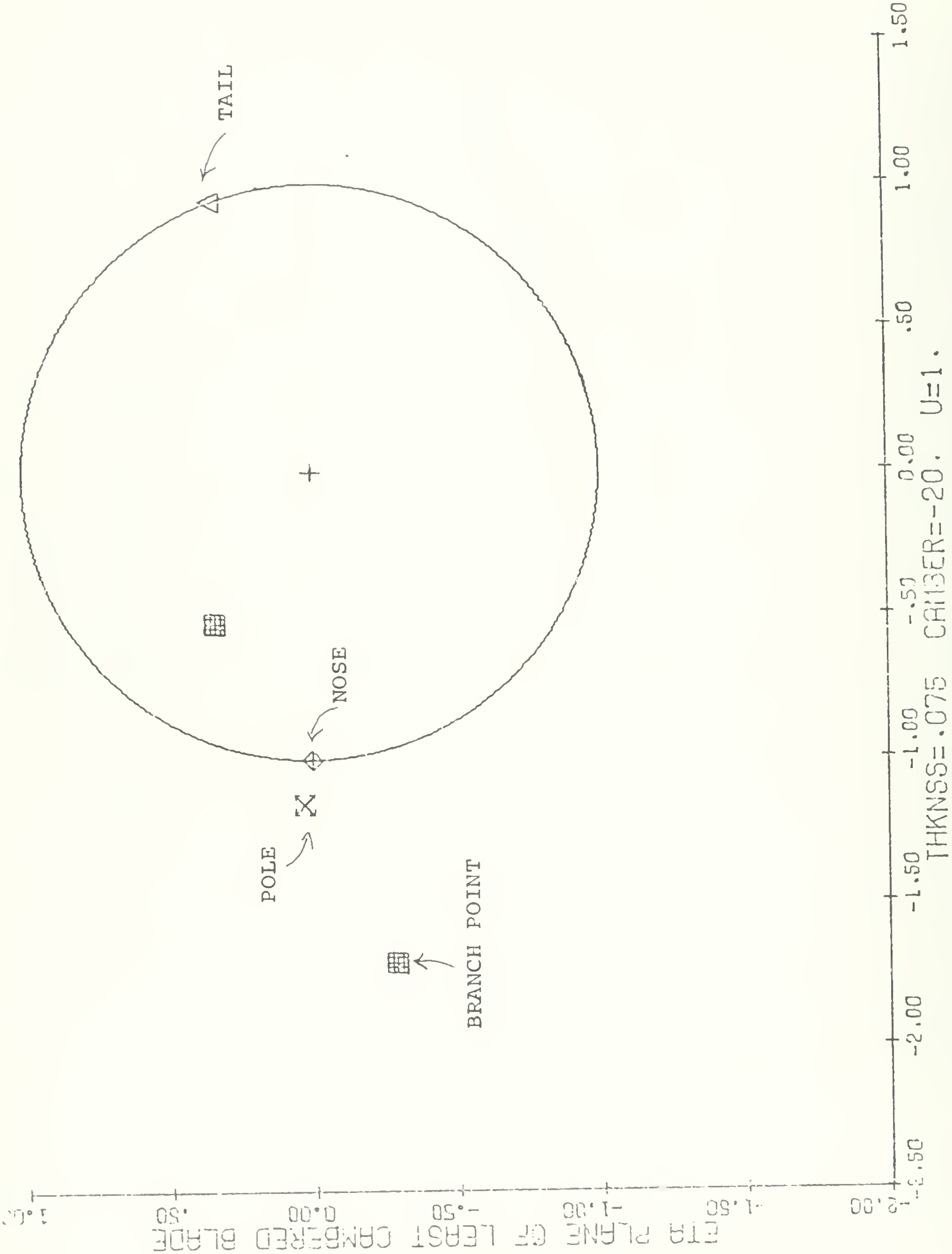
TAIL
NOSE
POLE
BRANCH POINT
-2.50
-2.00
-1.50
-1.00
-.50
0.00
.50
1.00
1.50
THKNSS=.075 CAMBER=-20. U=1.
-2.00
-1.50
-1.00
-.50
0.00
.50
1.00
ETA PLANE OF LEAST CAMBERED BLADE

Figure 19B

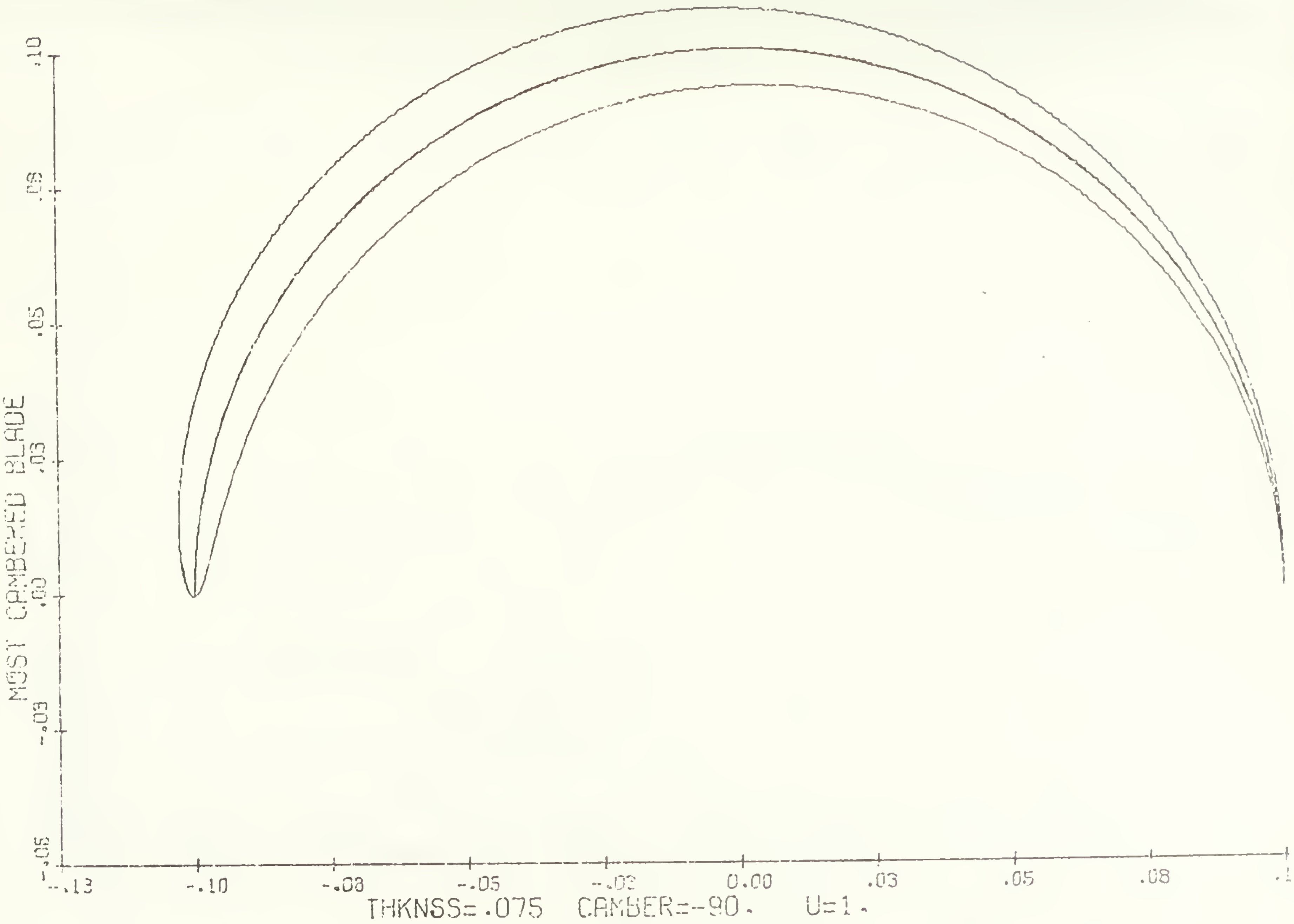
MOST CAMBERED BLADE
.10
.08
.05
.03
.00
-.03
-.05
-.13
-.10
-.08
-.05
-.03
0.00
.03
.05
.08
.10
THKNSS=.075 CAMBER=-90. U=1.

Figure 19C

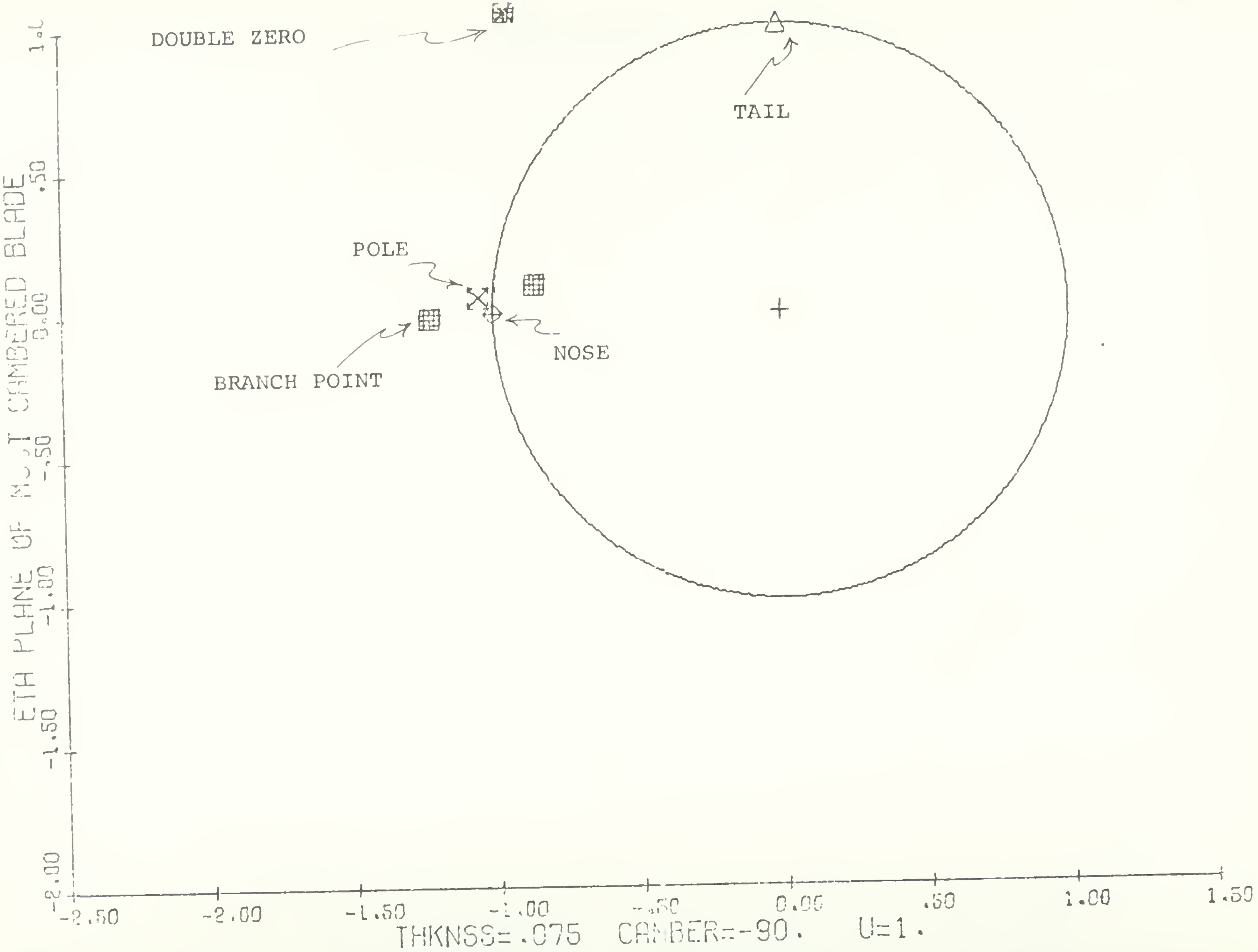
DOUBLE ZERO
TAIL
POLE
NOSE
BRANCH POINT
1.0
.50
0.00
-.50
-1.00
-1.50
-2.00
-2.50
-2.00
-1.50
-1.00
-.50
0.00
.50
1.00
1.50
ETH PLANE OF MOST CAMBERED BLADE
THKNSS=.075 CAMBER=-90. U=1.

Figure 19D

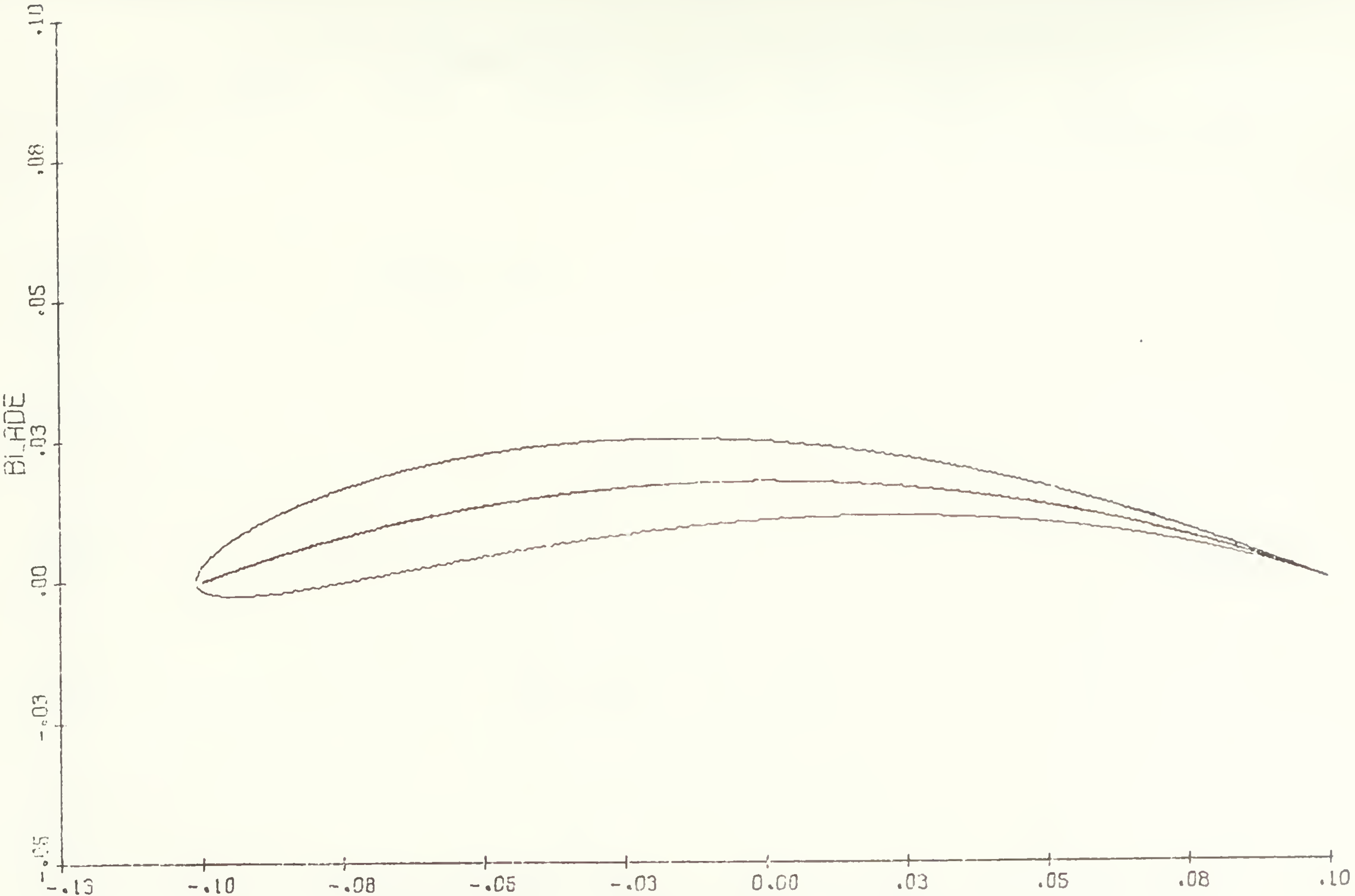

THKNSS=.075 CAMBER=-20. ANG=-10.

Figure 20A

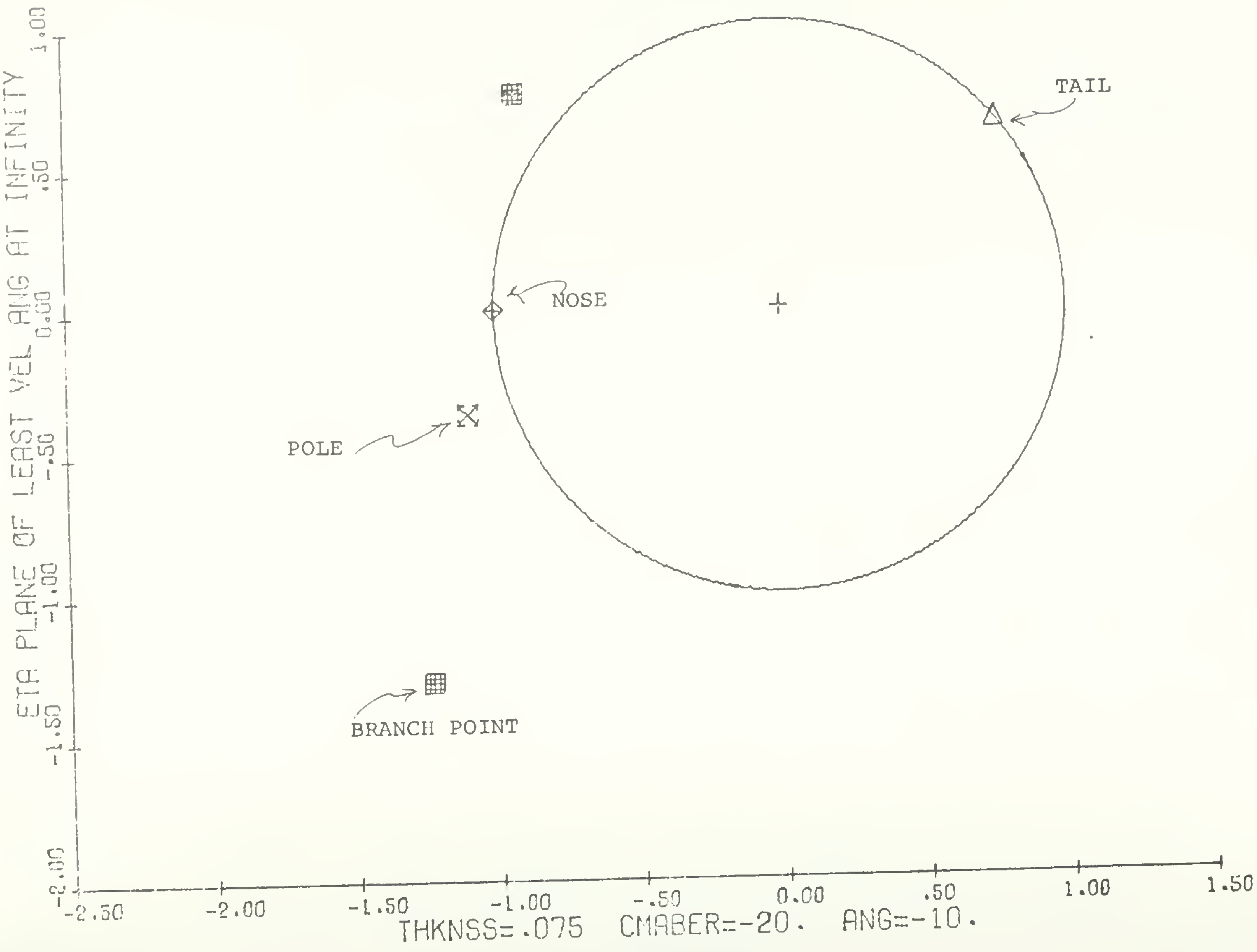
TAIL
NOSE
POLE
BRANCH POINT
ETA PLANE OF LEAST VEL ANG AT INFINITY
1.00
.50
0.00
-.50
-1.00
-1.50
-2.00
-2.50
-2.00
-1.50
-1.00
-.50
0.00
.50
1.00
1.50
THKNSS=.075 CMABER=-20. ANG=-10.

Figure 20B

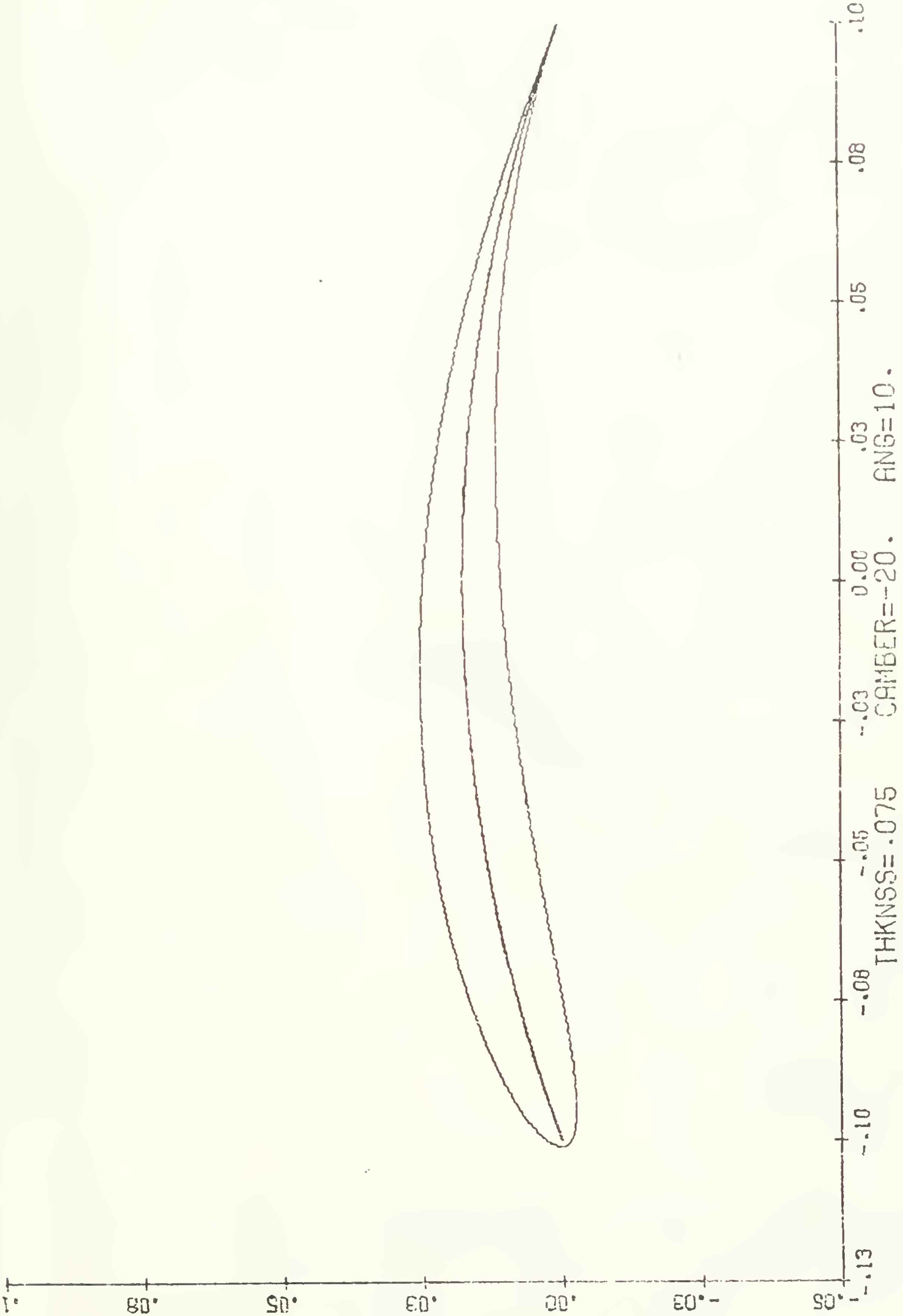
THKNSS=.075 CAMBER=-20. ANG=10.
BLADE
-.13
-.10
-.08
-.05
-.03
0.00
.03
.05
.08
.10
-.05
-.03
.00
.03
.05
.08
.10

Figure 20C

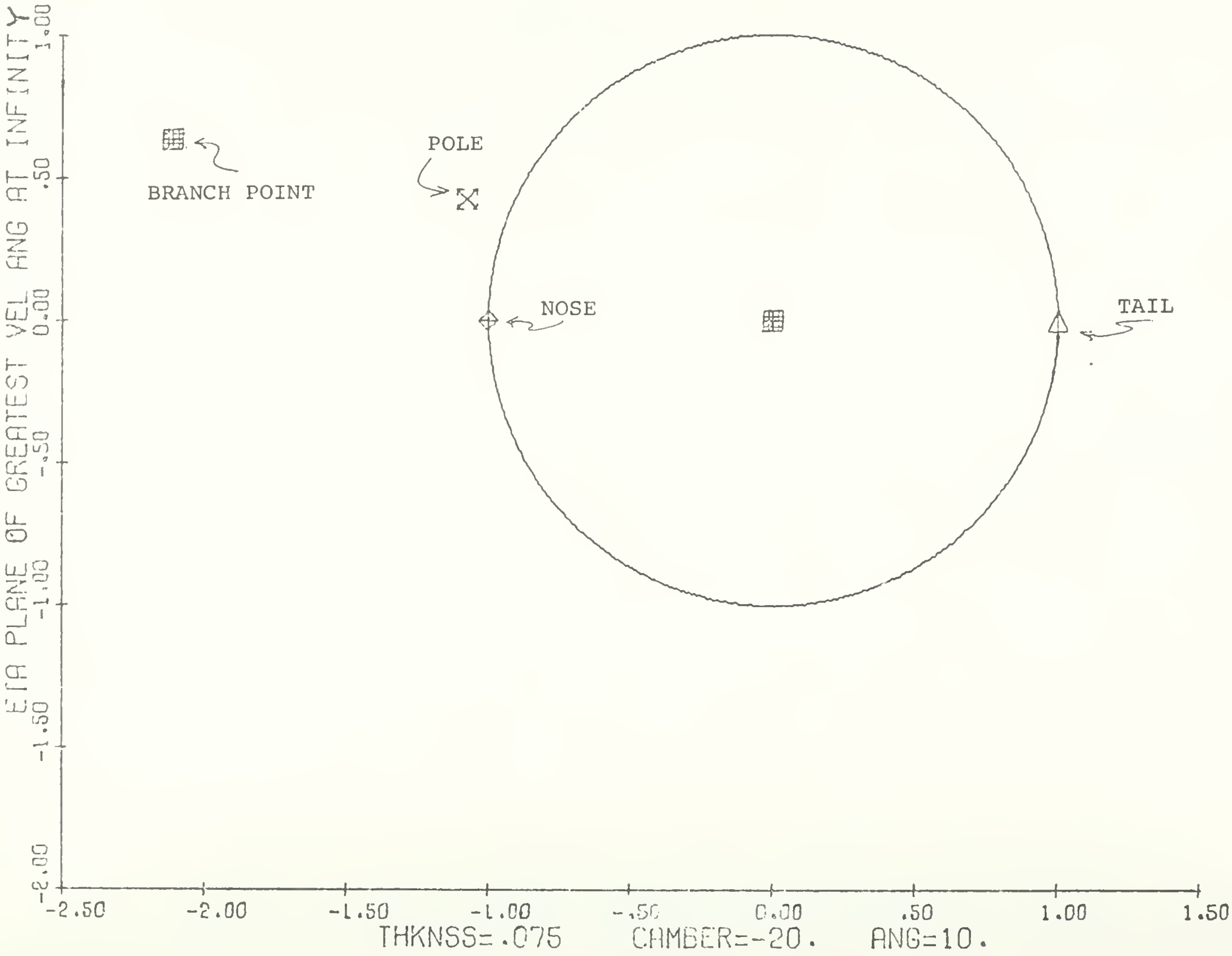
ETA PLANE OF GREATEST VEL ANG AT INFINITY
1.00
.50
0.00
-.50
-1.00
-1.50
-2.00
-2.50
-2.00
-1.50
-1.00
-.50
0.00
.50
1.00
1.50
BRANCH POINT
POLE
NOSE
TAIL
THKNSS=.075 CAMBER=-20. ANG=10.

Figure 20D

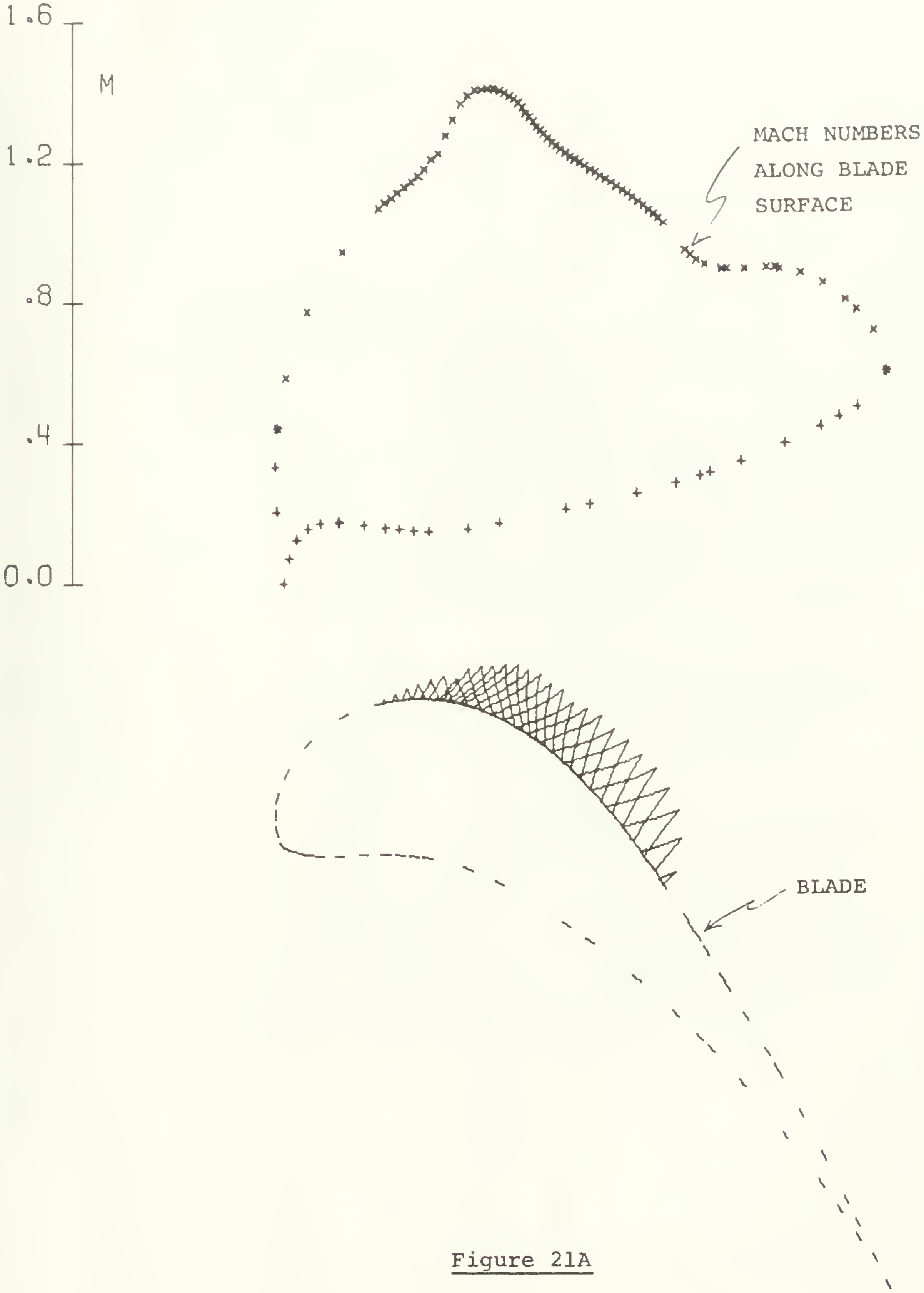

Figure 21A

M1=.340 M2=.800 DEL TH= 83.94 G/C=1.18

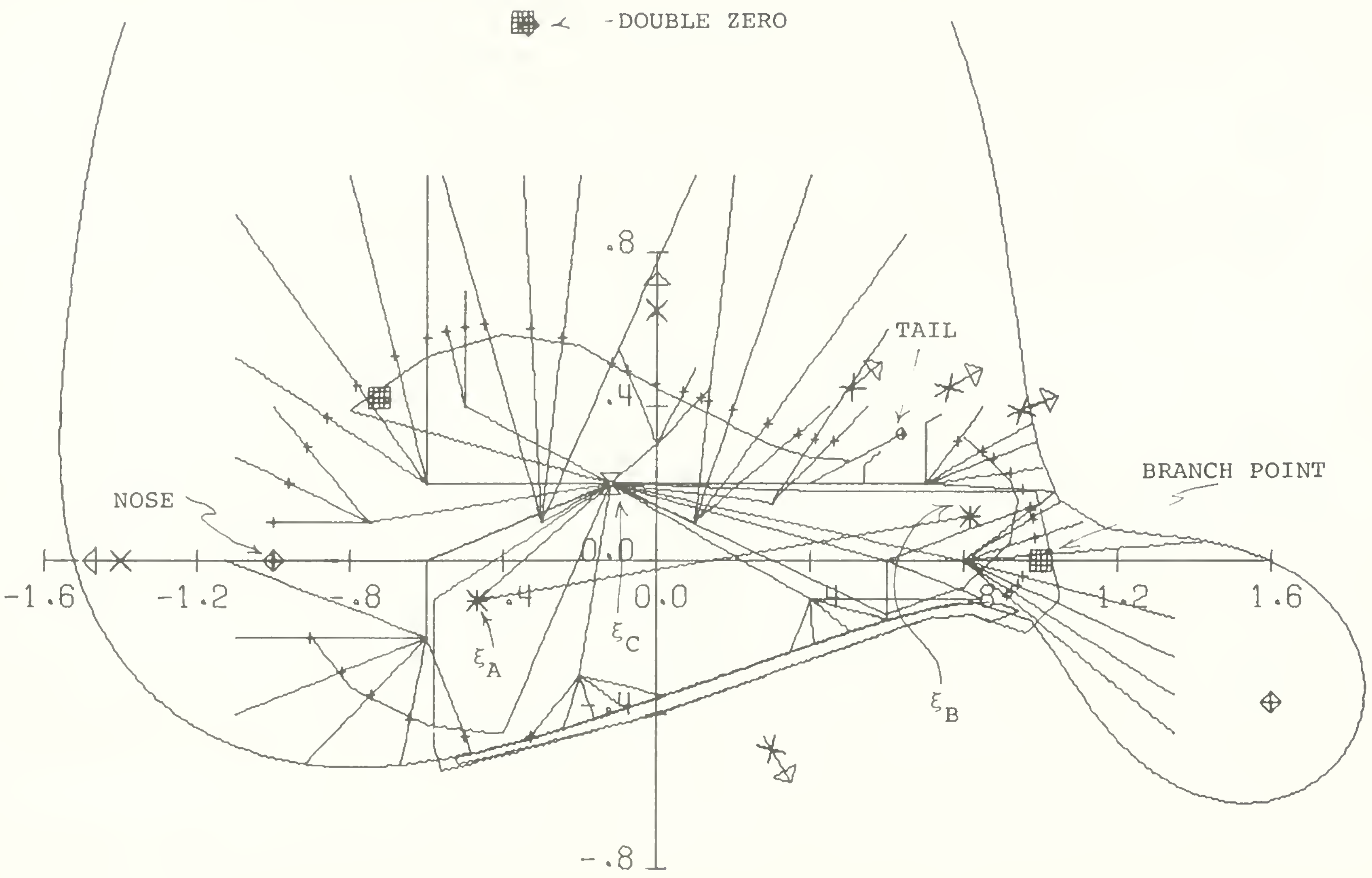

Figure 21B

RUN 473 EM1= .340 EM2= .800 M= .600

This report was prepared as an account of Government sponsored work. Neither the United States, nor the Administration, nor any person acting on behalf of the Administration:

A. Makes any warranty or representation, express or implied, with respect to the accuracy, completeness, or usefulness of the information contained in this report, or that the use of any information, apparatus, method, or process disclosed in this report may not infringe privately owned rights; or

B. Assumes any liabilities with respect to the use of, or for damages resulting from the use of any information, apparatus, method, or process disclosed in this report.

As used in the above, "person acting on behalf of the Administration" includes any employee or contractor of the Administration, or employee of such contractor, to the extent that such employee or contractor of the Administration, or employee of such contractor prepares, disseminates, or provides access to, any information pursuant to his employment or contract with the Administration, or his employment with such contractor.